Micromechanical Tuning Elements for Submillimeter Wave Integrated Circuits

Thesis by

Victor Manuel Lubecke

In Partial Fulfillment of the Requirements

for the Degree of

Doctor of Philosophy

California Institute of Technology

Pasadena, California

1996

(Submitted July 13, 1995)

To Whom it may concern

Acknowledgements

Most of the work described in this thesis was funded by a NASA GSRP Fellowship, and a contract with the NASA Jet Propulsion Laboratory. I owe a debt of gratitude to Rob McGrath for making these available to me, serving as technical advisor and research collaborator, originating the idea for a planar tuning element, and showing such enthusiastic interest throughout this work.

I would also like to express my deepest thanks to Phillip Stimson. I honestly cannot imagine how I would have made it through this ordeal without Phil's empathetic support, unrelenting encouragement, sound technical advice, and words of wisdom.

I have been privileged to work with many good people during my time at Caltech, and I am glad to have known them all. Without a doubt, the devoted friendship of Paul Bantz and Lars Foged pulled me through my first year. I am grateful for the continuing generous advice and long-term friendship provided me by Jon Hacker, Bobby Weikle, and Scott Wedge, as well as my renewed friendships with Moonil Kim, Karen Lee, and Yong Guo. I must also express my gratitude to Mike De Lisio and Alina Mousessian for making sure that I had too much fun to finish any sooner than I did, and to Jung-Chih Chiao for commiserating with me on our work in the *clean room*, when things weren't so fun. I would also like to thank Shi-Jie Li and Cheh-Ming Liu for tolerating my ubiquitous presence in our shared office.

A warm thank-you also goes to Kent Potter, for so many rescues, and Irene Loera for so many cakes. I have had the good fortune of receiving advice and friendship from Prof. Yu-Chong Tai, visiting Professors Erik Kollberg and Koji Mizuno, and alumni Gabreil Rebeiz and Dave Haub, for which I am also thankful. I spent a little more time at Caltech than I expected to, and I am glad to have had the consolation of meeting John Davis, Polly Preventza, and Prof. Minoru Saga.

I would also like to acknowledge my gratitude to Lance Riley and Dan Rascoe, for patiently counseling my return to school, and to Peter Siegel, for patiently supporting my return from school. I would also like to thank Tricia, Jessica, and Michael Stimson, along with Lisa De Lisio, Dee Weikle, and the Fay clan, for providing me with a much appreciated refuge from *nerdom*.

I cannot express how truely grateful I am to my loving parents for their unwavering support and selfless commitment to me, but I think they already know. I would also like to thank my beloved wife for being there, and for not killing me.

Finally, I am grateful to my advisor David Rutledge, who welcomed me to Caltech, provided me with a wealth of ideas, and never stopped trying to figure me out.

The trouble with doing something right the first time
is that nobody appreciates how difficult it was.

–Anonymous

Micromechanical Tuning Elements for Submillimeter Wave Integrated Circuits

Abstract

Monolithic integrated circuit technology promises a practical means for realizing reliable and reproducible planar millimeter and submillimeter wave circuits. Planar circuits are fabricated through photolithographic techniques, which allow for the cost-effective production of intricate designs not possible with waveguide technology. Such circuits however, do not typically allow for post-fabrication optimization of performance. This can be a critical problem for the millimeter and submillimeter band, where device parasitics and fabrication tolerances are difficult to control and characterize. In this thesis, a micromechanical tuning element suitable for integration in a variety of monolithic millimeter and submillimeter wave circuits is presented. It is called a *sliding planar backshort* (SPB) and it can be fabricated as an integral part of a dielectric-coated coplanar transmission line. The SPB forms a movable short-circuit over a useful bandwidth, which allows for the variation of the transmission line's electrical length. A semiempirical approach was employed in its design. Measurements of $|s_{11}|$ for the SPB at 2 GHz, were better than –0.5 dB over a bandwidth of at least 50% on both coplanar strip and coplanar waveguide transmission lines. A frequency-scaled version of the SPB was photolithographically fabricated and tested in a planar quasi-optical 100 GHz detector circuit. The response of a Schottky diode was successfully varied over a range of almost 14 dB, creating a 3 dB improvement over the untuned response. A technique for fabricating a micromechanical version of the SPB was developed. Two of these SPB's were fabricated as integral parts of a quasi-optical 620 GHz monolithic integrated detector circuit, where they were used to vary the measured response over a range of almost 15 dB. Such tuning elements can be used for characterizing developmental circuits, and for optimizing the in-use performance of various millimeter and submillimeter wave integrated circuits.

Contents

Chapter 1

Introduction

Although nearly invisible to the naked eye, micrometer scale structures will form the building blocks of powerful new instruments which will enable scientists to better explore the external world and the inner-workings of the human body. An important application of this technology is in remote sensing molecular-line spectroscopy, which is providing insight into the chemical make-up and dynamics of stars, the intergalactic medium, and the earths atmosphere. Such measurements are often performed using millimeter and submillimeter radiation which can penetrate gas and dust, yet conveys interesting spectral information. This field of research utilizes instrumentation with detectors for which physical dimensions are less than a wavelength of the radiation used. Conventional component fabrication techniques are difficult at this scale. Improved fabrication technologies are being investigated and may benefit from recent advances in other fields which involve structures on the micron scale. Techniques recently developed to enable the fabrication of micromechanical structures from silicon offer an attractive means for improving the technology of these tiny electromechanical circuits. These techniques have been employed to fabricate microsensors and novel machines, and may someday provide tools that will assist physicians in diagnosis and treatment, and researchers in understanding body processes.

1.1 Millimeter and Submillimeter Wave Circuits

The field of millimeter and submillimeter wave circuit technology is open to innovation. Mature radio circuit technology has been widely used in communica-

tions, telemetry, and numerous other applications at lower frequencies, and highly developed optical technology has been applied to remote-sensing and metrology at near-infrared frequencies and beyond, but the spectrum in between 100 GHz and 10 THz remains open to the development of new and diverse approaches offering their own distinct advantages.

The primary application of this spectrum has so far been astronomical and terrestrial remote sensing. At millimeter and submillimeter wavelengths, this science is mainly passive, and thus relies heavily on the use of highly sensitive, low-noise receivers to observe electromagnetic emissions. Blackbody and spectral emissions are monitored for physical and chemical phenomena which provide information on the cosmic background, newly formed distant galaxies, and the initial stages of star formation within clouds of gas in our galaxy [1],[2]. Information on the earth's atmosphere, climate, and ecology is also obtained in this way, and is becoming increasingly important [3].

Before the advent of molecular line radio astronomy it was largely believed that the interstellar regions of our galaxy were relatively empty, consisting mainly of scattered hydrogen atoms. The earliest detection of spectral emissions were in the centimeter range, and indicated the presence of the OH radical, ammonia and then water. This and other observations indicated the possibility of an interstellar medium with far greater chemical complexity than previously considered, and prompted a search for new molecules. Collision induced photon emissions from fundamental and higher-order transitions for many of these molecules were anticipated to be in the 50–150 GHz range [4]. The first of these emission to be detected were from the CO molecule at 115 GHz in 1970 [5], and so came the birth of millimeter wave molecular line radio astronomy. Many different species of molecules were detected soon afterwards. Early results prompted the building of large aperture radio telescopes, followed by the development of multielement interferometers, and even intercontinental very-long-baseline interferometers.

As the field matured, an interest has grown in molecular emissions at higher frequencies. Submillimeter wave heterodyne spectroscopy has played a critical role in the study of star formation. Stars are known to be formed within dense gas and dust clouds found in our own, and in distant, galaxies. When a protostellar cloud of mass comparable to a stellar mass becomes gravitationally unstable, it collapses to form a star. Much of the heavily processed mass in the outer envelope of the star, is later released back into the interstellar medium. The study of the atomic and molecular make-up of the interstellar medium provides information on the star-formation process itself, as well as the degree of stellar activity for a specific region. Emissions from many molecular species present in these regions, as well as specific accretion activities, each have there own distinct submillimeter spectroscopic signatures.

The strength of these emissions however, is low and tends to decrease with increasing frequency. Weak sources, combined with the interfering effects of the earth's atmosphere, provide a challenge to the development of instruments for detecting emissions in the submillimeter spectrum. The first receivers for molecular line radio astronomy functioned at room temperature and used a Schottky diode mounted in a waveguide as a heterodyne mixer, with a reflex klystron as the local oscillator (LO). The adoption of cryogenic cooling and solid state (Gunn) LO sources served to refine this technique, and such receivers are now used well into the low-frequency end of the submillimeter band. The most sensitive of these receivers utilize a whisker-contacted Schottky diode, mounted in a reduced-height waveguide with an adjustable backshort behind it, as shown in Figure 1.1.

Schottky diodes, as well as others devices used in this frequency band, have a parasitic reactance associated with their physical structures. This reactance degrades the device performance as the inverse of frequency, a phenomena which is usually the predominant effect on performance in the submillimeter band. Minimizing this reactance for a device typically involves performance trade-offs. The

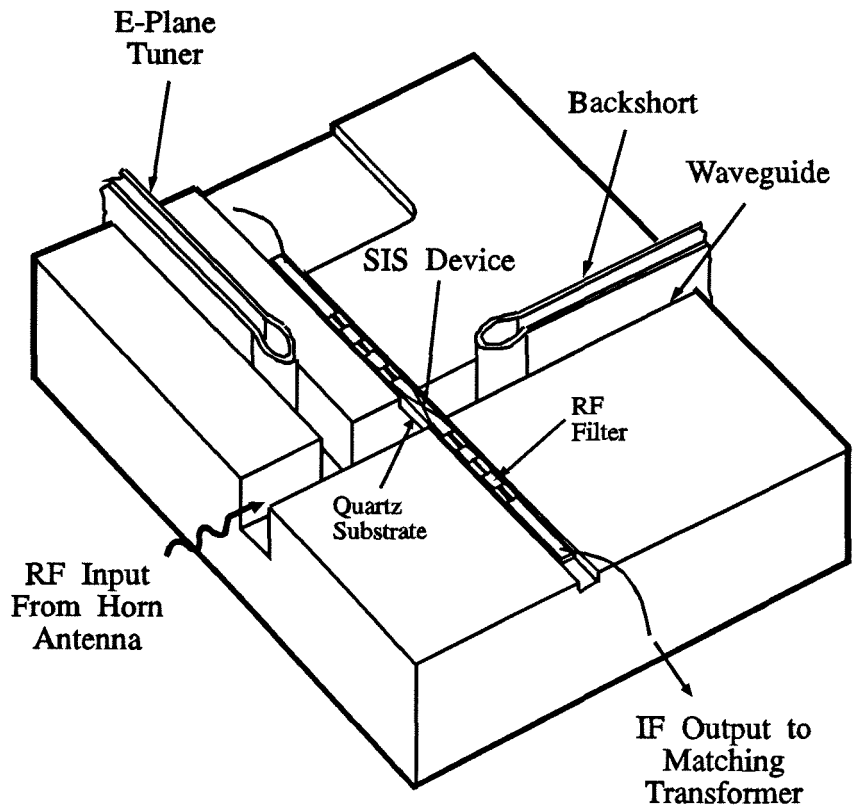

Figure 1.1 A typical waveguide mixer block with adjustable backshorts [11]. An SIS device is embedded in the waveguide cavity, and backshorts are used to provide an impedance match.

movable backshort in these mixer circuits however, can be positioned in the guide to create a susceptance in parallel with the diode, which compensates for the parasitic reactance in the device.

Parasitic reactance has such a deleterious effect at frequencies above 600 GHz that waveguide receivers are often replaced by a so called *corner cube* mount [6], in which a diode chip, surrounded be a corner cube reflector, is contacted by a thin free-standing whisker. This enables the circuit capacitance to be reduced somewhat and Schottky diode receivers at 2.5 THz [7], critical for the observation of the OH molecule, have been made by this means. Parasitics are still the dominating factor in these receivers, which require skilled manufacture and painstaking assembly. Their reliability is also in question for many applications.

The development of the superconductor-insulator-superconductor (SIS) tunnel junction mixer came in the late 1970's. An SIS mixer can offer conversion gain, requires LO power which is typically 30 dB lower than that needed in a Schottky diode mixer [4], and offers a sensitivity which can approach the quantum limit [8]. The first SIS mixers were made by simply replacing the Schottky diode in a reduced-height waveguide mount, with an SIS tunnel junction connected by coupling probes on a flat quartz substrate. The SIS junction has a large inherent geometric capacitance, typically 50 fF for a 1 μm^2 junction [9] compared with about 6 fF for submillimeter Schottky diodes [10]. This is due to the thin barrier in SIS junctions, which may approach one atomic layer in thickness for high performance devices. This makes backshort tuning more critical, and often the addition of an E-plane tuner, placed ahead of the mixing device, is needed to further improve the impedance match. An integral resonant tuning structure is sometimes fabricated along with the naturally planar SIS junction to further facilitate the matching of its impedance [11],[12]. Another drawback for SIS mixers is the requirement for cooling to temperatures less than 10 K, whereas the performance of Schottky diode mixers degrades gracefully as temperature is increased, and operation at

higher temperatures, like those attained by immersion in liquid nitrogen (77 K) or through conventional refrigeration techniques, is possible. Furthermore, there may be a fundamental frequency limit at which an SIS junction can no longer function; this is not the case for Schottky diodes. The development of mixer circuits for both of these devices is continuing, especially at higher frequencies.

Receiver performance can be further enhanced by combining several devices in a focal plane imaging array as a means of increasing the rate at which the receiver can obtain data. Much of the science thrust in millimeter and submillimeter wave astronomy involves mapping of extended sources or searching large areas for discrete objects of interest. This is because the field is relatively immature, and the sky has not yet been mapped at all wavelengths of interest, and because the sources of interest are often extended clouds. Mapping extended sources with a single receiver necessitates repositioning the telescope beam to record each pixel of the image. This is time consuming, cumbersome, and expensive. An array receiver can record the same data N times faster (assuming equivalent receiver noise temperature) where N is the number of elements. In addition, data may be recorded within the small time window of favorable atmospheric conditions, or within other time constraints, enabling some tasks which would be impossible with single element receivers. A focal plane imaging array of waveguide embedded Schottky diodes has been demonstrated at 115 GHz [13].

Building precise waveguide components is an exacting process, particularly at frequencies above 400 GHz where the physical dimensions place extreme demands on conventional machining techniques. While waveguide components and circuits have been demonstrated at frequencies in excess of 800 GHz, these items are extremely difficult to produce. Such circuits involve intricate mechanical structures like patterned noncontacting backshorts, tiny corrugated feed-horns, as well as the waveguides themselves. Various techniques have been used to miniaturize the elements. Corrugated feedhorns formed with a conventionally lathed man-

drel, have been demonstrated at 3 THz [14], and conventional machined resonant insertable waveguide backshorts have been used in receivers at 840 GHz [15]. Micromachining techniques are now being investigated for the fabrication of these components, but this work in still in its infancy [16],[17]. Silicon waveguides and planar whiskers have been developed. All of these efforts, however, are exceptional, and the manufacture of waveguide circuits for the submillimeter spectrum remains a sophisticated endeavor. The construction of complex focal plane imaging arrays, using waveguide technology at these frequencies, seems even more impractical.

The planar geometry of the SIS junction, and the advancing development of planar Schottky diodes [10],[18] has made possible an alternative approach. These devices can be fabricated with integral planar antennas and planar impedance matching elements to form fully integrated mixer circuits. They are manufactured through lithographic techniques alone, and are far simpler to fabricate at increasingly higher frequencies. This approach provides better reproducibility and reliability, allows for the creation of focal plane imaging arrays without an increase in the complexity of the fabrication process, and could potentially allow for the inclusion of IF circuitry to form fully integrated receivers.

Various circuits of this type have already been demonstrated utilizing SIS junctions and planar Schottky diodes as mixing elements [19],[20]. These circuits employ a substrate lens to quasi-optically couple to millimeter and submillimeter wavelength radiation, as illustrated in Figure 1.2, entirely avoiding the use of waveguide components. These circuits, however, are not without drawbacks. As previously mentioned, SIS junctions and Schottky diodes have an inherently large parasitic reactance. The radiation impedance of broadband planar antennas and resonant narrow-band antennas on the other hand, is real. In existing circuits, the impedance match between circuit elements is created using fixed-tuned elements. This makes characterization of the component elements critical, and it is not usually possible to achieve optimal results without multiple iterations.

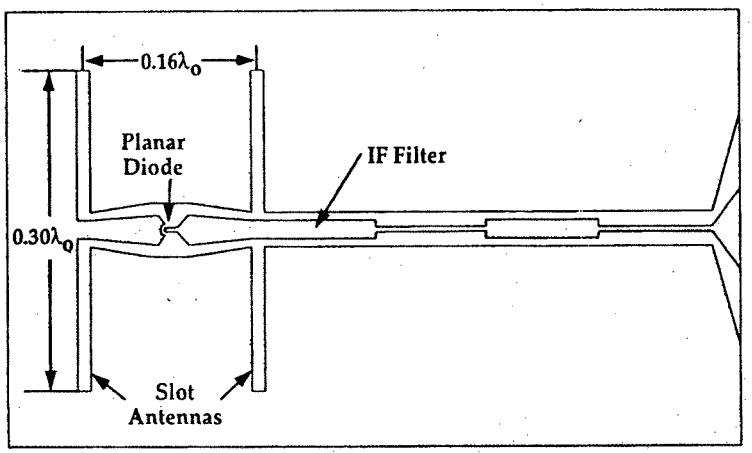

(a)

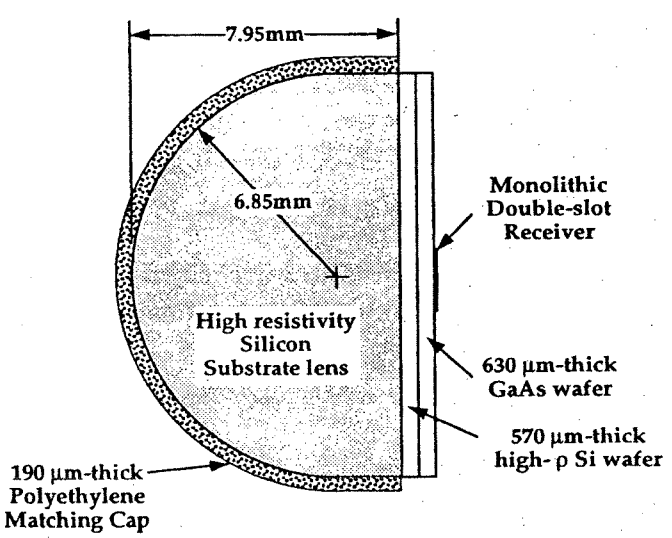

(b)

Figure 1.2 A planar quasi-optical mixer circuit [19]. A planar diode is integrated with planar slot antennas (a) and mounted on a substrate lens (b).

An adjustable planar tuning element, which could function in a planar circuit analogously to a backshort in a waveguide circuit, would be beneficial to the further development of these circuits [21]-[25]. Its interaction with a device could be studied in developmental circuits as an aid to characterizing the device. Ultimately, it could provide an integrated submillimeter wavelength receiver with a means for the same type of real-time performance optimization which is available in waveguide circuits.

1.2 Microelectromechanical Systems

Another field in which there is growing interest in structures with micron-scale dimensions is that of microelectromechanical systems (MEMS). This deals with the fabrication of micromechanical transducers through the use of photolithographic techniques, like those widely employed in the fabrication of integrated circuits. This work has largely involved the development of various techniques for the micromachining of silicon. Recent advances have extended this work from the manufacture of rigid fittings and deformable sensors, to fully rotatable joints, translating members, mechanical-energy storage units, and even micro-motors [26]. While many practical uses have already been found, these structures are expected to be used for extraordinary future applications, such as the fabrication of micro-robots capable of autonomous in vivo exploration and surgical repair of the human body.

Early work in the field was limited to rigid and semi-rigid structures such as cantilevers, bridges and diaphragms. Structures of this type have been successfully combined to create accelerometers, pressure sensors, flow sensors, nozzles, and valves [27]. The structures are usually fabricated by the selective etching of silicon, utilizing a wafer's crystallographic orientation to anisotropically etch a limited number of geometries. This is known as bulk micromachining, and is the most mature MEMS fabrication technology.

More recent work has extended the field to the manufacture of kinematic

pairs. These are devices such as rotating joints and linear translation elements which operate within the plane of a substrate, and hinged structures which can move out of the substrate plane [28],[29]. These include gears and gear trains, hinges, cranks, springs, sliders, and similar structures. They have been combined to form micro-tongs, micro-switches, turbines, and even micro-motors. Most of these structures have been fabricated through the use of sacrificial-layer techniques to create polysilicon structures anchored to a silicon substrate. This technique is known as surface micromachining, and the process can be as simple as the following example of the fabrication of a simple rotating joint.

A thermal oxide layer is first grown on a silicon wafer, and then appropriately patterned using photolithography and reactive-ion etching techniques. Next, a layer of polysilicon is deposited using low pressure chemical vapor deposition (LPCVD), and etched to form another pattern (on top of the thermal oxide), using photolithography. A second layer of oxide is then deposited over these layers using chemical vapor deposition (CVD), and openings are then etched in it to allow access to the bare substrate below. A second layer of polysilicon is subsequently deposited and patterned as before, forming a structure which is in-part anchored to the substrate, and in-part overlapping the now oxide-covered, first polysilicon structure. Finally, the sacrificial oxide layers are dissolved with a wet etch, releasing the structure formed by the first polysilicon step to move freely in the plane, constrained only by the overlapping edge of the anchored second polysilicon layer. The process is shown in Figure 1.3.

Another recently developed process allows for the fabrication of microstructures with larger vertical aspect ratios (over 100 to 1), and the use of materials other than silicon. This process, illustrated in Figure 1.4, is known as LIGA (a German acronym meaning lithography, electroforming, and molding) [30], and can be combined with surface micromachining techniques to create substrate anchored structures as well. This procedure allows for the batch production of three-dimensional

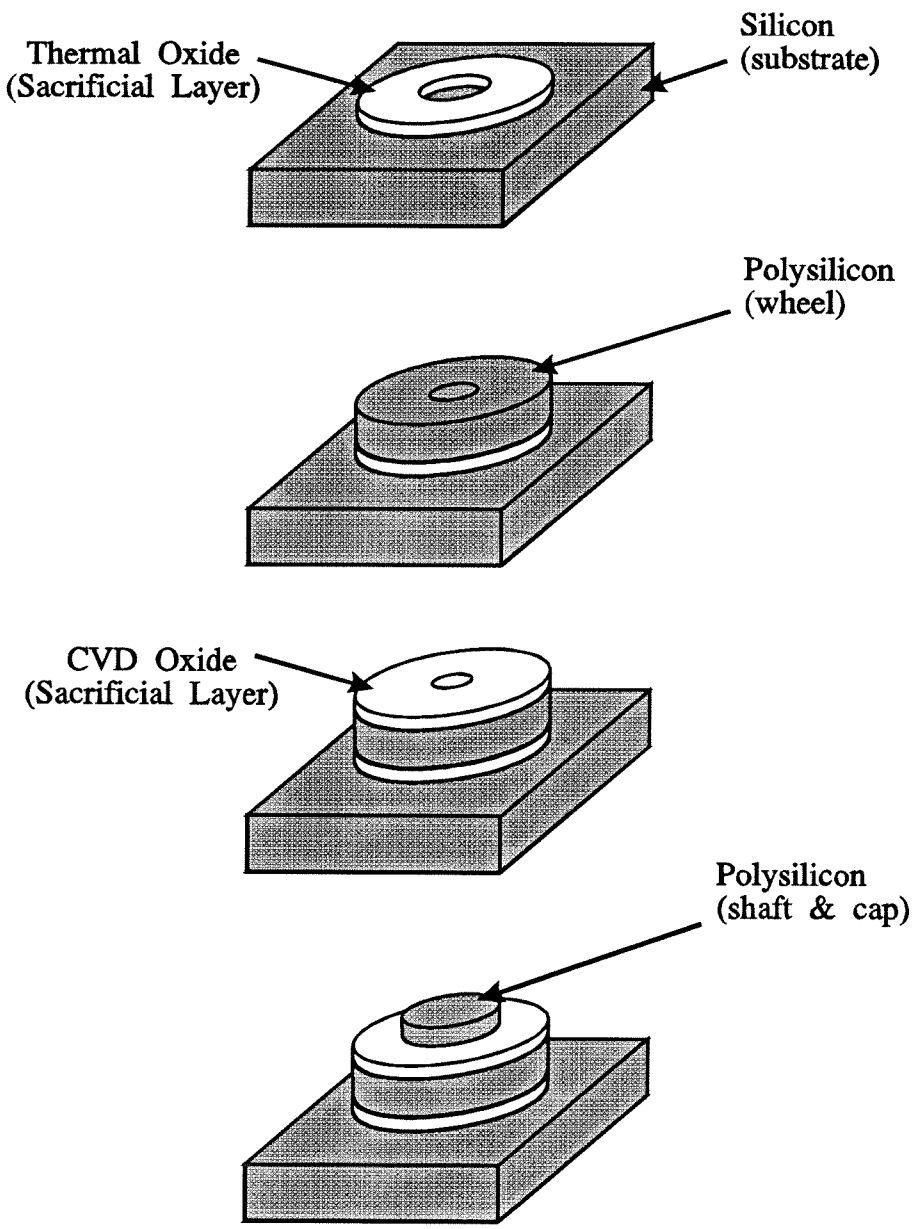

Figure 1.3 Illustration of a simple surface micromachining process. Sacrificial layers are used to make a rotating joint.

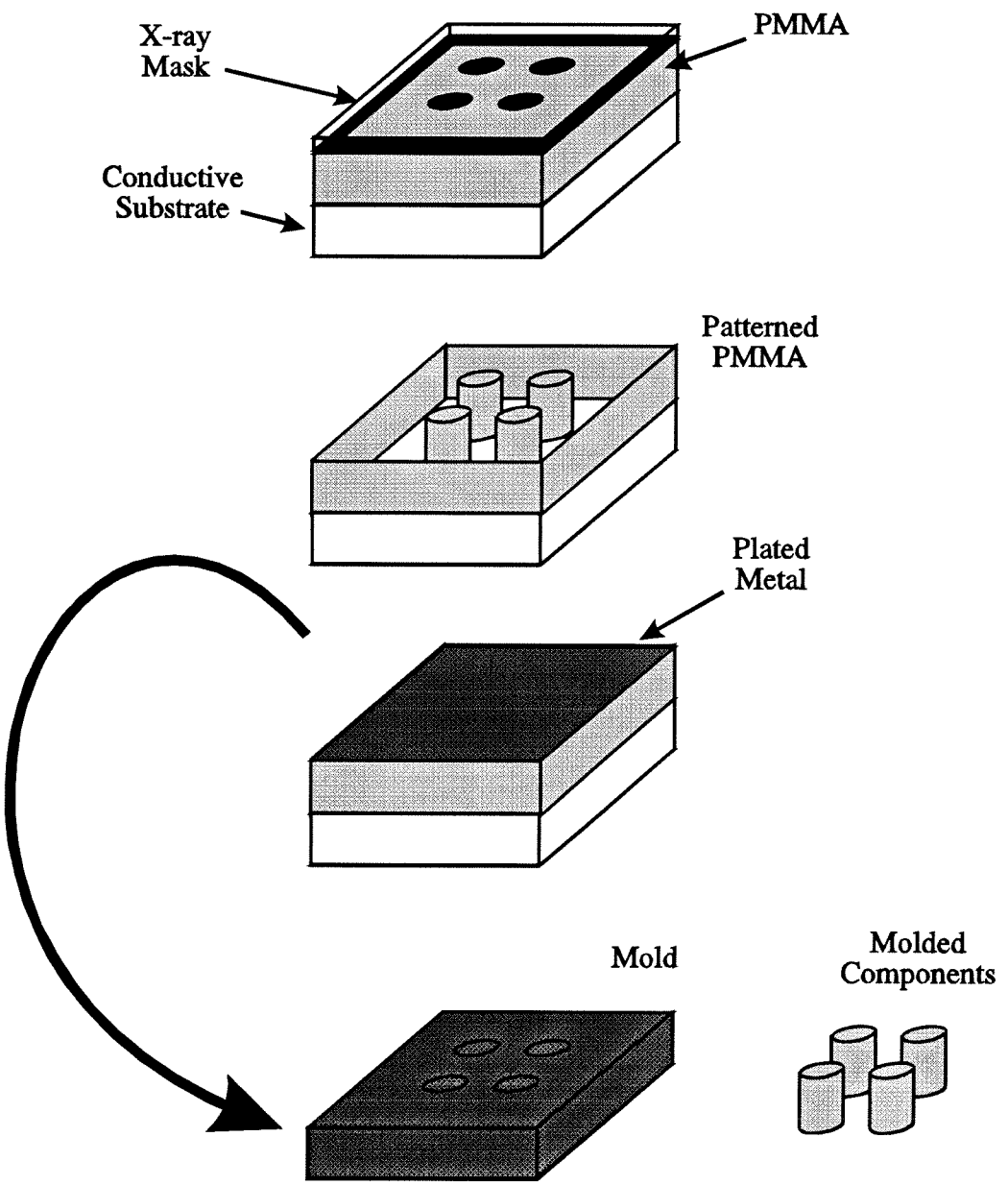

Figure 1.4 Illustration of the LIGA process. A micro-mold is formed which can be used to form micro-components.

structures within a micro-fabricated cast or mold. This technique has been used to form couplers for multimode optical fibers and various refractive and difractive micro-optical components, as well as more conventional mechanical structures like gears and bearings [27],[31].

The LIGA process begins with the deposition of a thick layer of X-ray sensitive photoresist, typically poly-methylmethacrylate (PMMA), on a conductive substrate. The resist is then exposed through an X-ray mask, using a highly collimated X-ray source to achieve high, yet vertical, sidewalls when the resist is developed. The openings formed in the resist can then be partially filled with metal through selective electroplating, forming metallic structures with large vertical aspect ratios as an end product. Alternatively, the openings in the resist can be filled above the brim in order to form a unified structure, patterned as the compliment of the X-ray mask, which when removed from the resist can be used as a mold or micro-cast for a low-viscosity polymer. The mold can be used to repetitively form high-aspect-ratio copies of the original pattern, from the cured polymer material.

The dimensions of these MEMS are consistent with those needed for resonant structures in millimeter and submillimeter wavelength circuits. The fabrication processes described and the associated materials, however, are not consistent with the processes and materials used in the fabrication of existing millimeter and submillimeter wavelength circuits. It is conceivable, however, that a hybrid process can be developed which is suitable for fabricating a micromechanical element as an integral component in such a circuit, in order to allow for the post-fabrication optimization of its performance [32]-[34]. Such an element could potentially help to close the gap in performance between waveguide circuits and planar circuits at lower frequencies, and make possible the fabrication of otherwise impractical circuits at higher frequencies.

1.3 Organization of the Thesis

This thesis details the development of a mechanically adjustable planar tuning element suitable for integration with otherwise conventional submillimeter wavelength integrated circuits. Its design and development with a microwave model, and subsequent development for millimeter and submillimeter wavelength applications, are chronicled in that order. Performance tests, ultimately at 620 GHz, are described.

In Chapter 2 the theory necessary for the development of a tuning structure for use on planar transmission lines is summarized. The focus is on the use of a sliding planar metallic pattern to form a movable low-impedance termination, on dielectric-coated coplanar strip and coplanar waveguide transmission lines.

Development of the tuning element is carried out with a 2 GHz model in Chapter 3. Useful dimensions for both coplanar strip and coplanar waveguide transmission lines are determined, along with the critical dimensions for a frequency scalable tuning element which works well on either type of line.

In Chapter 4, a frequency scaled version of the tuning element is shown to be effective in a 100 GHz quasi-optical detector circuit. The tuning element is fabricated through photolithographic techniques, and its effect on the response of a beam-lead Schottky diode is demonstrated.

A mechanically tunable 620 GHz monolithic integrated circuit is demonstrated in Chapter 5. Fabrication of the tuning element through a novel micromachining technique is described, as well as the effect of two integrated tuning elements on the response of a self-heated bismuth thermocouple to submillimeter radiation.

Chapter 6 summarizes the results of this work, and discusses the implications. Additional applications and improvements are also described as suggestions for future work.

Development of the fabrication process for the micromechanical submillimeter

wave integrated circuit formed a major part of this thesis. An appendix which details the process has been included.

References

[1] G.D. Watt and A.S. Webster, *Submillimetre Astronomy*, Dordrecht, The Netherlands: Kluwer Academic Publishers, 1990.

[2] T.G Phillips and J. Keene, "Submillimeter Astronomy," *Proceedings of the IEEE*, vol. 80, no. 11, pp. 1662–1678, November 1992.

[3] G.L. Manny, L. Froidevaux, J.W. Waters, "Chemical Depletion of Ozone in the Arctic - Lower Stratosphere During Winter 1992-93," *Nature*, vol. 370, no. 6489, pp. 429–434, August 11, 1994.

[4] J.M. Payne, "Millimeter and Submillimeter Wavelength Radio Astronomy," *Proceedings of the IEEE*, vol. 77, no. 7, pp. 993–1017, July 1989.

[5] R.W. Wilson, K.B. Jefferts, and A.A. Penzias, "Carbon Monoxide in the Orion Nebula," *Astrophysical Journal*, vol. 161, pp. L87–L89, August 1970.

[6] H.R. Fetterman, P.E. Tannenwald, B.J. Clifton, C.D. Parker, W.D. Fitzgerald, and N.R. Erickson, "Far-IR Heterodyne Radiometric Measurements with Quasioptical Schottky Diode Mixers," *Applied Physics Letters*, vol. 33, pp. 151–154, 1978.

[7] P.A.D Wood, D.W. Porterfield, W.L. Bishop, and T.W. Crowe, "GaAs Schottky Diodes for Atmospheric Measurements at 2.5 THz," *Fifth International Symposium on Space Terahertz Technology - Symposium Proceedings*, pp. 355–368, May 1994.

[8] J.R. Tucker, "Quantum Limited Detection in Tunnel Junction Mixers," *IEEE Journal of Quantum Electronics*, vol. 15, no. 11, pp. 1234–1258, November 1979.

[9] R. Blundell and C.-Y.E. Tong, "Submillimeter Receivers for Radio Astronomy," *Proceedings of the IEEE*, vol. 80, no. 11, pp. 1702–1720, November 1992.

[10] T.W. Crowe, R.J. Mattauch, H.P. Roser, W.L. Bishop, W.C.B. Peatman, and

X. Liu, "GaAs Schottky Diodes for THz Mixing Applications," *Proceedings of the IEEE*, vol. 80, no. 11, pp. 1827–1841, November 1992.

[11] M. Salez, P. Febvre, W.R. McGrath, B. Bumble, and H.G. Leduc, "An SIS Waveguide Heterodyne Receiver for 600 GHz-635 GHz," *International Journal of Infrared and Millimeter Waves*, vol. 15, no. 2, pp. 349–368, February 1994.

[12] J. Zmuidzinas, H.G. Leduc, J.A. Stern, and S.R. Cypher, "Two Junction Tuning Circuits for Submillimeter SIS Mixers," *IEEE Transactions on Microwave Theory and Techniques*, vol. 42, no. 4, pp. 698–706, April 1994.

[13] N.R. Erickson, P.F. Goldsmith, G. Novak, R.M. Grosslein, P.J. Viscuso, R.B. Erickson, and C.R. Premore, "A 15 Element Focal Plane Array for 100 GHz," *IEEE Transactions on Microwave Theory and Techniques*, vol. 40, no. 1, pp. 1–11, January 1992.

[14] B.N. Ellison, M.L. Oldfield, D.N. Matheson, B.J. Maddison, C.M. Mann, and A.F. Smith, "Manufacture and Test of a 2.5 THz Corrugated Feedhorn," *Fifth International Symposium on Space Terahertz Technology - Symposium Proceedings*, pp. 851–860, May 1994.

[15] G. deLange, *et al.*, "Quantum Limited Responsivity of a $Nb/Al_2O_3/Nb$ SIS Waveguide Mixer at 460 GHz and First Results at 750 GHz and 840 GHz," *Fourth International Symposium on Space Terahertz Technology - Symposium Proceedings*, pp. 41–49, March 1993.

[16] W.R. McGrath, C. Walker, M. Yap, and Y.-C. Tai, "Silicon Micromachined Waveguides for Millimeter-Wave and Submillimeter-Wave Frequencies," *IEEE Microwave and Guided Wave Letters*, vol. 3, no. 3, pp. 61–63, March 1993.

[17] D.A. Brown, A.S. Treen, and N.J. Cronin, "Micromachining of Terahertz Waveguide Components with Integrated Active Devices," *Nineteenth International Symposium on Infrared and Millimeter Waves - Conference Digest*, pp. 359–360, October 1994.

[18] I. Mehdi and P.H. Siegel, "Effect of Parasitic Capacitance on the performance of Planar Subharmonically Pumped Schottky Diode Mixers," *Fifth International Symposium on Space Terahertz Technology - Symposium Proceedings*, pp. 379–393, May 1994.

[19] S.S. Gearhart and G.M. Rebeiz, "A Monolithic 250 GHz Schottky-Diode Receiver," *IEEE Transactions on Microwave Theory and Techniques*, vol. 42, no. 12, pp. 2505–2511, December 1994.

[20] P.A. Stimson, R.J. Dengler, H.G. LeDuc, S.R. Cypher, and P.H. Siegel, "A Planar Quasi-optical SIS Receiver," *IEEE Transactions on Microwave Theory and Techniques*, vol. 41, no. 4, pp. 609–615, April 1993.

[21] V.M. Lubecke and W.R McGrath, "Tuners for Coplanar-Strip Transmission Lines," *NASA Tech Briefs Magazine*, submitted September 1990.

[22] V.M. Lubecke, W.R. McGrath, and D.B. Rutledge, "Sliding Backshorts for Planar Circuits," *International Journal of Infrared and Millimeter Waves*, vol. 12, no. 12, pp. 1387–1397, December 1991.

[23] V.M. Lubecke, W.R. McGrath, and D.B. Rutledge, "An Adjustable RF Tuning Element for Microwave, Millimeter Wave, and Submillimeter Wave Integrated Circuits," *Proceedings of the NASA Technology 2001 Conference*, vol. 2, no. 3136, pp. 239–245, December 1991.

[24] W.R. McGrath, V.M. Lubecke, and D.B. Rutledge, "Adjustable RF Tuning Elements for Planar Millimeter Wave and Submillimeter Wave Circuits," *Fifteenth International Conference on Infrared and Millimeter Waves: Conference Digest*, pp. 344–346, December 1990.

[25] W.R. McGrath and V. M. Lubecke, "RF Tuning Element," *U.S. patent no. 5,115,217*, granted May 19, 1992.

[26] W.D. Marbach, "A Small World Grows Tinier," *Newsweek*, November 30, 1987.

[27] J. Bryzek, K. Peterson, and W. McCully, "Micromachines on the March," *IEEE Spectrum*, pp. 20–31, May 1994.

[28] L.-S. Fan, Y.-C. Tai, and R.S. Muller, "Integrated Movable Micromechanical Structures for Sensors and Actuators," *IEEE Transactions on Electron Devices*, vol. 35, no. 6, pp. 724–730, June 1988.

[29] M. Mehregany, K.J. Gabriel, and W.S.N. Trimmer, "Integrated Fabrication of Polysilicon Mechanisms," *IEEE Transactions on Electron Devices*, vol. 35, no. 6, pp. 719–723, June 1988.

[30] In German: LIthographie, Galvanoformung, Abformung.

[31] A. Müller, J. Göttert and J. Mohr, "LIGA Microstructures on top of Micromachined Silicon Wafers Used to Fabricate a Micro-Optical Switch," *Journal of Micromechanics and Microengineering*, vol. 3, pp. 158–160, September 1993.

[32] V.M. Lubecke, W.R. McGrath, and D.B. Rutledge, "A 100 GHz Coplanar Strip Circuit Tuned With a Sliding Planar Backshort," *IEEE Microwave and Guided Wave Letters*, vol. 3, no. 12, pp. 441–443, December 1993.

[33] V.M. Lubecke, W.R. McGrath, and D.B. Rutledge, "A Micromechanical Tuning Element for a 620 GHz Circuit," *Nineteenth International Conference on Infrared and Millimeter Waves: Conference Digest*, pp. 431–432, October, 1994.

[34] V.M. Lubecke, W.R. McGrath, D.B. Rutledge "Millimeter Wave Performance of a Sliding Planar Backshort," *SPIE International Conference on Millimeter and Submillimeter Waves and Applications-Conference Digest*, pp. 543–544, January, 1994.

Chapter 2

Planar Tuning Elements

Circuits developed for use at centimeter to submillimeter wavelengths have long capitalized on the advantages of simple and cost-effective planar circuit technology. Essential to these circuits are planar transmission line structures such as microstrip, stripline, slotlines, and coplanar lines. Common to each of these, is the fact that their characteristics can be controlled by dimensions in a single plane. Impedance and propagation for these lines can be set by choosing the width of conductive strips, or slots, over a dielectric substrate. Fabrication of these lines, as well as various other circuit elements, can be accomplished through practical photolithographic techniques. This has made possible the cost-effective manufacture of fully integrated planar circuits for use at microwave, and higher, frequencies. Unfortunately, such circuits once fabricated, have electrical characteristics that are not easily adjusted. A mechanically adjustable tuning element which could be included in planar transmission lines, without sacrificing the benefits of photolithographic fabrication, would be highly advantageous.

2.1 Planar Circuits

Circuits for use at these high frequencies, typically route signals between key functional components using one or more types of planar transmission lines. Additionally, terminated lengths of planar line, called *stubs*, are themselves used as reactive elements [1]. Each key component has its own impedance, and the proper choice of transmission lines and stubs allows for the most efficient transfer of signal between them by making the necessary impedance transformations. Ideally,

knowledge of the operating impedance of each component allows for the use of a fixed circuit design to accomplish this matching of impedances. In practice, however, it is quite difficult to accurately characterize many components, particularly at high frequencies.

As a result, some post fabrication tuning in the form of circuit modification is usually required. This type of tuning is difficult and more tuning is required as the design frequency is increased. At millimeter and submillimeter wavelengths, typical planar circuits cannot be altered by any practical means, nor in any reversible manner. It is therefore desirable to incorporate into planar circuits impedance matching elements which can be adjusted after fabrication in order to relax the constraint of component characterization, and thus allow the circuit design to be extended to use at higher frequencies.

The same tuning issue is also encountered in circuits which use nonplanar transmission lines. In a waveguide circuit, such tuning is accomplished with a mechanically adjustable backshort which is inserted into the waveguide [2], [3]. This creates a waveguide tuning stub with an adjustable electrical length. This type of tuner can be used to determine impedance characteristics for a device, as well as to optimize the performance of a circuit. Of course waveguide circuits do not share the practical fabrication benefits of planar circuits. It would be desirable, however, to reproduce this sort of tuning element in a purely planar circuit. Thus, an analogous approach for a movable, noncontacting *planar backshort* which can be used to vary the electrical length of a planar transmission line tuning stub is examined here.

2.2 Coplanar Transmission lines

The term *coplanar line* is used to describe a transmission line in which all of the conductors are in the same plane. This makes the shunt or series interface, between such lines and planar components, a seamless transition across the surface

of a substrate. Additionally, since the electric and magnetic fields for such lines extend across the surface of the substrate, they can easily be electromagnetically coupled to other surface structures. This makes them suitable for integration with an adjustable, surface-mounted tuning element.

Two well suited coplanar transmission line structures are coplanar strips (CPS), and its dual, coplanar waveguide (CPW). The basic theory and design of these lines have been well documented [4], [5]. Additional theory, which extends the application of such lines to the terahertz frequency range, has also been reported in numerous articles which are widely scattered in the technical literature [6]–[12]. A summary of closed-form expressions which pertain to the development of the planar tuning element are presented here. The geometries for CPS and CPW are shown in Figure 2.1.

The dielectric constant for the substrate is ϵ_r and its thickness is h. The thickness of the conductors is t. For CPS, W is the width of each conductive strip and S is the spacing between them. For CPW, S is the width of the center conductor and W is the distance from the ground plane on either side.

It is useful to define the parameter k as

$$k = \frac{S}{S + 2W} . \tag{2.1}$$

Results from a quasi-static numerical analysis have been fitted to provide an expression for the effective dielectric constant for either type of line [4]:

$$\begin{aligned} \epsilon_{re} = {} & \frac{\epsilon_r + 1}{2} \tanh\left[0.785 \log\left(\frac{h}{W}\right) + 1.75\right] + \cdots \\ & + k\frac{W}{h}\left[0.04 - 0.7k + 0.01(1 - 0.1\epsilon_r)(0.25 + k)\right] . \end{aligned} \tag{2.2}$$

This holds for thin conductors, where $\frac{t}{W} \leq 0.16$. This is typically the case for the high frequency integrated circuits of interest. Modifications exist [4], [5] for other

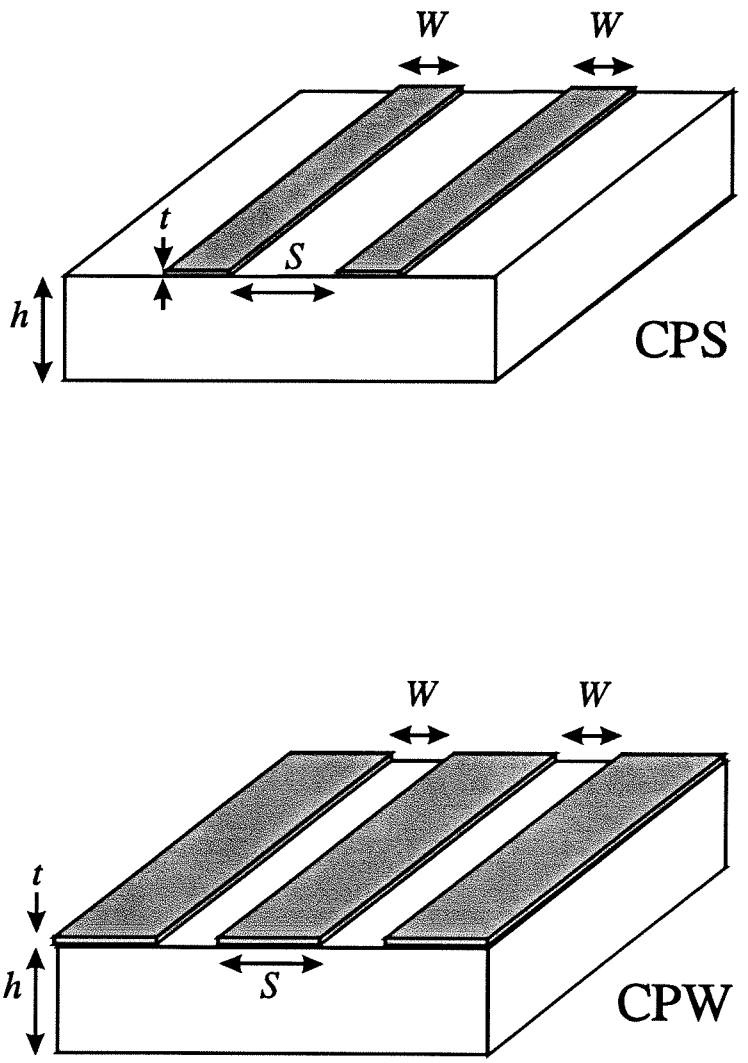

Figure 2.1 Geometries for Coplanar Strip (CPS) (a), and Coplanar Waveguide (CPW) (b) transmission lines.

cases.

Approaching the terahertz frequency range, dispersion can have a significant effect, particularly when the substrate is thin. An analytical approximation has been derived by Hasnain *et al.* [6], by fitting data from a numerical simulation to an empirical formula. It provides a useful modification which makes the previous quasi-static expression frequency-dependent, becoming

$$\epsilon_{re}(f) = \left(\sqrt{\epsilon_{re}} + \frac{\sqrt{\epsilon_r} - \sqrt{\epsilon_{re}}}{1 + a\left(\frac{f}{f_{TE}}\right)^{-b}} \right)^2 \tag{2.3}$$

where the f is the frequency, $f_{TE} = 4\sqrt{\epsilon_{re} - 1}/h$ is the cut-off frequency for the lowest order TE mode, $b \approx 1.8$ is a computed constant, and $a \approx 10^{u \log\left(\frac{S}{W}\right)+v}$ is a constant computed from the conductor dimensions. The additional constants

$$u \approx 0.54 - 0.64 \log\left(S/h\right) + 0.015 \log^2\left(S/h\right),$$

and

$$v \approx 0.43 - 0.86 \log\left(S/h\right) + 0.540 \log^2\left(S/h\right),$$

depend on the substrate thickness.

The characteristic impedance for each line is given by the application of $\epsilon_{re}(f)$ to quasi-static solutions. For CPS this becomes

$$Z_0^{cps} = \frac{120\pi}{\sqrt{\epsilon_{re}(f)}} \frac{K(k)}{K'(k)} \quad \Omega \tag{2.4}$$

and for CPW

$$Z_0^{cpw} = \frac{120\pi}{\sqrt{\epsilon_{re}(f)}} \frac{K'(k)}{4K(k)} \quad \Omega \tag{2.5}$$

where $K(\xi) = \displaystyle\int_0^{\pi/2} \frac{d\phi}{\sqrt{1 - \xi^2 \sin^2 \phi}}$ is the complete elliptic integral of the first kind, and $K'(\xi) = K(\sqrt{1 - \xi^2})$ [12].

The guide-wavelength can be written as

$$\lambda_g = \frac{c}{f\sqrt{\epsilon_{re}(f)}}\,. \tag{2.6}$$

Losses to the conductors, the dielectric, and radiation are accounted for in the form of attenuation constants. The attenuation constant describing ohmic losses to the conductor [4] for CPS is

$$\alpha_c^{cps} = 2.00\frac{R_s}{Z_0^{cps}}\frac{P'}{\pi S}\Big(1+\frac{W}{S}\Big)\frac{\dfrac{1.25}{\pi}\ln\dfrac{4\pi W}{t}+1+\dfrac{1.25t}{\pi W}}{\Big[1+2\dfrac{W}{S}+\dfrac{1.25t}{\pi S}\Big(1+\ln\dfrac{4\pi W}{t}\Big)\Big]^2} \tag{2.7}$$

and for CPW is

$$\alpha_c^{cpw} = 5.61\times10^{-5}R_s\epsilon_{re}(f)Z_0^{cpw}\frac{P'}{\pi W}\Big(1+\frac{S}{W}\Big)\frac{\dfrac{1.25}{\pi}\ln\dfrac{4\pi S}{t}+1+\dfrac{1.25t}{\pi S}}{\Big[2+\dfrac{S}{W}+\dfrac{1.25t}{\pi W}\Big(1+\ln\dfrac{4\pi S}{t}\Big)\Big]^2} \tag{2.8}$$

both in nepers per unit length, where R_s is the surface resistivity for the conductors. For the case where $0 \le k \le 0.707$

$$P' = \frac{k}{(1-\sqrt{1-k^2})(1-k^2)^{3/4}}\Big(\frac{K(k)}{K'(k)}\Big)^2 \tag{2.9a}$$

and when $0.707 \le k \le 1.0$

$$P' = \frac{1}{(1-k)\sqrt{k}}\,. \tag{2.9b}$$

For both CPS and CPW, the attenuation constant due to dielectric loss [4] is

$$\alpha_d = 3.14\frac{\epsilon_r}{\sqrt{\epsilon_{re}(f)}}\frac{\epsilon_{re}(f)-1}{\epsilon_r-1}\frac{\tan\delta_{loss}}{(c/f)} \tag{2.10}$$

in nepers per unit length, where $\tan\delta_{loss}$ is the loss tangent for the dielectric. The accuracy of the dielectric loss model has not been well established for coplanar lines. However, this model should be sufficient in this case since it is anticipated that dielectric loss will be the least significant loss mechanism.

These transmission lines also have some loss due to radiation into the dielectric substrate. The radiation occurs because the guided signal travels with a velocity which is greater than that for electromagnetic propagation within the dielectric. Thus, the guided signal loses energy through an electromagnetic shock-wave which is emitted into the substrate [7]. According to Frankel *et al.* [6], the radiative attenuation constant for CPS can be calculated as

$$\alpha_r^{cps} = \pi^5 \frac{(3-\sqrt{8})}{2} \sqrt{\frac{\epsilon_{re}(f)}{\epsilon_r}} \left(1 - \frac{\epsilon_{re}(f)}{\epsilon_r}\right)^2 \frac{(S+2W)^2 \epsilon_r^{3/2}}{c^3 K'(k) K(k)} f^3, \tag{2.11}$$

and for CPW,

$$\alpha_r^{cpw} = \left(\frac{\pi}{2}\right)^5 2 \frac{\left(1 - \frac{\epsilon_{re}(f)}{\epsilon_r}\right)^2}{\sqrt{\frac{\epsilon_{re}(f)}{\epsilon_r}}} \frac{(S+2W)^2 \epsilon_r^{3/2}}{c^3 K'(k) K(k)} f^3, \tag{2.12}$$

both in nepers per unit length. To obtain these attenuation constants in units of dB/λ_g, multiply the corresponding expression by $8.686\lambda_g$. The total loss for either line can be expressed as a sum of these three attenuation constants:

$$\alpha = \alpha_c + \alpha_d + \alpha_r \,. \tag{2.13}$$

2.3 The Sliding Planar Backshort

At high frequencies, it is difficult to form a movable short-circuit across a planar transmission line through ohmic contact. However, a similar effect can be

attained over a specific bandwidth, without ohmic-contact. By simply placing a solid metallic plate across one of these coplanar transmission lines, with a thin dielectric layer in between, a section of lower-impedance transmission line can be formed. The impedance discontinuity at the leading edge of the plate would result in the partial reflection of any incident signal being guided along the coplanar line. If instead of a solid metal plate, a judiciously chosen metal pattern were used, this reflection could be greatly increased and made to function over a well defined and broad bandwidth. An optimal metal pattern would create an impedance which was low enough to act as movable short-circuit over this bandwidth; this planar element would act as a backshort on a planar transmission line, which could slide to vary the electrical length of the line. Furthermore, the *sliding planar backshort* (SPB) [14]-[18] could be designed in such a way that it could be fabricated photolithographically along with the rest of the planar circuit.

The key to optimizing the effect of this element lies in the coherent combining of reflections caused by multiple sub-elements. This type of approach is commonly and successfully used to create fixed terminations, or bandstop filters, in circuits for use at microwave through optical frequencies [19], [20]. Ideally, the metal pattern of the SPB covers the coplanar line for a distance of one quarter-wavelength of the desired working frequency, creating a section of lower-impedance line. The pattern then opens up to restore the original higher-impedance line for a distance of one quarter-wavelength. This can be repeated several times to create several impedance discontinuities, which together have a cumulative effect equivalent to one very large impedance discontinuity at the leading edge of the first section. In this simple model, illustrated in Figure 2, the impedance at the edge of an SPB with n sections would be

$$Z = \left(\frac{Z_{low}}{Z_{high}}\right)^{n} Z_{low} \tag{2.14}$$

where Z_{low} is the impedance of the sections of line covered by the metal pattern,

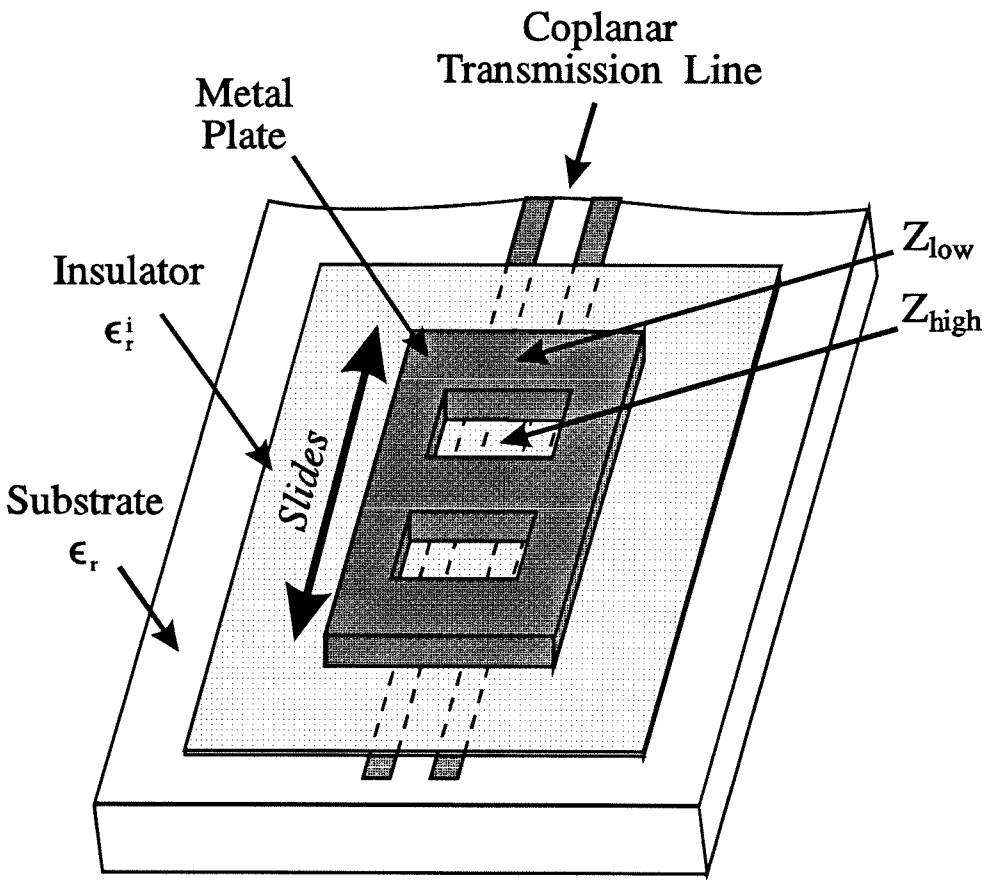

Figure 2.2 Conceptual diagram of the Sliding Planar Backshort (SPB) shown on CPS transmission line.

and Z_{high} is the characteristic impedance of the line were it is left uncovered. In this equation it is evident that with a large number of sections, Z can be made much lower than the Z_{low} created by a single covered section.

In a real circuit, only a few sections can be used before losses in the line render additional sections ineffective. For this reason, it is important that the covered sections have as low an impedance as possible.

When used on CPS line, the impedance for the sections covered by the metal pattern can be determined with an approximate model. Each covered strip, looks like a parallel-plate transmission line, with the thin dielectric coating acting as its substrate. Twice this impedance would be seen across the two differential strips. The approximate impedance at the transition can be found using

$$Z_{low}^{cps} \approx 2\frac{120\pi}{\sqrt{\epsilon_r^i}}\frac{h^i}{W} \quad \Omega \tag{2.15}$$

where ϵ_r^i is the dielectric constant of the thin dielectric coating, and h^i is its thickness. Clearly it is important to keep the dielectric coating thin, and the metal pattern as flat as possible.

Similarly for the covered region of a CPW, the covered center conductor appears as a parallel-plate transmission line. It appears in series with the parallel combination of the two parallel-plate transmission lines formed by the covered groundplanes. Taking the impedance caused by the covered center conductor as the dominant impedance, the approximate impedance at the transition is

$$Z_{low}^{cpw} \approx \frac{120\pi}{\sqrt{\epsilon_r^i}}\frac{h^i}{w} \quad \Omega \tag{2.16}$$

which is about half the impedance on CPS.

Ohmic and dielectric losses for these covered sections would be of the same order of magnitude as those for the parallel-plate analogies. Radiation loss does not

apply to this structure as the fields are mainly confined between two conducting plates.

These assumptions and formulas are simplified approximations which are useful in the design of an effective SPB. In a real circuit, the fields are not restricted to the modes which have been considered and the structures cannot be created precisely as described. These ideal relationships can, however, provide a starting point for the selection of appropriate materials and dimensions, and these can be refined through the use of a frequency-scaled model or computer based field-simulations.

References

[1] R.E. Collin, *Foundations for microwave engineering*, New York, NY: McGraw-Hill, 1966.

[2] A.R. Kerr, "An Adjustable Short-Circuit for Millimeter Waveguides," *Electronics Division Internal Report No. 280, NRAO*, July 1990.

[3] W.R. McGrath, T.M. Weller, and L.P.B. Katehi, "A Novel Noncontacting Waveguide Backshort for Submillimeter-wave Frequencies," *International Journal of Infrared and Millimeter Waves*, vol. 16, no. 1, pp. 237–256, January 1995.

[4] K.C. Gupta, R. Garg, and I.J. Bahl, *Microstrip Lines and Slotlines*, Dedham, MA: Artech House, 1979.

[5] R.K. Hoffman, *Handbook of Microwave Integrated Circuits*, Norwood, MA: Artech House, 1987. Translation form the German *Integrierte Mikrowellenschaltingen*, Heidelberg, Germany: Spinger-Verlag, 1983.

[6] G. Hasnain, A. Dienes, and J.R. Whinnery, "Dispersion of Picosecond Pulses in Coplanar Transmission Lines," *IEEE Transactions on Microwave Theory and Techniques*, vol. 34, no. 6, pp. 738–741, June 1986.

[7] D. Grischkowsky, I.N. Duling III, J.C. Chen, and C.-C. Chi, "Electromagnetic Shock Waves from Transmission Lines," *Phys. Rev. Lett.*, vol. 59, no. 15, pp. 1663–1666, October 12, 1987.

[8] M.Y. Frankel, S. Gupta, J.A. Valdmanis, and G.M. Mourou, "Terahertz Attenuation and Dispersion Characteristics of Coplanar Transmission Lines," *IEEE Transactions on Microwave Theory and Techniques*, vol. 39, no. 6, pp. 910–916, June 1991.

[9] D.B Rutledge, D. P. Neikirk, and D.P. Kasilingham, in *Infrared and Millimeter Waves: Millimeter Components and Techniques , Part II, Volume 10*, K.J. Button, Ed., New York, NY: Academic Press, Inc., 1983.

[10] D.S. Phatak and A.P. Defonzo, "Dispersion Characteristics of Optically Excited Coplanar Striplines: Pulse Propagation," *IEEE Transactions on Microwave Theory and Techniques*, vol. 38, no. 5, pp. 654–661, May 1990.

[11] U.D. Keil, D.R. Dykaar, A.F.J. Levi, R.F. Kopf, L.N. Pfeiffer, S.B. Darack, and K.W. West., "High-Speed Coplanar Transmission Lines," *IEEE Journal of Quantum Electronics*, vol. 28, no. 10, pp. 2333–2342, October 1992.

[12] J.F. Whitaker, R Sobolewski, D.R. Dykaar, T.Y. Hsiang, and G.A. Mourou, "Propagation Model for Ultrafast Signals on Superconducting Dispersive Striplines," *IEEE Transactions on Microwave Theory and Techniques*, vol. 36, no. 2, pp. 277–285, February 1988.

[13] M. Abamowitz and I.A. Stegun, *Handbook of Mathematical Functions*, New York, NY: Dover Publications, Inc, 1965.

[14] V.M. Lubecke and W.R McGrath, "Tuners for Coplanar-Strip Transmission Lines," *NASA Tech Brief Magazine*, submitted September 1990.

[15] V.M. Lubecke, W.R. McGrath, and D.B. Rutledge, "Sliding Backshorts for Planar Circuits," *International Journal of Infrared and Millimeter Waves*, vol. 12, no. 12, pp. 1387–1397, December 1991.

[16] V.M. Lubecke, W.R. McGrath, and D.B. Rutledge, "An Adjustable RF Tuning Element for Microwave, Millimeter Wave, and Submillimeter Wave Integrated Circuits," *Proceedings of the NASA Technology 2001 Conference*, vol. 2, no. 3136, pp. 239–245, December 1991.

[17] W.R. McGrath, V.M. Lubecke, and D.B. Rutledge, "Adjustable RF Tuning Elements for Planar Millimeter Wave and Submillimeter Wave Circuits," *Fifteenth International Conference on Infrared and Millimeter Waves: Conference Digest*, pp. 344–346, December 1990.

[18] W.R. McGrath and V. M. Lubecke, "RF Tuning Element," *U.S. patent no. 5,115,217*, granted May 19, 1992.

[19] G.L. Matthaei, L. Young, E.M.T. Jones, *Microwave Filters, Impedance Matching Networks, and Coupling Structures*, New York, NY: Mcgraw-Hill, 1964.

[20] M. Born and E. Wolf, *Principles of Optics*, Oxford, England: Pergamon Press Ltd., 1959.

Chapter 3

Microwave Modeling

Much of the analysis presented for SPB structures has assumed TEM and quasi-TEM propagation conditions within the sections, and ideal coupling in the transitions between them. This is a useful starting point for choosing a structure for the SPB, but its optimization must include consideration for additional modes and forms of coupling. An empirical approach to optimization was applied here.

A microwave implementation was used to develop and demonstrate the SPB [1]-[5]. The process involved the use of copper tape to form various transmission line patterns on thick dielectric substrates, planar-to-coaxial transitions to allow measurements with a network analyzer, and the evaluation of the behavior of various dielectric sheets, metal plates, and other structures in the device. The process was used both to demonstrate that such a tuning element can work, and to provide a vehicle for optimizing its physical parameters for electrical performance and mechanical scaling.

3.1 Empirical Design

Several approaches were considered. A promising configuration consisted of a movable planar structure over CPS transmission line, like the one outlined in Chapter 2. Coplanar strips can be easily integrated with common printed-circuit antennas such as dipoles and bowties, and a completely planar mechanical element promised straight-forward scaling to higher frequencies.

A large scale model of this SPB was built and the magnitude of its reflection

coefficient was measured with an HP 8510B network analyzer, over a frequency range of 50 MHz to 5 GHz. The measurement required a transition between the coaxial input of the network analyzer, and the coplanar transmission line. Unfortunately, no standard transition with low VSWR is readily available. For this reason, several measurement techniques were devised in order to obtain reliable results.

A natural choice of calibration technique for an HP8510B is the *Thru-Reflect-Line* method which allows for measurements in nonstandard transmission media such as coplanar line [6]. The transition between coaxial and coplanar line can, in principle, be accounted for in the calibration procedure. However, reproducible calibration standards in coplanar line are required. In practice, reflections at connections between segments of coplanar line and uncertainties in the reflection standard used, lead to nonrepeatable results and unacceptable errors. As a result, this method was not pursued further.

A second technique, a simple one-port measurement of a circuit which employs a direct connection between coaxial and coplanar lines, was investigated. This measurement of $|s_{11}|$ was made over a 1.5 GHz to 2.5 GHz frequency range. Figure 3.1 shows the test arrangement. The abrupt transition from coaxial line to coplanar line was formed at the edge of the Stycast® [7] substrate with a flange mount SMA connector. The measurement was recorded with the reference plane of the backshort adjusted to coincide with the SMA connector. The line was terminated in an open-circuit, covered by a layer of Eccosorb®LS [7] microwave absorber.

While this transition resulted in large unwanted reflections (which increased the uncertainty of the measurement), the technique was useful because it allowed the reflection coefficient for the SPB to be directly monitored as its dimensions were varied. The performance of the SPB was then optimized by systematically varying the length of the low- and high-impedance sections, the number of sections,

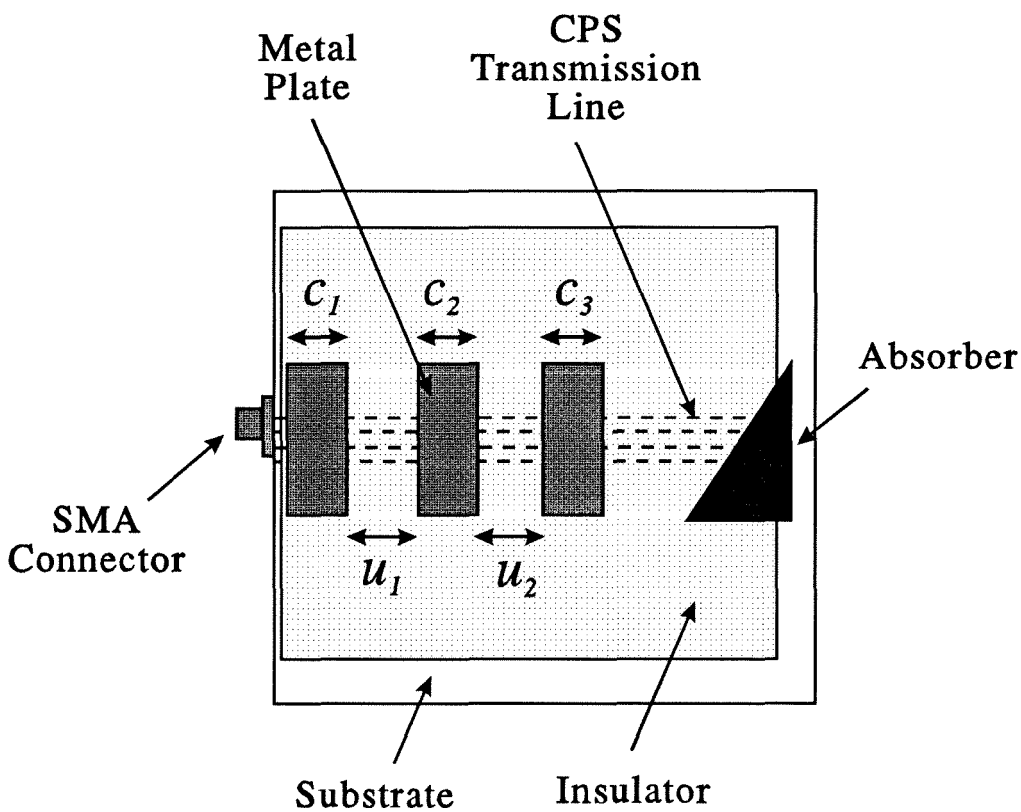

Figure 3.1 Circuit used for optimizing the SPB. The dimensions of the metal plates, transmission lines, and various insulators were varied to optimize the performance of the structure as a backshort.

the dimensions of the transmission line, and the thickness of the insulator in order to achieve the largest reflection of RF power.

Good performance over a useful bandwidth was obtained for a coplanar transmission line with 2.1 mm wide copper strips, separated by a 5.2 mm gap and mounted on a 6 mm thick Stycast®substrate with a dielectric constant of $\epsilon_{re} = 4$. From Equations 2.4 and 2.2, the characteristic impedance and effective dielectric constant of this transmission line were determined to be 203 Ω, and 2.4, respectively. A 25 μm thick sheet of Mylar ($\epsilon_r^i \approx 2.9$) was used to insulate the transmission line from the sliding plate. Using Equation 2.14, the impedance of the covered sections was determined to be approximately 5 Ω. This noncontacting, 76 mm-wide, 6 mm-thick aluminum plate contained two rectangular holes with dimensions and spacing of $c_1 = 24.3$ mm, $u_1 = 19.4$ mm, $c_2 = 24.0$ mm, $u_2 = 23.0$ mm, and $c_3 = 24.4$ mm. This resulted in uncovered high impedance sections, u_1 and u_2, and covered low impedance sections, c_1, c_2 and c_3, which were each approximately $\lambda_g/4$ long on the coplanar line.

A plot of $|s_{11}|$ versus frequency is shown in Figure 3.2. This optimized planar backshort produced an $|s_{11}|$ better than –0.3 dB over a 20% bandwidth. That is, a reflection of more than 90% of the power in the incident wave. The center frequency was measured to be 2 GHz, which agrees exactly with the design frequency.

This direct-connection measurement technique was useful for evaluating the effects of potential tuning element configurations. Various transmission line, dielectric layer, and SPB configurations were examined in this way. Other distinct circuit arrangements included a 3-strip transmission line, and one in which SPB elements which were extended into a groove between two coplanar strips. It appeared that a fully planar SPB on CPS would be a promising configuration to pursue.

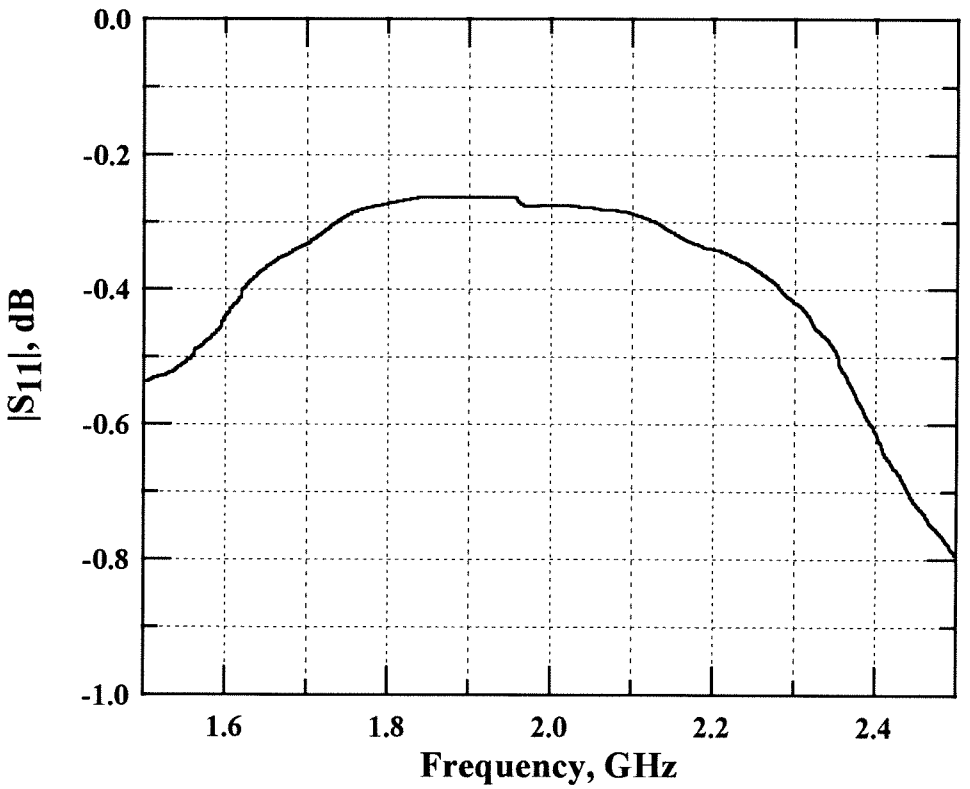

Figure 3.2 Performance of optimized SPB. The reflection coefficient, $|s_{11}|$, is better than –0.3 dB over a 20% bandwidth.

3.2 Variations and Other Measurements

It was apparent that the proximity of the front edge of the sliding metallic plate to the physical transition at the SMA connector in the direct-measurement scheme would introduce some undesirable electromagnetic coupling between them. The error caused by this unwanted interference, along with the lack of a transmission measurement, motivated the design of a third measurement technique.

The system used for this technique is shown in Figure 3.3. Here, the 204 Ω coplanar line was connected to the 50 Ω network analyzer inputs by means of two baluns of identical length. These baluns were made by gradually trimming the shield and teflon insulation from a semirigid, 3.5 mm wide coaxial line over a distance of approximately one wavelength at 2 GHz. This created a smoother transition to the coplanar line which minimized the power reflected at the connection. The return loss for these baluns was measured at approximately –10 dB and the remaining undesired reflections from these transitions were gated out of the measurement using the *low-pass* time domain mode of the network analyzer. The measurement frequency was swept from 50 MHz to 20 GHz so that an accurate transformation between frequency and time could be made using the low-pass mode of the network analyzer.

The full two-port scattering parameters for the system were measured under three different conditions. First, a reference measurement was made which corresponded to an ideal short. The baluns were identical in length and hence, the test model was symmetric about the midpoint of the coplanar line. Thus, the magnitude of the transmission measurement of this circuit with no short in place is equal to the reflection measurement with an ideal short at the midpoint. Reflection measurements for the SPB were then made with the metal plate arranged to reflect an incident wave from Port 1 at the midpoint of the system and then, Port 2. The values obtained for $|s_{11}|$ from the first reflection measurement, and for $|s_{22}|$ from the second, were normalized by dividing each by the values for $|s_{21}|$ and

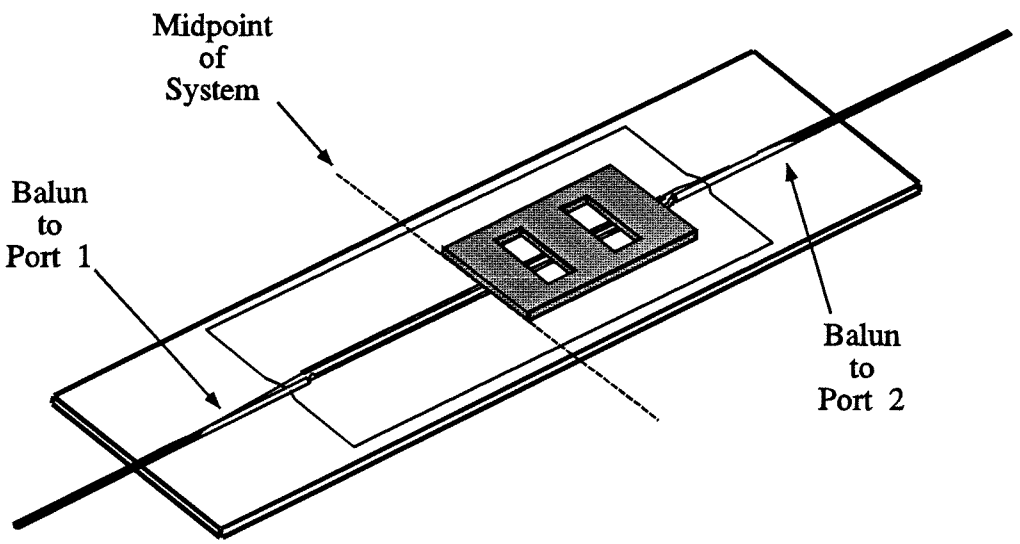

Figure 3.3 Circuit used to measure two-port scattering parameters for the SPB. The baluns create a gradual transition between coaxial and coplanar line, which reduces measurement uncertainty due to unwanted reflections at the transition.

$|s_{12}|$ from the reference measurement. The two results were averaged to cancel the effect of any asymmetry in the system. Transmission measurements for the SPB were similarly normalized and averaged. The requirement of processing the measured data, along with the large frequency scan, prohibited the direct monitoring of the 2 GHz reflection coefficient during this measurement.

The results for the averaged, normalized $|s_{11}|$ and $|s_{21}|$ are shown in Figure 3.4. The plot shows that $|s_{11}|$ was better than –0.5 dB over approximately an 80% bandwidth and the center frequency was slightly higher than 2 GHz. Over the frequency range between 1.5 GHz and 2.5 GHz, $|s_{11}|$ is better than –0.3 dB over a 16% bandwidth and the center frequency is slightly lower than 2 GHz. This agrees well with the previous results shown in Figure 3.2.

The rippled-peak characteristic seen in the averaged result for $|s_{11}|$ also appeared in individual measurements for this circuit, and is assumed to be an artifact of the gating technique employed. The time-domain response for the SPB could not be completely isolated from the response for the transmission line transitions. Thus, it was not possible to completely gate out the transition response while completely preserving the SPB response. This artifact also appears in a similar measurement for the same SPB on 90 Ω CPS, shown in Figure 3.5. These strips were 12.7 mm wide and spaced 1.3 mm apart, and the measured $|s_{11}|$ was better than 1 dB over a 100% bandwidth.

A measurement comparing the performance of the metal plate SPB to that of a one inch thick block of Stycast®backed by similarly patterned copper tape, was also made using this technique and yielded almost identical results for both.

The same measurement technique was also used to test the performance of the optimized metal plate SPB on a CPW transmission line. In this case no balun was necessary, so an SMA connector was soldered directly to a quarter-wave matching section of CPW on each end of the circuit. Beyond the matching section, the width of the gaps in the line was opened up to 2.1 mm, with a 5.2 mm-wide

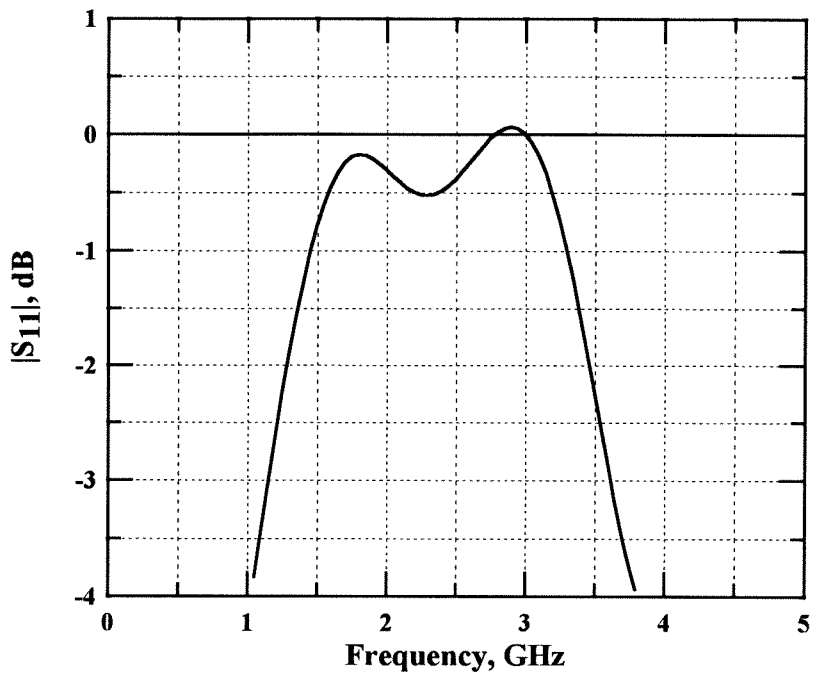

(a)

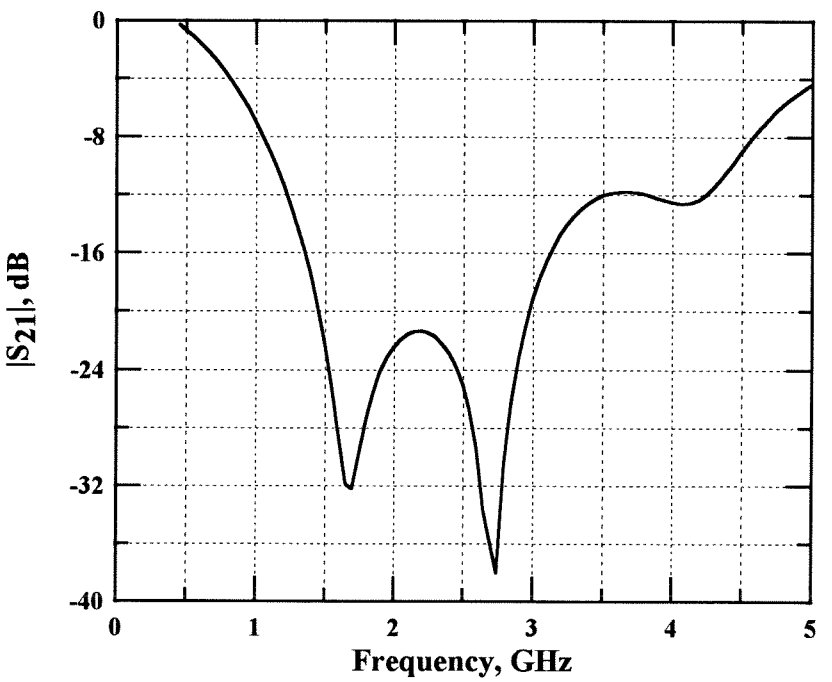

(b)

Figure 3.4 Plot of reflection coefficient (a) and transmission coefficient (b) for SPB on 203 Ω CPS line, using baluns for transmission line transitions.

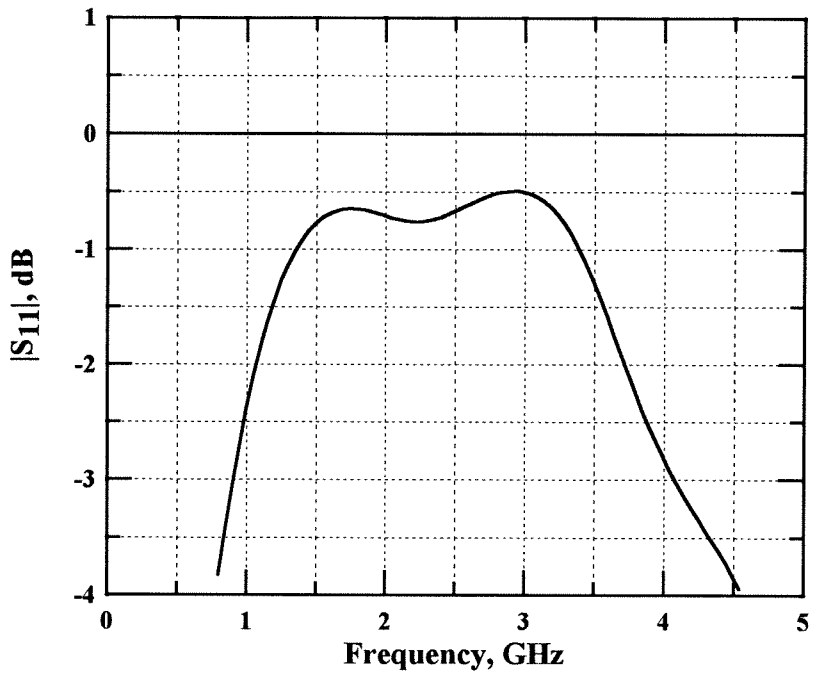

(a)

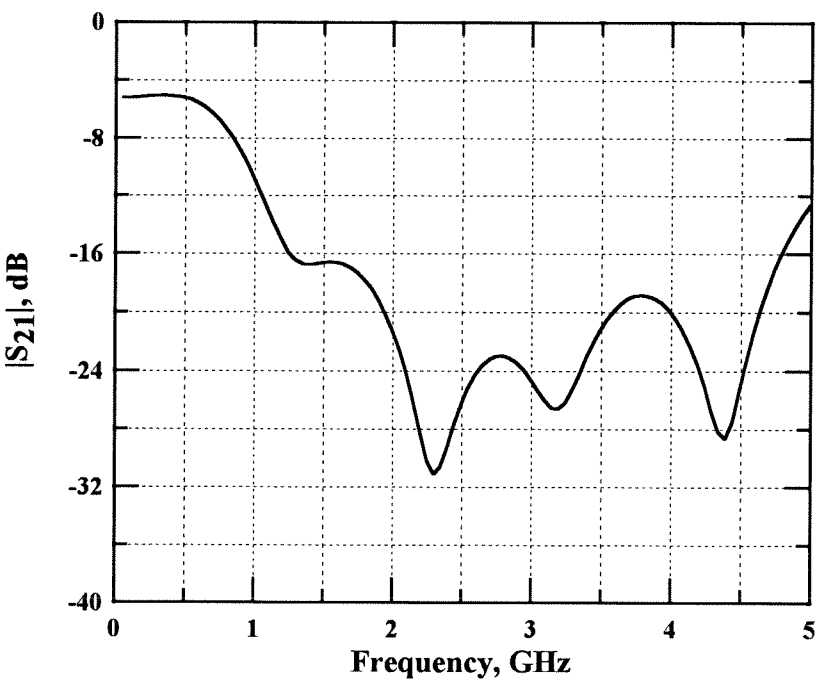

(b)

Figure 3.5 Plot of reflection coefficient (a) and transmission coefficient (b) for SPB on 90 Ω CPS line, using baluns for transmission line transitions.

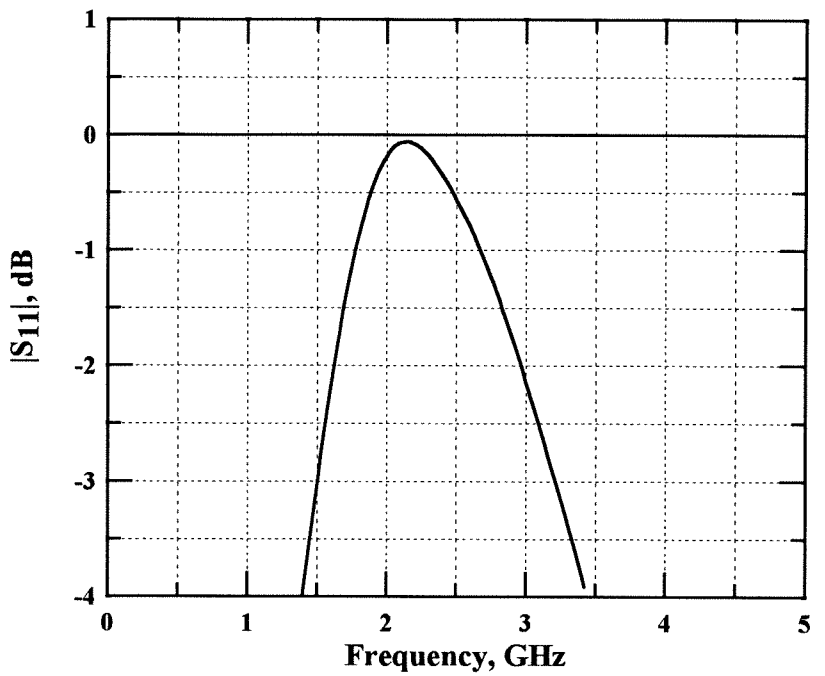

(a)

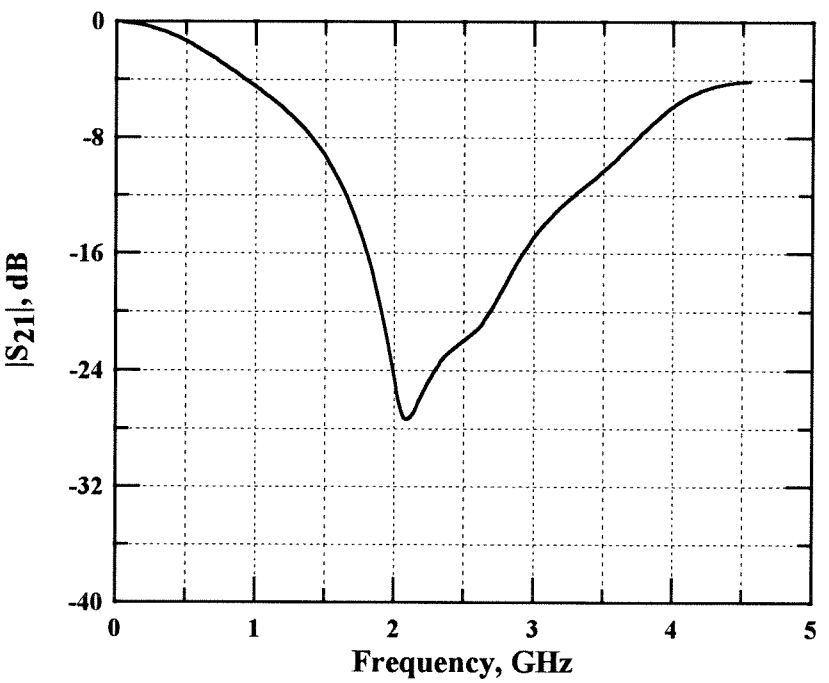

(b)

Figure 3.6 Plot of reflection coefficient (a) and transmission coefficient (b) for SPB on 78 Ω CPW line, using baluns for transmission line transitions.

center conductor. This is the physical compliment of the previously tested CPS circuit. The impedance was calculated as 78 Ω, using Equation 2.5. Both $|s_{11}|$ and $|s_{21}|$ were measured for this circuit and are shown in Figure 3.6. The peak return loss was $|s_{11}| = -0.02$ dB at 2.1 GHz, and $|s_{11}|$ was less than (0.5 dB) over a (50%) bandwidth. The time-domain response for the SPB on CPW was more easily isolated when gating than it was on CPS. This response does not show any rippled-peak characteristics.

3.3 Circuit Application

As an example of the tuning range accessible using SPB's in a planar circuit, a double shunt-stub tuner which incorporates two SPB's on CPS transmission lines was built [8]. Figure 3.7 shows both the equivalent circuit and the circuit arrangement as measured. The characteristic impedance of the coplanar line was 90 Ω and the stub spacing was $\lambda_g/8$. A 90 Ω resistor was used to simulate the impedance of a planar antenna and a 3.5 mm-wide semirigid coaxial probe was used to measure the range of impedances to which the antenna resistance could be transformed. The calibration reference plane for this measurement was set at the end of the shield for the coaxial probe. The same measurement was also performed using a 203 Ω CPS transmission line circuit, and agreed with theory.

Figure 3.8 is a Smith chart, normalized to the characteristic impedance of the line, which shows the accessible impedance region at 2 GHz. The overlap for the tuning region and the impedance region necessary for matching SIS devices implies that a circuit of this type would be useful for such matching applications. Variations in the shape of this tuning region can be achieved by changing the spacing between the tuning stubs. The solid and dashed boundary lines in Figure 3.8 show a comparison between the measured impedance range of the double stub tuner and a computer simulation of the circuit using *Puff* [9], respectively. The simulation agrees well with the measured data. The reflection coefficient of the shorting element used in the computer model was adjusted to fit the simulation

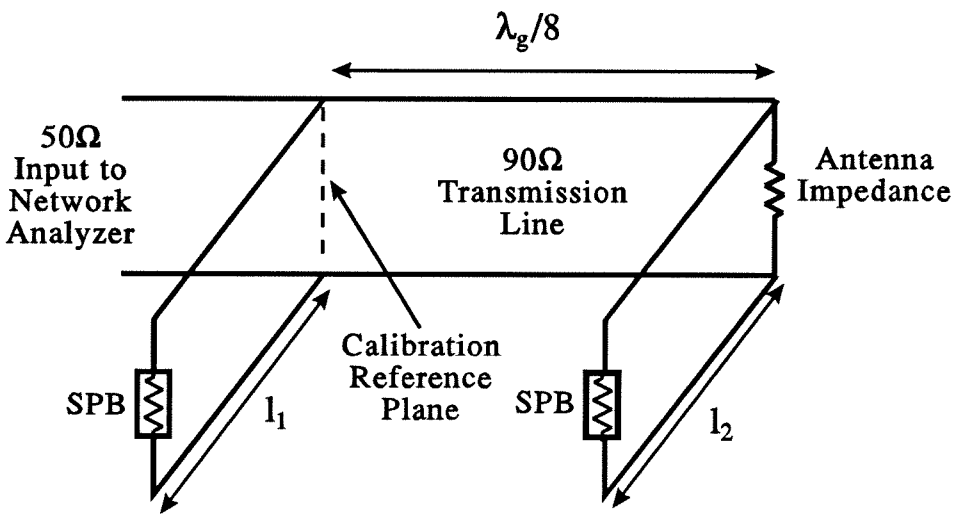

(a)

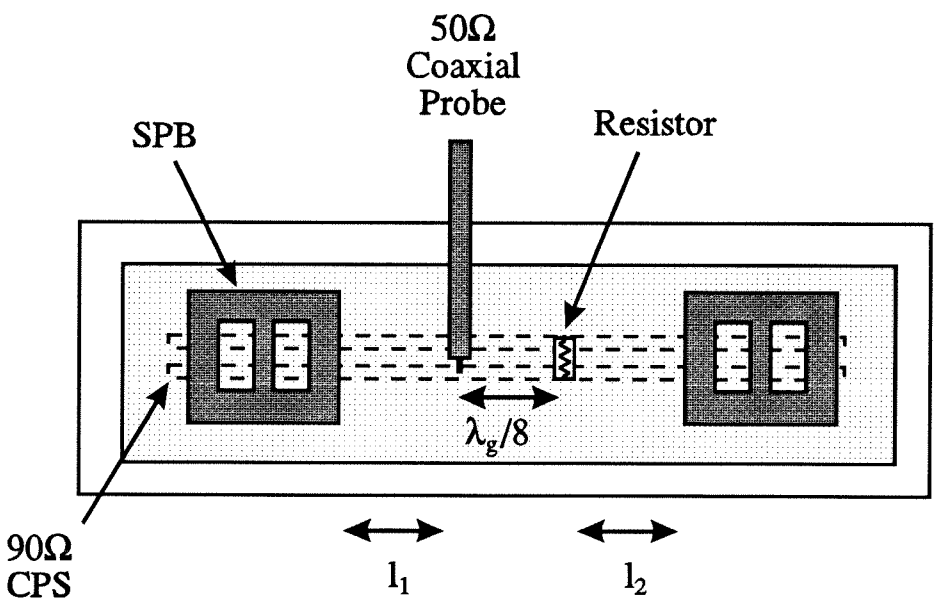

(b)

Figure 3.7 Schematic diagram for equivalent double-shunt stub tuner circuit (a) and circuit arrangement used for measurements (b).

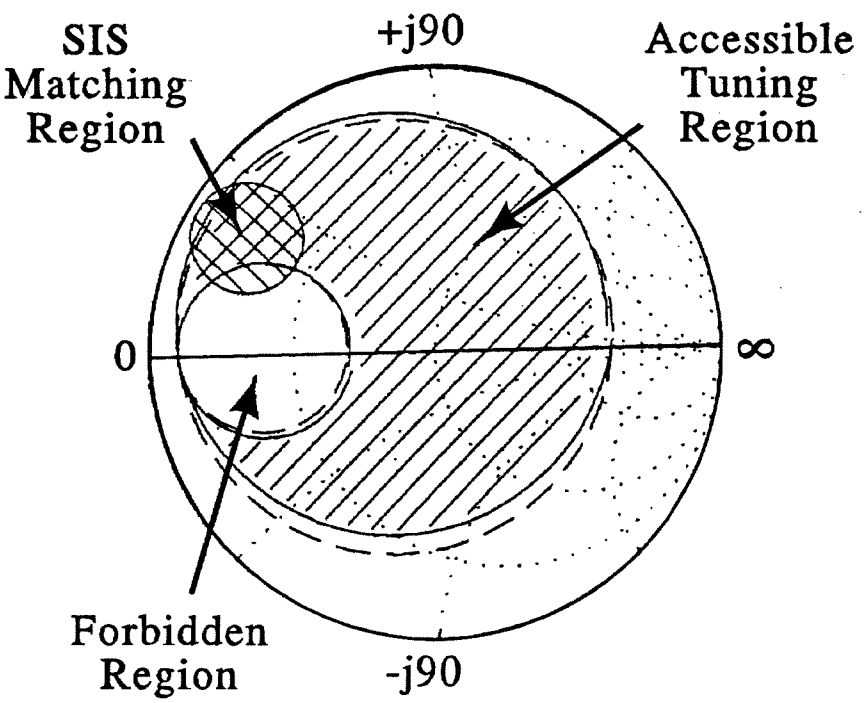

Figure 3.8 Smith chart showing measured (solid boundary) and fitted (dashed boundary) tuning region for double shunt-stub tuning circuit. The available tuning region covers the impedance region needed for matching to an SIS device.

to the measured Smith chart data. The resulting fitted $|s_{11}|$ for the backshort was –1.0 dB, which is similar to the –0.7 dB result that was measured for the same backshort alone on a 90 Ω transmission line at 2 GHz. A phase shift of 4° was also fitted at the coaxial probe transition in order to account for the calibration reference plane uncertainty.

The SPB developed in this chapter was shown to act as an effective backshort on a variety of coplanar transmission lines. Both a solid metal plate version, and a metal pattern on a superstrate were evaluated at 2 GHz, and found to be equally effective. The structures are suitable for scaling to millimeter and submillimeter wavelengths, where they can be fabricated using integrated circuit photolithographic techniques [10]-[12].

References

[1] V.M. Lubecke and W.R McGrath, "Tuners for Coplanar-Strip Transmission Lines," *NASA Tech Brief Magazine*, submitted September 1990.

[2] V.M. Lubecke, W.R. McGrath, and D.B. Rutledge, "Sliding Backshorts for Planar Circuits," *International Journal of Infrared and Millimeter Waves*, vol. 12, no. 12, pp. 1387–1397, December 1991.

[3] V.M. Lubecke, W.R. McGrath, and D.B. Rutledge, "An Adjustable RF Tuning Element for Microwave, Millimeter Wave, and Submillimeter Wave Integrated Circuits," *Proceedings of the NASA Technology 2001 Conference*, vol. 2, no. 3136, pp. 239–245, December 1991.

[4] W.R. McGrath, V.M. Lubecke, and D.B. Rutledge, "Adjustable RF Tuning Elements for Planar Millimeter Wave and Submillimeter Wave Circuits," *Fifteenth International Conference on Infrared and Millimeter Waves: Conference Digest*, pp. 344–346, December 1990.

[5] W.R. McGrath and V. M. Lubecke, "RF Tuning Element," *U.S. patent no. 5,115,217*, granted May 19, 1992.

[6] G.F. Engen and C.A. Hoer, "Thru-Reflect-Line: An Improved Technique for Calibrating the Dual Six-Port Automatic Network Analyzer," *IEEE Transactions on Microwave Theory and Techniques*, vol. 27, no. 12, pp. 987–993, December 1979.

[7] Registered trademark of *W.R Grace & Co.*, Canton, MA, USA.

[8] R.E. Collin, *Foundations for microwave engineering*, New York, NY: McGraw-Hill, 1966.

[9] S.W. Wedge, R. Compton, D. Rutledge, *Puff: Computer Aided Design for Microwave Integrated Circuits*, Pasadena, CA: California Institute of Technology, 1991.

[10] V.M. Lubecke, W.R. McGrath, and D.B. Rutledge, "A 100 GHz Coplanar Strip Circuit Tuned with a Sliding Planar Backshort," *IEEE Microwave and Guided Wave Letters*, vol. 3, no. 12, pp. 441–443, December 1993.

[11] V.M. Lubecke, W.R. McGrath, and D.B. Rutledge, "A Micromechanical Tuning Element for a 620 GHz Circuit," *Nineteenth International Conference on Infrared and Millimeter Waves: Conference Digest*, pp. 431–432, October 1994.

Chapter 4

Implementation of SPB's at Millimeter Wavelengths

Over the past two decades, waveguide circuits have been used to make sensitive measurements in the millimeter wave spectrum. Though this technology is well developed, fabrication remains a difficult and costly procedure. There is a growing interest in alternative technologies which are better suited for focal plane array applications, and offer improved mechanical integrity for air and space borne applications.

An attractive option is the use of planar devices in integrated planar mixers. Planar technology promises reliability and simplicity of fabrication. The planar structure of the SIS junction for example, makes it highly suitable for integration with planar antenna structures and substrate lenses, thus entirely eliminating the need for complex waveguide mounts. Great progress has also been made in the development of planar Schottky diodes, and in their application. The main circuit challenge for the use of these devices is to overcome the parasitic reactances inherent in their physical structures. In waveguide circuits this is accomplished with mechanically adjustable tuners. Planar circuits have thus far been limited to fixed tuning elements, resulting in a greater need for accurate device and circuit characterization, and optimization through iterative fabrication. In this chapter, the potential for using SPB's to allow for the post-fabrication optimization of planar millimeter wave circuits is examined [1].

4.1 The Millimeter Wave SPB

At millimeter wavelengths, realization of the SPB posed some interesting challenges. The dimensions of the SPB are still large with respect to those used in micromachining applications. It would be difficult to achieve by photolithographic means alone, the fabrication of a metal-film SPB with a large enough vertical aspect ratio to provide sufficient mechanical integrity. On the other hand, the dimensions are still small enough to be difficult to attain by conventional machining.

A first attempt was made to manufacture a millimeter wave SPB as the tip of a metallic probe. Photoresist was patterned on both sides of a 25 μm-thick sheet of beryllium-copper, and various probes were etched from it. The tip of each probe was a scaled version of the perforated metal plate used in the 2 GHz realization of the SPB. Each probe was then bent in such a way that its tip could be pressed against a dielectric-coated transmission line on a 100 GHz circuit. The probes were annealed, hardening them sufficiently to provide the spring-tension necessary for pressing them firmly onto the test circuit.

At 100 GHz, the scaled thickness (from the microwave model) of the dielectric coating between the transmission line and metal plate is 5000 Å. The impedance of the covered sections should increase in direct proportion with an increase in this thickness, according to Equation 2.14. The total impedance created by the SPB varies with the $(n + 1)$'th power of this impedance, according to Equation 2.14. While some increase in this gap between the metal plate and transmission line can be tolerated, it is clear that the flatness of the plate must keep this gap within a few microns, in order to maintain a sufficiently low impedance for it to function as a backshort. It was found that this was not feasible.

A different implementation approach was used successfully. At 100 GHz, the horizontal dimensions of a scaled SPB must be on the order of one millimeter. The thickness required to give adequate mechanical integrity to a self-supporting metal structure would be too great to attain through photolithographic techniques.

Instead, this realization the SPB consisted of a thin-film metal pattern, formed photolithographically on the surface of a quartz wafer. The wafer was then diced so that the metal-film SPB could be laid flat on top of a dielectric-coated transmission line, with the diced quartz superstrate acting as a structural support. This is illustrated in Figure 4.1.

4.2 The Planar Quasi-Optical Detector Circuit

In 1992, Stimson *et al.* [2] demonstrated a planar quasi-optical millimeter wave receiver in which ten antennas and SIS mixing devices were combined in the form of a 230 GHz focal plane imaging array. All ten mixer circuits were fabricated on a single quartz-wafer, and each consisted of a thin-film dipole antenna with an integral SIS device. Incident millimeter wave radiation was passed through the circuit, reflected off a quartz-filled gold parabola beneath the substrate, and focused onto the group of antennas. Radiation from the LO entered through an opening in the rear of the parabola, and coplanar strip transmission lines were used to extract the IF signal from each mixer. Thin-film capacitors were included across each CPS transmission line, to isolate the IF signal by blocking the RF. The performance of each individual array element was evaluated separately.

This circuit, shown in Figure 4.2, demonstrated a practical means of providing a compact, lightweight array receiver with simple frequency scaling, device replacement, and photolithographic fabrication. While the mixer noise temperature for a single element in this receiver (148 K DSB) was consistent with that of a waveguide circuit using a similar device (48 K DSB), it was still significantly higher. This was attributed in part, to the lack of tuning capability inherent in such planar circuits, compared to the excellent tuning provided by movable waveguide backshorts. This is particularly important with state of the art SIS devices, whose properties are quite variable from one fabrication run to the next, reducing the effectiveness of fixed tuning. A circuit of this type appeared to be an appropriate vehicle for the evaluation of a millimeter wave SPB.

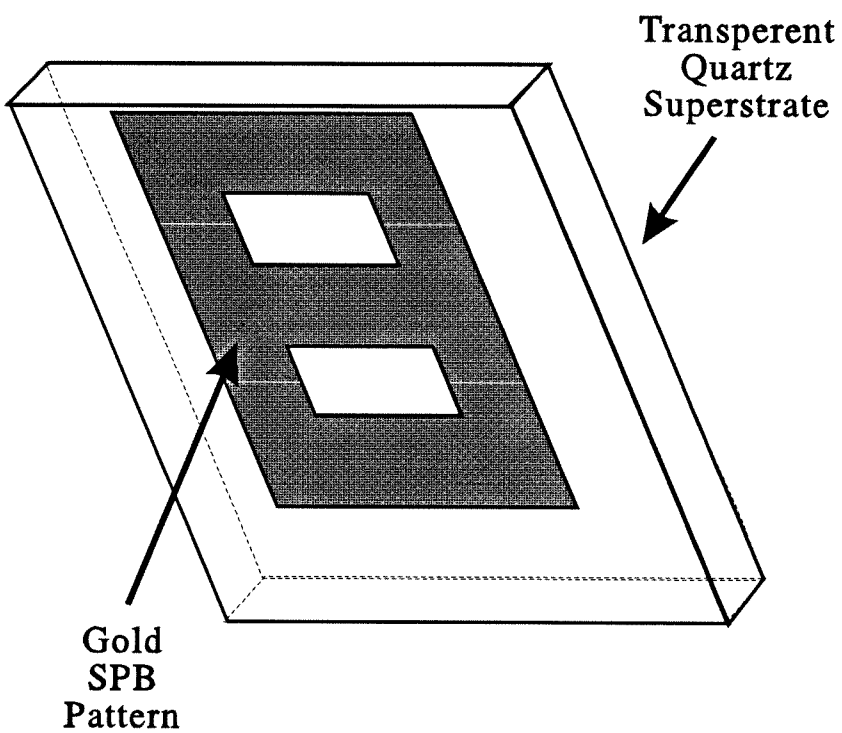

Figure 4.1 The millimeter wave SPB. It was diced from a fused-quartz wafer, photolithographically patterned with a thin-film gold SPB.

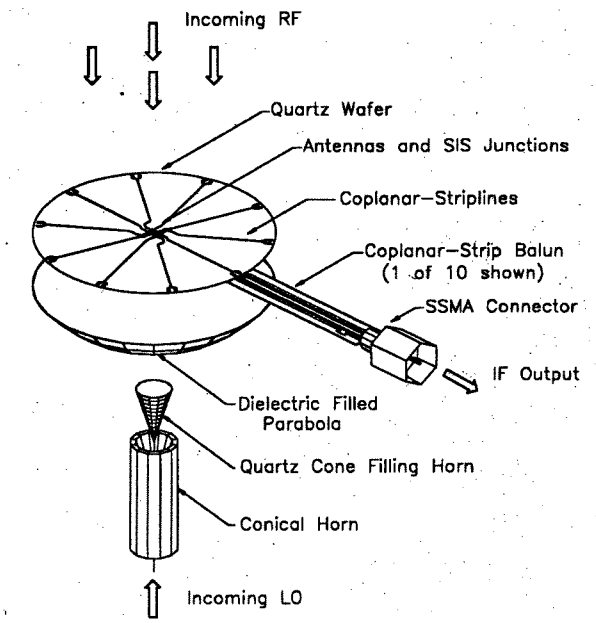

(a)

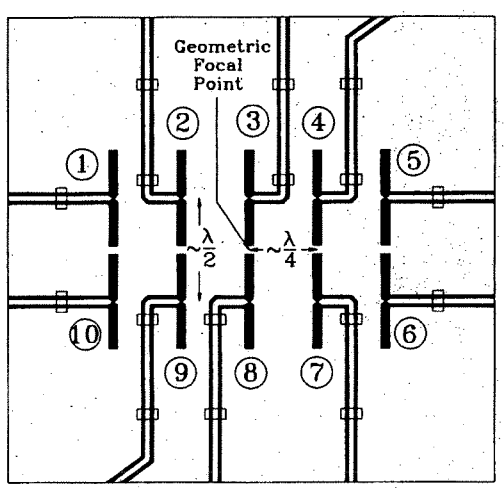

(b)

Figure 4.2 Diagram of the quasi-optical planar SIS receiver used by Stimson *et al.* [2]. An exploded view of the receiver (a) is shown along with a close-up view of the focal plane array of dipole mixers (b).

A 100 GHz single-element detector circuit was designed, based on the aforementioned mixer circuits. It included a dipole antenna, scaled from the SIS mixer, and a beam-lead diode as a detector element. A CPS transmission line was used to extract the DC detector output, and a 100 GHz SPB was implemented on this line both to isolate the DC response from the millimeter wave signal, and to form an adjustable length CPS tuning stub in parallel with the diode, which could be used to compensate for its parasitic reactance.

4.3 Circuit and SPB Fabrication

The antenna circuit and the SPB were fabricated by thermal evaporation of thin conducting films onto separate quartz wafers, each 250 μm in thickness. A 2,800 Å chrome-gold film was used for the antenna circuit and a 2,700 Å chrome-gold-chrome film was used for the SPB. The thin (100 Å) chrome layers were used to promote adhesion to the substrate and the subsequently deposited dielectric layer. A photoresist lift-off stencil was used to define the geometry for each of these circuits. The quartz wafer served as the dielectric substrate for the antenna circuit. For the sliding short however, the quartz wafer merely served as a support structure, providing a convenient means for achieving the high degree of flatness required for making an effective SPB at this frequency.

The antenna circuit consisted of a 936 μm-long, 87 μm-wide metal-film dipole, center fed by two 50 μm-wide metal-film strips as shown in Figure 4.3. A 100 μm gap separated the two strips and split the dipole. The SPB consisted of a rectangular metal-film pattern with two centered rectangular holes along its length. When positioned as shown in Figure 4.3, three 486 μm sections of transmission line are covered by the metal film, forming the lower impedance sections, with two sections, 388 μm and 460 μm long, left uncovered by the holes. A dicing saw was used to cut the quartz-backed SPB's to an appropriate size.

Several attempts were made to evaporate an oxide or alkali halide as the dielectric coating for the CPS transmission line. Silicon monoxide, silicon dioxide,

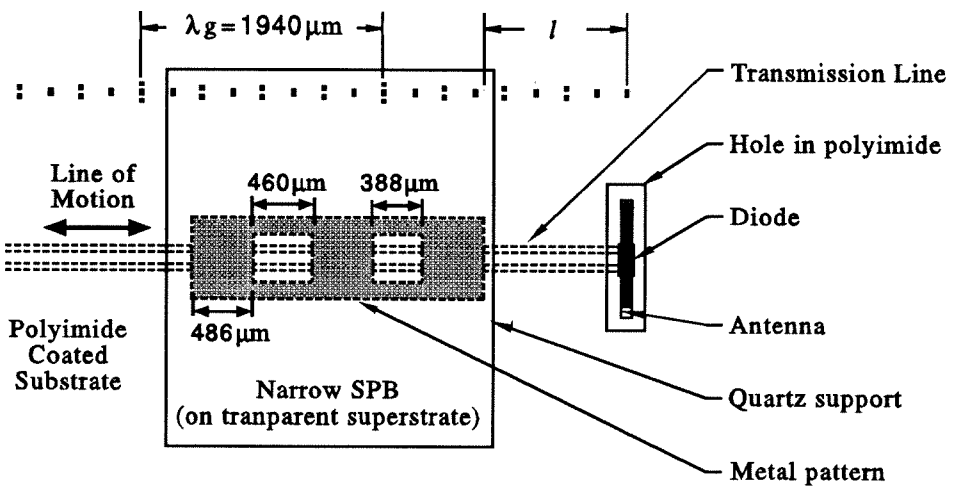

(a)

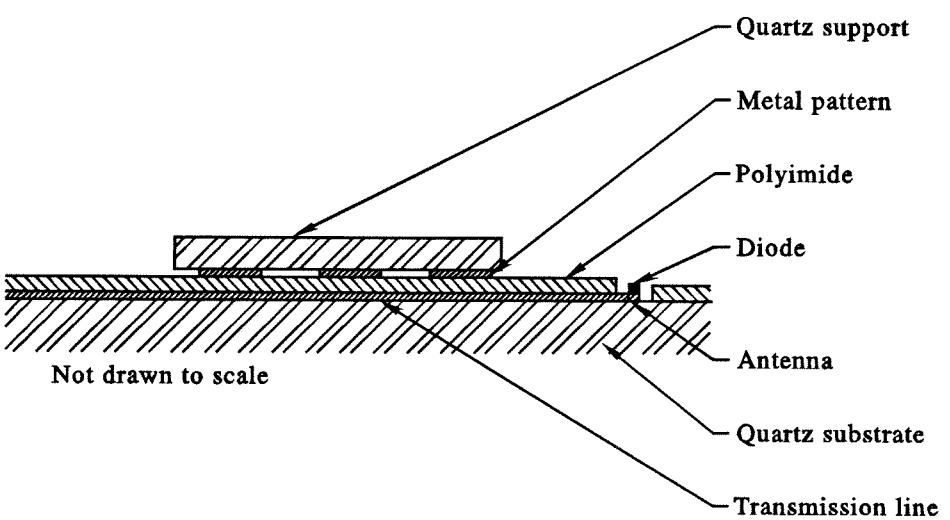

(b)

Figure 4.3 Plan view (a) and cross section (b) of the mechanically tunable planar detector circuit. The SPB creates a variable susceptance in parallel with the diode by varying the electrical length of the CPS tuning stub.

and magnesium fluoride were each tried through thermal evaporation over a photoresist lift-off stencil, at various rates and chamber pressures. In each case, severe mechanical stresses resulted in films which cracked or flaked too easily to function as reliable coatings [3]. Ultimately, a thin layer of polyimide plastic was spun onto the circuit and cured to a final thickness of 5,000 Å. Using a photolithographically patterned aluminum film as a mask, small windows were reactive ion etched from the polyimide in an oxygen plasma, to allow for soldering of the diode to the antenna and bonding of DC-wires to the other end of the transmission line.

While practical for this application, polyimide is rather soft and mechanical wear caused by repetitive use of the SPB would be pronounced. A photograph of the circuit appears in Figure 4.4 which shows the wear sustained by the dielectric layer during measurements.

4.4 Quasi-Optical Measurement of Tuning Effects at 100 GHz

Measurements were made with the detector circuit mounted over a dielectric-filled parabola with the SPB, positioned metallization side down, resting freely on the polyimide-coated transmission line. The circuit was positioned horizontally beneath a flat copper reflector aligned to direct a 100 GHz signal onto the circuit. An HP 83620A synthesized oscillator with an HP 8355A millimeter wave source module was used as the signal source. The source power was set to 0 dBm with an internal 1 kHz square wave modulation and an EG&G 5210 lock-in amplifier used to monitor the detected power [4]. The measurement set-up is illustrated in Figure 4.5. A plot showing the linearity of the detector response with respect to the source power is shown in Figure 4.6. The detected power was derived from the voltage measured across the diode, v_d, while biased with 300 μA of DC current. The source power was read form the signal generator display. The measured DC I-V curve for the diode, is also shown in Figure 4.6.

Positioning marks were defined in the antenna circuit pattern so that the SPB could be aligned at various distances, the dimension l in Figure 4.3, from

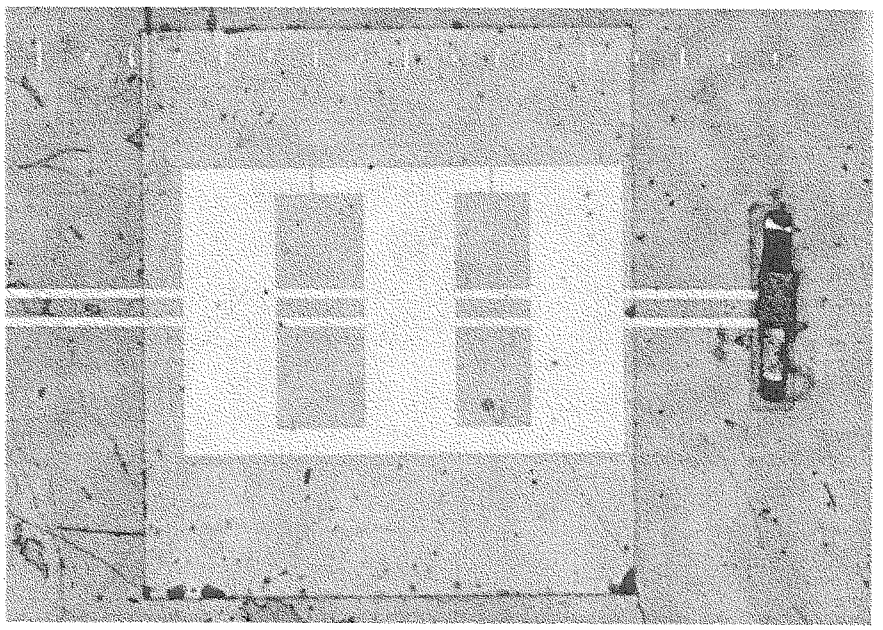

(a)

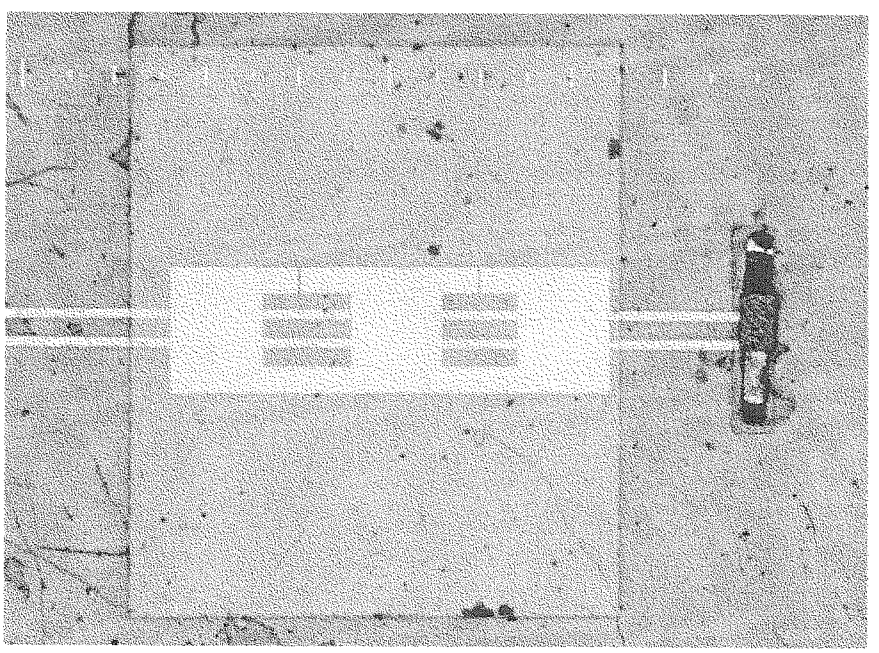

(b)

Figure 4.4 Photographs of the 100 GHz planar detector circuit with wide (a) and narrow (b) SPB's taken after measurements. Scratches are evident in the polyimide coating.

the antenna and diode with the aid of a microscope. The circuit was tested by manually aligning the SPB, with the aid of a sharp wooden probe, at increments of $\lambda_g/16$ along the transmission line and measuring the detector response at each position. The wavelength, λ_g, used here was that for the CPS transmission line (Equation 2.6), and the SPB was positioned up to three wavelengths away from the antenna and diode. This procedure was repeated using two SPB designs, both having identical dimensions along the transmission line, but one with a wider metallization pattern across the line. The diode was DC biased at $200\,\mu$A, and results for both the narrow (0.34-λ_g) and wide (0.77-λ_g) SPB's are shown in Figure 4.7, normalized to the response measured with no SPB present (typically $160\,\mu$V).

The detector response varied through peaks and nulls as the SPB was used to increase the electrical length of the CPS line. The largest responses occurred with the SPB near the $\lambda_g/2$ position, an increase of almost 3 dB over the untuned response. A slight increase in this position produced the deepest nulls (as low as -11 dB), indicating that the electrical length of the CPS tuning stub was extremely critical. This illustrates the advantage of including an adjustable tuning element, as it would be difficult to predict the optimal length for the line in a fixed-tuned circuit.

A theoretical model for the circuit was developed, and is shown in Figure 4.8. The theoretical circuit response is included in Figure 4.7, and was calculated using

$$P_n(l) = \frac{\left| \dfrac{R_d}{Z_{th}(l) + R_d} V_{th}(l) \right|^2}{\left| \dfrac{R_d}{Z_{th}(\infty) + R_d} V_{th}(\infty) \right|^2} \tag{4.1}$$

where l is the distance between the diode and the SPB, P_n is the power delivered to the diode as a function of l, normalized to that of $l = \infty$, and R_d is the differential resistance of the biased diode ($300\,\Omega$). The circuit has been reduced to a Thévenin equivalent voltage ($V_{th}(l)$) and impedance (Z_{th}), as seen by R_d. They are given by

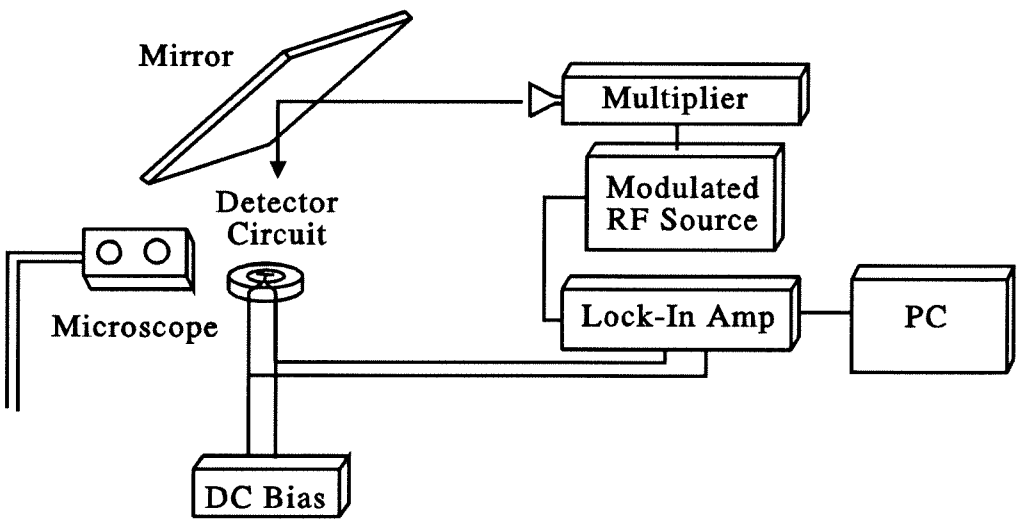

Figure 4.5 Test set-up used for quasi-optical measurements of the the detector circuit. The 100 GHz source was modulated with a 1 kHz square-wave and a lock-in amplifier used to monitor the detector output.

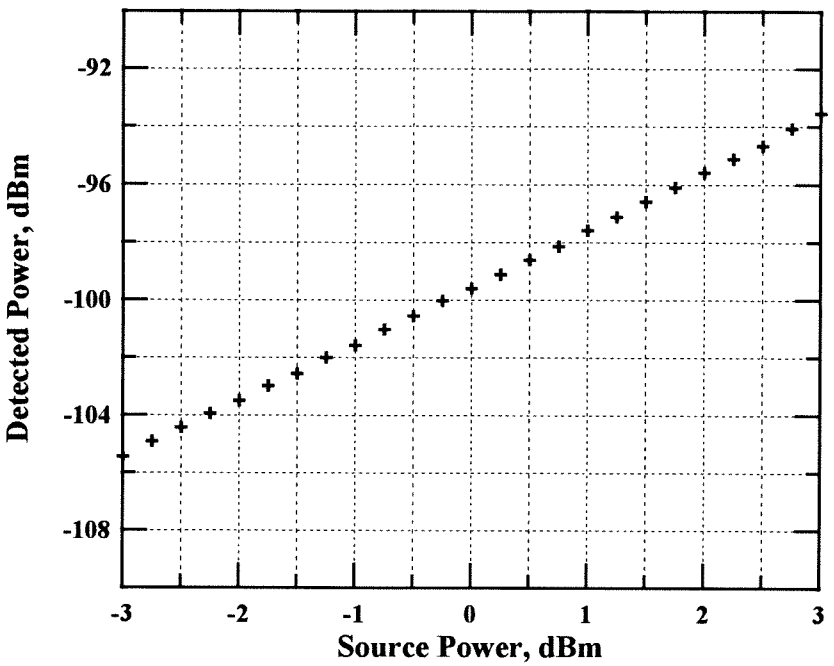

(a)

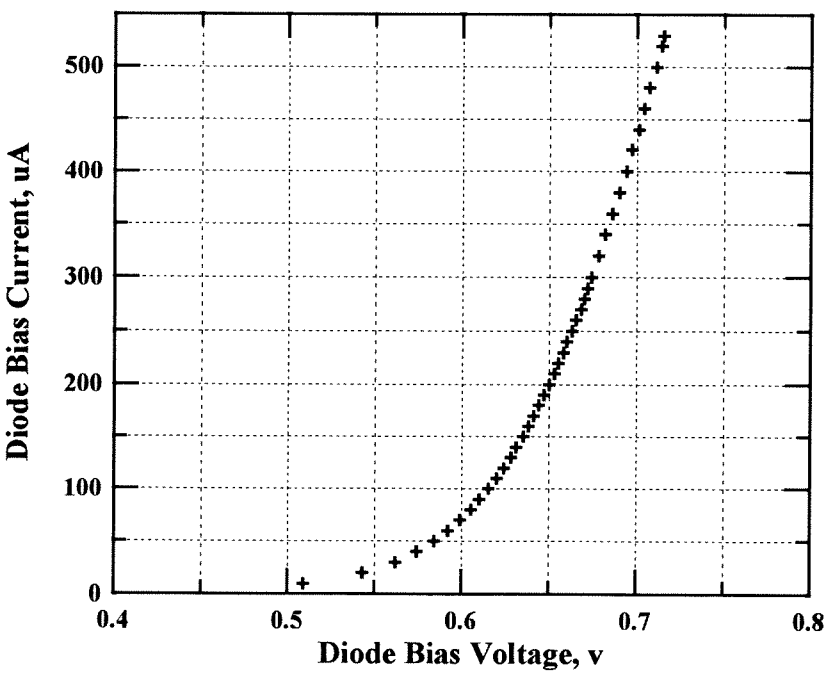

(b)

Figure 4.6 Detected power versus source power (a) and DC I-V curve for the beam-lead Schottky diode detector.

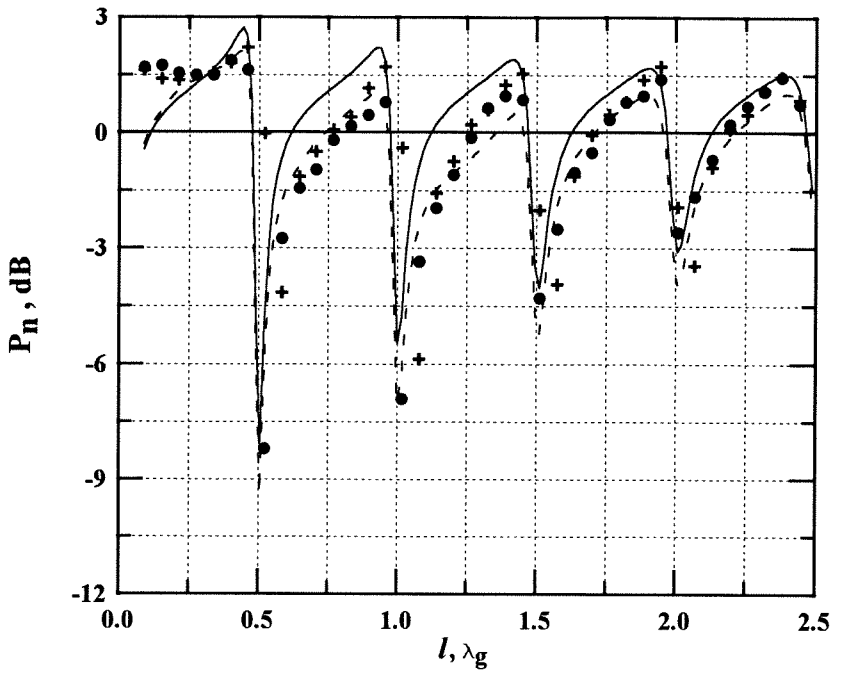

(a)

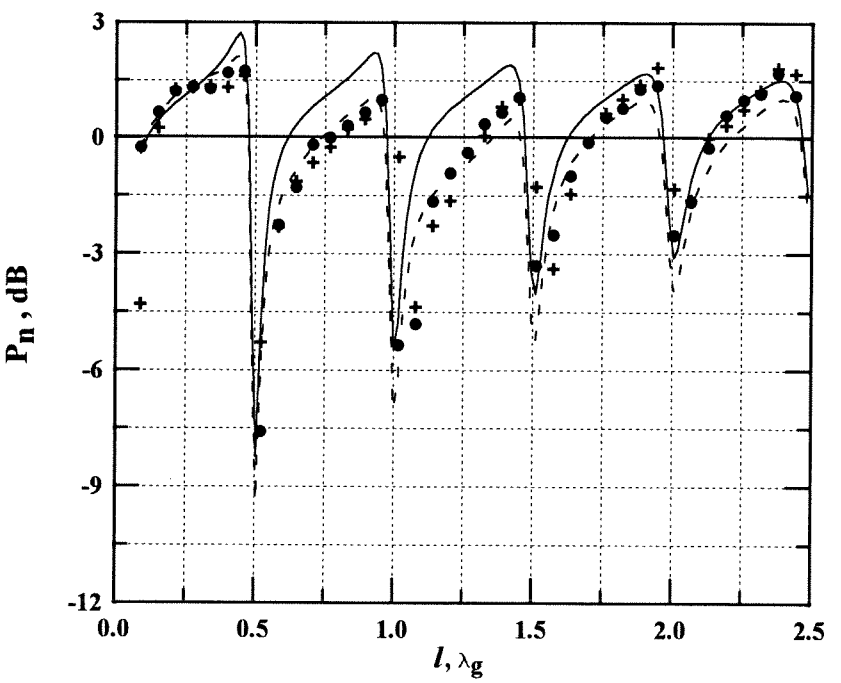

(b)

Figure 4.7 Data for two typical trials (•) (+) is shown for both the wide (a) and narrow (b) SPB's. Theory is shown both with (—) and without (- -) the coupling effect included.

$$V_{th}(l) = \left(\frac{Z_{tl}(l)}{R_a + Z_{tl}(l)}\right)\left(\frac{Z_C}{R_a \parallel Z_{tl}(l) + Z_L + Z_C}\right) \times \cdots \\ \times \left(\frac{Z_{Cd}}{[R_a \parallel Z_{tl}(l) + Z_L] \parallel Z_C + R + Z_{Cd}}\right) V_a, \tag{4.2}$$

in terms of the antenna voltage, V_a, and

$$Z_{th} = \Big([R_a \parallel Z_{tl}(l) + Z_L] \parallel Z_C + R\Big) \parallel Z_{Cd}, \tag{4.3}$$

respectively. The frequency dependent impedances Z_L, Z_C, and Z_{Cd} correspond to elements in the manufacturer's equivalent circuit for the beam lead diode (M/A-COM MA40417). Specifically, L (100 pH) and C (20 fF) are package parasitics, R (8.5 Ω) is the series resistance, and C_d (47 fF) is the junction capacitance. R_a is the antenna resistance (50 Ω) [5] and the impedance of the CPS transmission line tuning stub [6] is given by

$$Z_{tl}(l) = Z_0\left(\frac{Z_{spb}\cosh\gamma l + Z_0 \sinh\gamma l}{Z_0\cosh\gamma l + Z_{spb}\sinh\gamma l}\right) \tag{4.4}$$

where Z_0 is the characteristic impedance of the CPS line (190 Ω) from Equation 2.4 and

$$Z_{spb} = Z_0\frac{(1 - |s_{11}|^2)}{(1 + |s_{11}|^2)} \tag{4.5}$$

is the equivalent termination impedance of the SPB with $|s_{11}| = -0.3$ dB, a value taken from the 2 GHz scaled model. Changes due to material variations and increased skin effect at this frequency were not included because the experiment was not expected to be accurate enough to show these effects. Also,

$$\gamma = \alpha + j\beta \tag{4.6}$$

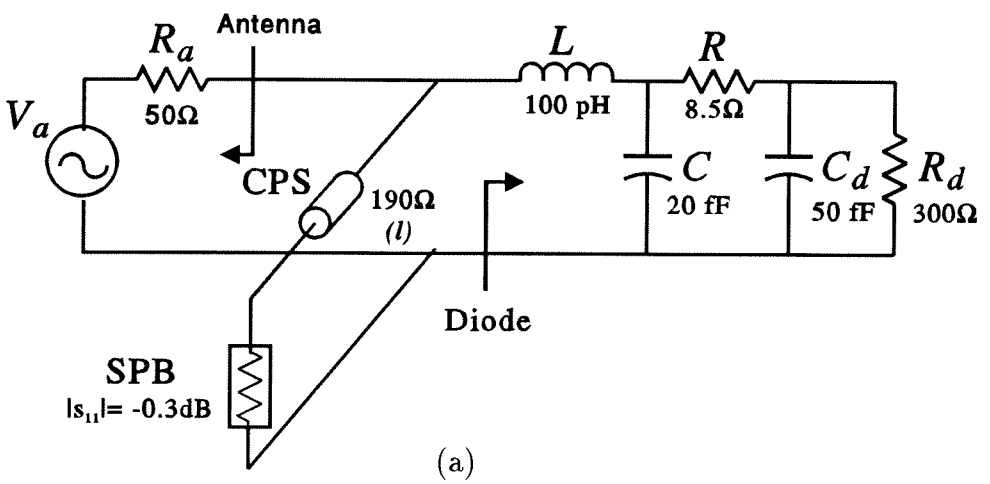

(a)

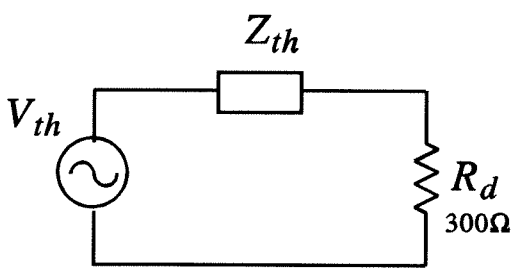

(b)

Figure 4.8 Schematic diagram for the tunable detector circuit. Both the full circuit (a) and the Thévenin equivalent (b) are shown.

is the propagation constant for a CPS line with phase constant $\beta = \frac{2\pi}{\lambda_g}$. Attenuation constant α ($0.83\,\mathrm{dB}/\lambda_g$) and λ_g (1.94 mm) come from Equations 2.13 and 2.6, respectively. The surface resistance for α_c in Equation 2.13 came from the measured DC conductivity (1.5×10^7 S/m) of the gold film.

A parasitic coupling effect between the SPB and the antenna was also observed. This was characterized by repeating the measurements with the SPB moved incrementally away from the antenna as before, but now positioned on the side of the antenna exactly opposite to the transmission line. In this way the parasitic coupling between the antenna and SPB could be recreated, isolated from the transmission line effect. The results of this measurement are shown in Figure 4.9. The average value of the measured coupling effect, a perturbation of as much as –2 dB, was then added to the theoretical response, and the result is also shown in Figure 4.7. This compensation is necessary to obtain good agreement between theory and measurement for positions less than $2\lambda_g$.

This experiment demonstrated a new approach for tuning planar circuits at millimeter wavelengths. A photolithographically generated SPB was used to vary the length of a CPS tuning stub in parallel with a Schottky diode detector. The detector response, at 100 GHz, was increased by more than 2 dB over the untuned response at the peak position and nulled by nearly 11 dB at the $\lambda_g/2$ position. These two extremes occurred at electrical lengths that were only $\lambda_g/10$ apart, illustrating the critical role of an adjustable tuning element in such circuits. Also, the theory was shown to adequately predict the circuit performance.

The circuit used here demonstrates the concept of planar tuning. Other circuits could be designed to take even better advantage of the SPB. A different device, such as a monolithically fabricated diode or SIS tunnel junction, could be used as the detector and a second tuning stub could be incorporated to provide further improvement in the response. The SPB could be fabricated as an integral part of the transmission line, captivated by a micromechanical guiding structure.

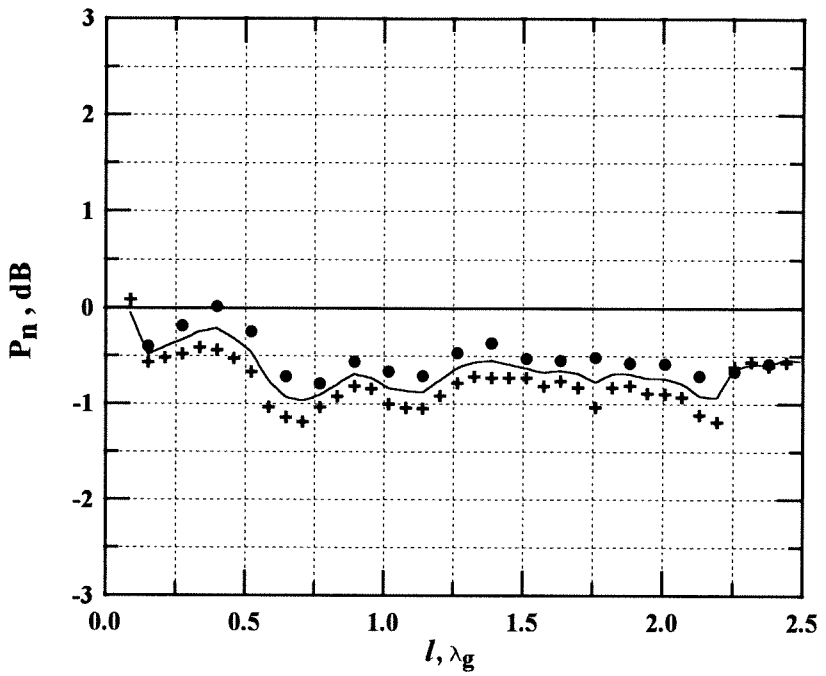

(a)

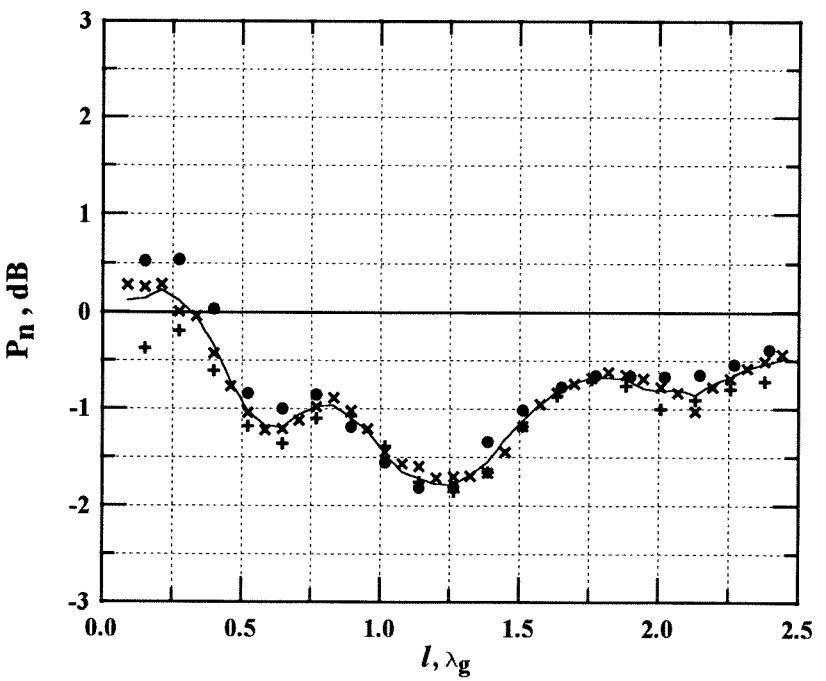

(b)

Figure 4.9 Measured coupling effect between antenna and SPB. The measured data (•)(+)(×) for the wide (a) and narrow (b) SPB's are shown, along with their average values (—).

A circuit of this type, scaled for use at submillimeter wavelengths, is described in the next chapter.

References

[1] V.M. Lubecke, W.R. McGrath, and D.B. Rutledge, "A 100 GHz Coplanar Strip Circuit Tuned With a Sliding Planar Backshort," *IEEE Microwave and Guided Wave Letters*, vol. 3, no. 12, pp. 441-443, December 1993.

[2] P.A. Stimson, R.J. Dengler, H.G. LeDuc, S.R. Cypher, and P.H. Siegel, "A Planar Quasi-optical SIS Receiver," *IEEE Transactions on Microwave Theory and Techniques*, vol. 41, no. 4, pp. 609-615, April 1993.

[3] L.I. Maissel and R. Glang, *Handbook of Thin Film Technology*, New York, NY: McGraw-Hill, 1970.

[4] M.L Meade, *Lock-In Amplifiers: Principles and Applications*, London, UK: Peter Peregrinus Ltd., 1983.

[5] P.H. Siegel and R.J. Dengler, "The Dielectric-Filled Parabola: a New Millimeter and Submillimeter Wavelength Receiver/Transmitter Front End," *IEEE Transactions on Antennas and Propagation*, vol. 39, no. 1, pp. 40–47, January 1991.

[6] S. Ramo, J.R. Whinnery, T. Van Duzer, *Fields and Waves in Communications Electronics*, New York, NY: John Wiley & Sons, Inc., 1965.

Chapter 5

Integration of SPB's for Submillimeter Wavelengths

State-of-the-art performance has been established in the submillimeter band through the use of technology extended from the millimeter spectrum; three-dimensional devices embedded in hollow waveguide structures have been used to make measurements at the highest frequencies. Devices in these circuits are often in the form of SIS tunnel junctions integrated with planar impedance matching circuits, or whisker contacted Schottky diodes. Optimization of the performance of these circuits is typically performed using mechanical tuning elements to compensate for the parasitic reactance inherent in these devices. The critical dimensions for these circuits are smaller than in millimeter wave circuits, making fabrication an even greater challenge. Planar technology offers an attractive alternative.

At submillimeter wave frequencies, the value of post-fabrication tuning is increased. Parasitic reactances are more deleterious to the performance of devices, devices are more difficult to characterize, and it is more difficult to physically realize circuits as designed. It would be desirable to add a means for post-fabrication to these planar integrated circuits. Technology from the emerging field of MEMS can make this possible. A procedure for fabricating an SPB, suitable for integration in a submillimeter wave monolithic circuit, has been developed. It is based on a combination of LIGA and surface micromachining techniques [1]. The work described here involves the development of this technique and the measured performance of SPB's in a monolithic submillimeter wave circuit [2].

5.1 Design of the Integrated Circuit

A number of promising planar circuit designs have emerged which involve the use of slot antennas and CPW transmission lines on a plano-convex substrate-lens [3]-[5]. These circuits couple to incident signals quasi-optically, focusing radiation incident on the convex surface of the lens onto an antenna on a substrate which is attached to the planar surface of the lens. These lenses can absorb radiation through a hemispherical or elliptical convex surface, or alternatively through the planar surface of a lens which employs a metallized parabolic reflecting surface. This was the case in the millimeter wave demonstration of the SPB on a CPS transmission line described in Chapter 4. The placement of a ground plane between the focused radiation in the substrate-lens, and the mechanical SPB structure on a CPW line, has a particular appeal. It should act to reduce the coupling between the near-field radiation and SPB, which was seen in the millimeter wave experiment.

A quasi-optical 620 GHz monolithic direct-detection circuit was developed to demonstrate the operation of an integrated SPB. This circuit used a dielectric-filled parabola to focus radiation onto a slot antenna, and coupled this radiation to a bismuth detector by means of two CPW transmission lines, each with integrated SPB's. One SPB creates a variable series reactance between the antenna and the detector, potentially serving to compensate for any off-resonance reactance of the slot. The other SPB creates a variable susceptance in parallel with the detector, and acts to compensate for the parasitic capacitance found in otherwise desirable submillimeter wave devices.

The dielectric-filled parabola consisted of a plano-convex fused-quartz lens, with the convex surface shaped into a parabola with an f/D ratio of 0.25. The parabolic side is metallized and functions analogously to a conventional parabolic dish antenna, focusing incident paraxial radiation to a small beam-waist. The integrated detector circuit was fabricated on a fused-quartz wafer and positioned

on the lens so that the antenna coincided with this beam-waist.

The integrated circuit design is illustrated in Figure 5.1. The CPW transmission lines were designed to optimize the effect of the tuning elements, and the antenna was designed to be compatible with the dimensions of the CPW and SPB. The antenna was a full-wave resonant slot, designed to have a feed impedance of 24 Ω at 620 GHz. This was calculated following the work of Eleftheriades *et al.* [6]. It consisted of a 261 μm-long, 5 μm-wide opening, etched in a 1000 Å gold film.

The CPW consists of a 16 μm-wide center conductor, with 8 μm gaps on each side, and is designed to have a characteristic impedance of 78 Ω, as calculated using Equation 2.5. The line was also designed to minimize loss due to radiation into the substrate. Conductor loss for such a line can be minimized by the use of a highly conductive metal or superconducting film. Total loss for the lines in this experiment was calculated to be $0.6\,\mathrm{dB}/\lambda_g$, using the surface resistance of bulk gold along with Equation 2.13.

The critical dimensions of the SPB were scaled from the tuning element which was empirically designed at 2 GHz for use on a 204 Ω CPS transmission line, described in Chapter 3. The 78 Ω CPW used here is the physical dual of that transmission line, and the return loss of the SPB in this application was also measured at 2 GHz, as $|s_{11}| = -0.06\,\mathrm{dB}$. The frequency scaled SPB consisted of three covered sections, each approximately 80 μm long, and two uncovered sections, approximately 65 μm and 75 μm long. Additional uncovered and covered sections were added to the trailing end of the SPB, to better facilitate its manipulation with a mechanical probe. The width of the exterior of the 620 GHz SPB was 200 μm, and the holes were 110 μm wide. These dimensions were chosen to avoid lateral resonances at the design frequency.

For this experiment a small bismuth film was used to create a self-heating thermocouple for detection of the submillimeter radiation. It was patterned across the CPW near the antenna. Current induced in the antenna by a submillimeter

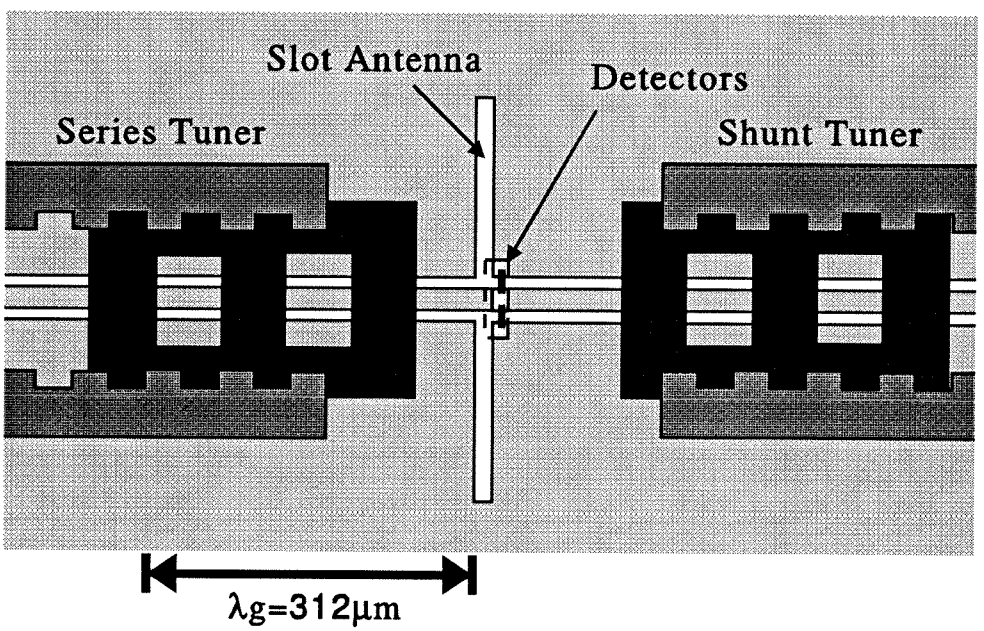

Figure 5.1 The 620 GHz detector circuit. Two micromechanical SPB's on dielectric coated CPW transmission lines form the adjustable impedance matching circuit.

signal passes though the film and heats it, and the physical asymmetry of the interface between the bismuth and the conductors of the CPW results in a thermal-electric voltage which is proportional to the power absorbed by the film. This circuit was designed to accommodate a four-wire resistance measurement, allowing the bismuth film to be used as a microbolometer as well [7]. The advantage of using the film as a thermocouple is that it requires no bias current, and thus has no $1/f$ noise [8]. Using a bismuth film which is much thicker than the metal layer contacts which the detector must overlap, insures good edge coverage and also results in a low-impedance detector which should closely match the 24 Ω antenna. This match, and consequently the output of the circuit, can be altered by varying the positions of the SPB's.

5.2 Fabrication Overview

The circuit was fabricated on a round fused-quartz substrate, 250 μm thick and 19 mm in diameter, and involved a combination of techniques commonly used in making millimeter and submillimeter wave circuits. The seven mask, seven layer process illustrated in Figure 5.2, contains many subtle details which are described in full in an Appendix. The development of this process formed a major part of this thesis. Facilities for thin-film evaporation and RF sputtering, electroplating, wet etching, and general photo-processing were used, but a dedicated clean-room was not required.

The first circuit layer proved to be most difficult in the absence of clean-room facilities, because it involved the production of a high-resolution pattern over a large area and was thus highly susceptible to contamination. A thorough cleaning of the wafer immediately preceded the first layer deposition. Electron-beam evaporation was used to first apply a 60 Å layer of chrome as an adhesion layer, followed by a 1000 Å layer of gold and then another 60 Å layer of chrome. Photoresist was then patterned over this metal film using the first mask to allow for wet etching of the antenna and CPW patterns. The photoresist was then stripped

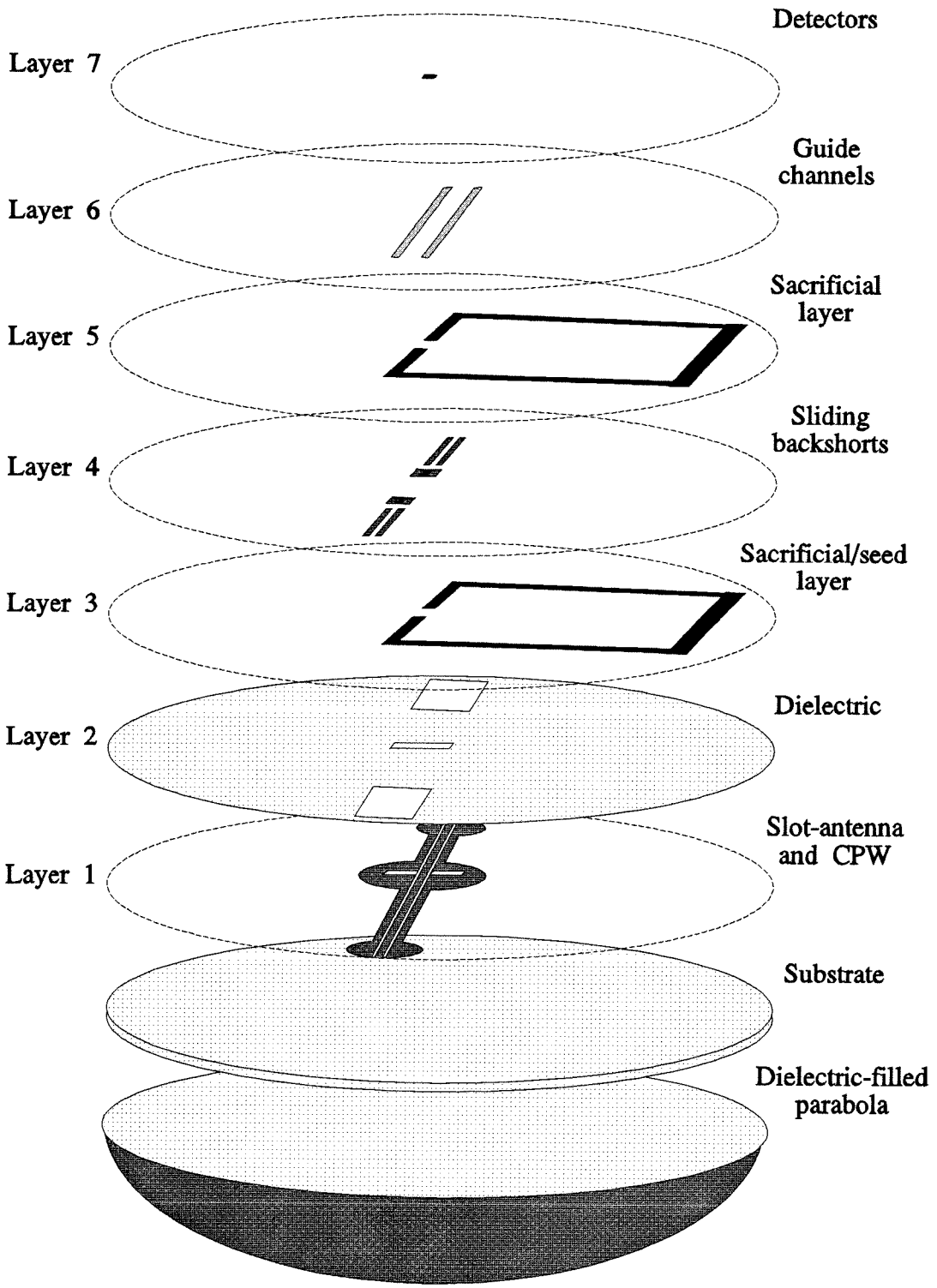

Figure 5.2 Exploded view of the integrated circuit. Seven circuit layers are fabricated on a dielectric substrate which is mounted over a dielectric-filled parabola.

and a new layer of photoresist applied, patterned with the second mask, and the metal-film ground plane etched away, except for the area immediately surrounding the CPW and antenna.

Next, a dielectric layer was used to electrically insulate the CPW transmission lines from the subsequently applied SPB structures. A layer of photoresist was applied and treated with chlorobenzene to form a lift-off stencil. It was patterned with the third mask to create openings in an 1000 Å layer of silicon-dioxide, which was deposited on the wafer by RF magnetron sputtering. The resist was severely hard-baked during the procedure and the assistance of ultrasonic agitation and mechanical probing were required to lift-off the pattern, in addition to soaking the wafer in acetone.

The procedure for fabricating each SPB is illustrated in Figure 5.3. A photoresist lift-off stencil was first applied, patterned with the fourth mask to define a sacrificial-seed layer. This layer consisted of two 200 μm-wide strips, the width of the SPB, which each ran approximately two millimeters along the two CPW lines. It also contained two 1 mm-square patches, and connecting lines which extended out to the edge of the wafer. The layer was formed by using electron-beam evaporation to deposit a 1700 Å layer of copper on top of a 70 Å chrome adhesion layer. The stencil and unwanted film were lifted in acetone.

Next, an 8 μm layer of photoresist was applied to the circuit, and patterned with the fifth mask to form a mold layer. This layer defined the shape of each SPB, several sacrificial pieces used to define the region into which each SPB would slide, and two 1mm^2 patches which served to increase the plating area to allow for the use of a higher, less variable plating current. The photoresist mold was hard-baked, then soaked in distilled water and dipped briefly in an ultrasonic bath to remove any trapped gasses [9]. An electrode was then clipped onto the edge of the wafer, connecting a current source to the sacrificial-seed layer, and the circuit was dipped in a cyanide-based gold electroplating solution. The exposed regions

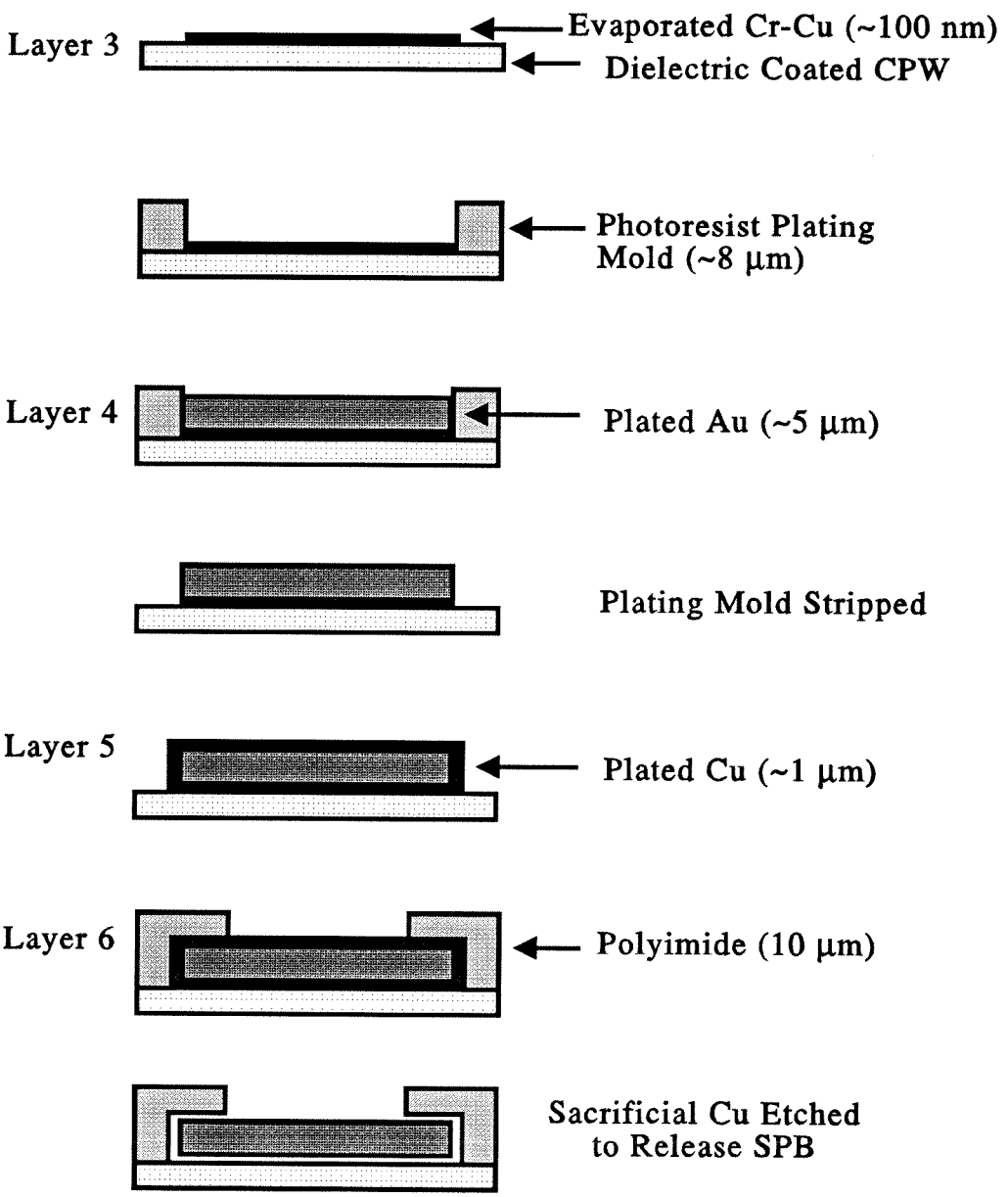

Figure 5.3 Simplified illustration of the SPB fabrication process. Sacrificial layers are used to form an SPB which is constrained by guide structures.

of copper were then plated with 5 μm of gold. The thick, hard-baked resist was then removed in 60°C N-methyl 2-pyrrolidone.

A sacrificial coating was then applied to each SPB by connecting the bare circuit again to an electrode and immersing it this time in an acid-based copper electroplating solution. The exposed gold and copper structures were plated with approximately 1 μm of copper. Next, a 13 μm layer of photosensitive polyimide-precursor was spun onto the circuit, and patterned with the sixth mask to form two digitate strips, each overlapping one side the copper-coated gold structures. The strips were then cured to form 9 μm-thick polyimide guide structures. The overlapping digits not only served to minimize the area in which a defect in the plating surface might ultimately bind the SPB to the polyimide-guide, but also as a reference scale for positioning the SPB during measurements.

Finally, the circuit was soaked in a copper etchant to dissolve the copper plating and sacrificial-seed layer, releasing each remaining gold SPB structure to slide along the substrate within its polyimide guide-structure. The chrome remaining from the sacrificial-seed layer, as well as the chrome exposed by the windows in the sputtered dielectric layer, was then removed with chromium mask etchant. SEM's of a mechanically operable circuit are shown in Figures 5.4 and 5.5.

After meticulous removal of the sacrificial gold pieces, which served only as structural supports for the formation of the polyimide guide-structures, photoresist was applied to the circuit and patterned using the seventh mask to form a lift-off stencil for the bismuth detector. A 6000 Å layer of bismuth was then deposited onto the wafer by thermal evaporation, and the stencil was again lifted using acetone, leaving only the patterned bismuth.

5.3 Quasi-Optical Measurement of Tuning Effects at 620 GHz

The circuit was mounted in a brass fixture, over a recess containing the fused-quartz parabola with gold-film backing. Aluminum bond wires were used to con-

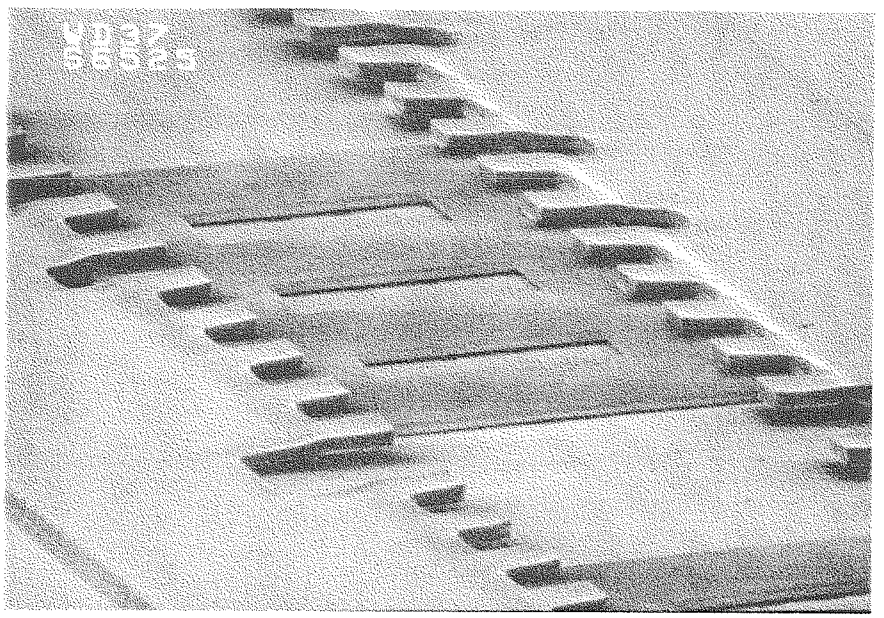

(a)

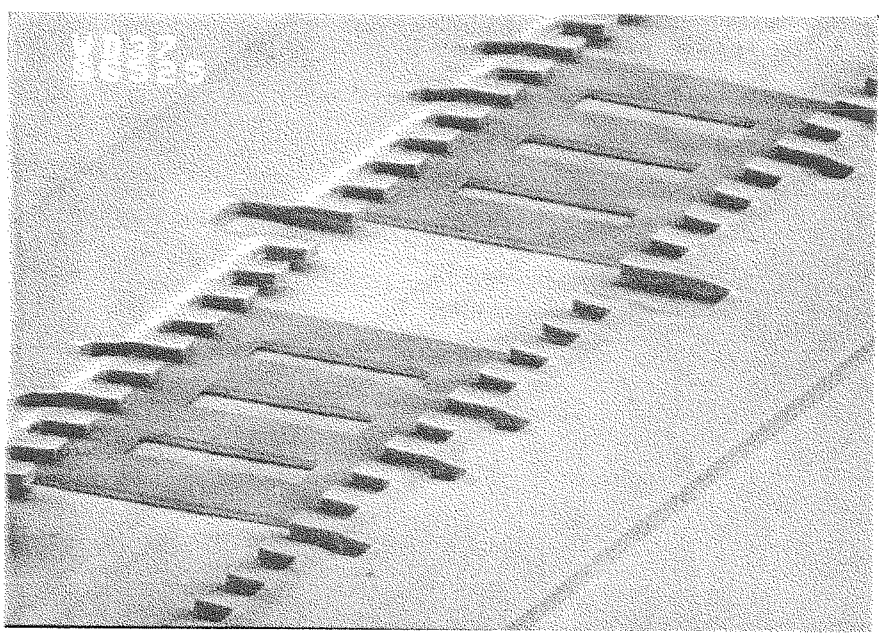

(b)

Figure 5.4 SEM's of the micromechanical integrated circuit. The same circuit is shown from two vantage points.

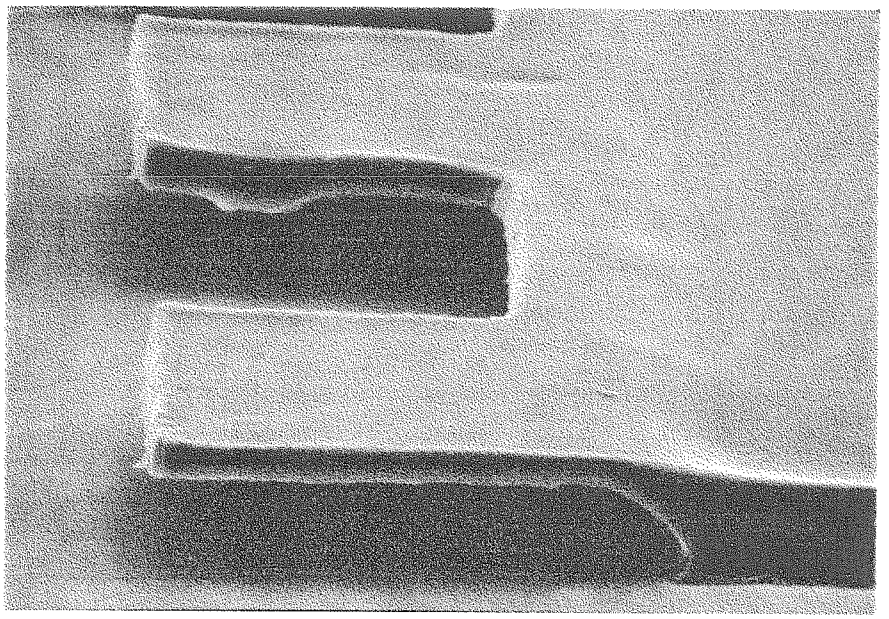

(a)

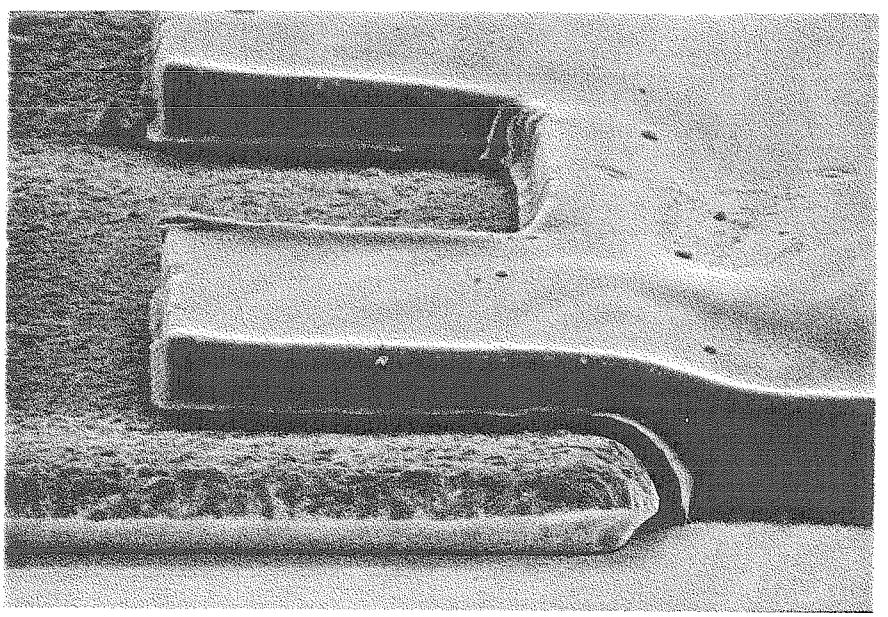

(b)

Figure 5.5 SEM's of the micromechanical integrated circuit. The polyimide guide structure is shown with (a) and without (b) the SPB underneath it.

nect the center and outer conductors on each end of the CPW, to individual printed circuit boards on the mount, each terminated with an SSMA connector. This was done in order to allow various connection methods to be tried for measurement of the detected signal. The fixture was attached, with the circuit facing upwards, to an adjustable gimbal-mount on top of two orthogonal linear-translation stages mounted on an optical-measurement table. A gold mirror mounted on translational and rotational stages was used to direct a horizontally incident signal onto the circuit. A microscope with a magnification of 1000× was positioned at an angle above the circuit, to aid in the manipulation of the SPB's. The set-up is illustrated in Figure 5.6.

A Backward Wave Oscillator (BWO) was used as a 620 GHz source [10]. This source provided only a couple of milliwatts of multimoded power, with much less than 1 mW present in the fundamental mode which couples to the circuit. It was positioned behind a 25 Hz chopper and as close as possible to the gold mirror. A PAR 125A lock-in amplifier was used to measure the output voltage of the detector. The system was first aligned to maximize the detected signal (approximately 2 μV) with the tuning elements in somewhat arbitrary positions. The voltage was measured across the two detectors in series. The DC I-V characteristics for each detector are shown in Figure 5.7. A probe was fashioned with a 50 μm-diameter ox hair at its tip, and this was used to manually position the SPB for each measurement.

It would be desirable to implement probes on micrometer driven positioners to move the SPB's. This was planned, but proved difficult to implement in the actual circuit tested. The small amount of power available at 620 GHz necessitated placement of the circuit very close to the tube output (an overmoded waveguide horn) in order to minimize losses. This left no room for the positioners.

Data obtained by sweeping the position of the series tuning element over a distance of one guide-wavelength, for one position of the parallel tuning element,

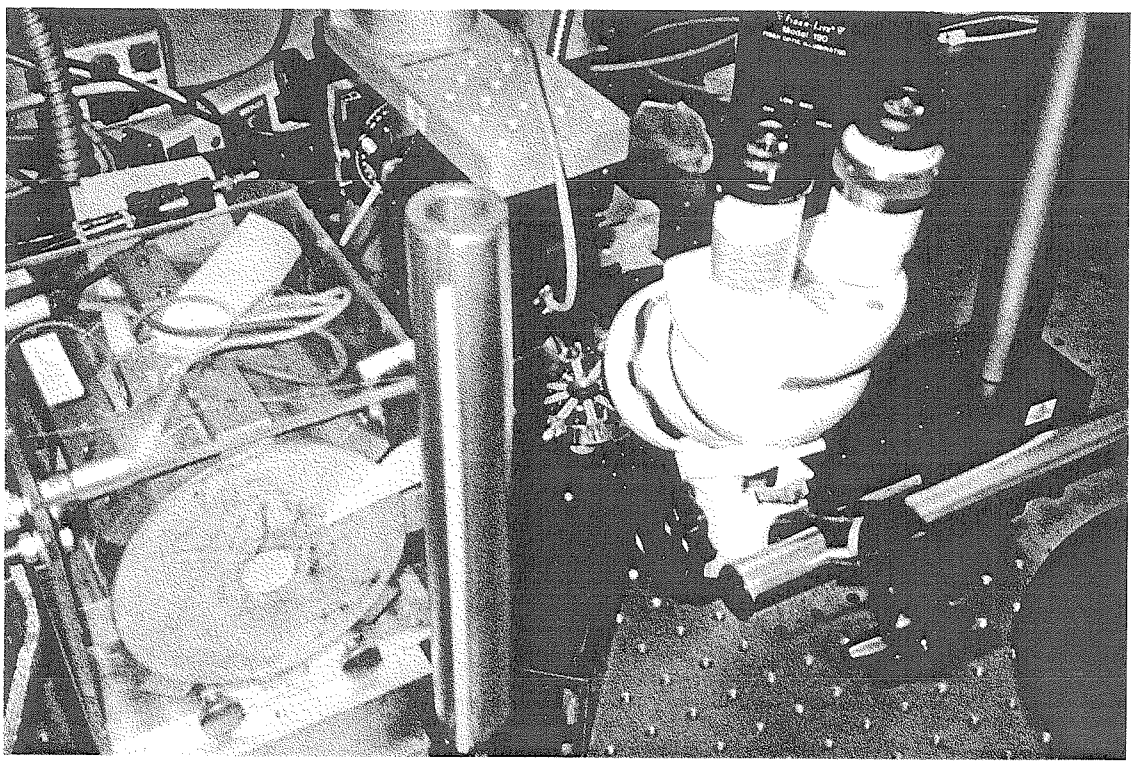

(a)

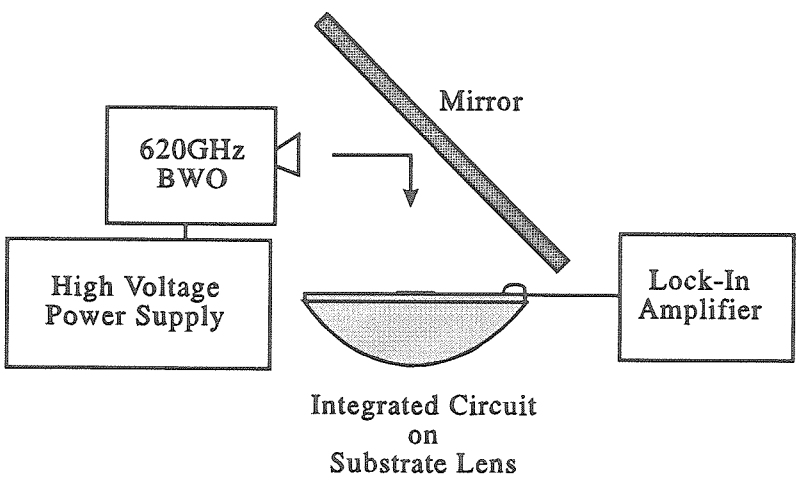

(b)

Figure 5.6 Photograph (a) and diagram (b) of the quasi-optical measurement set-up for the 620 GHz integrated circuit. A mirror was used to direct a test signal to the dielectric-filled parabola.

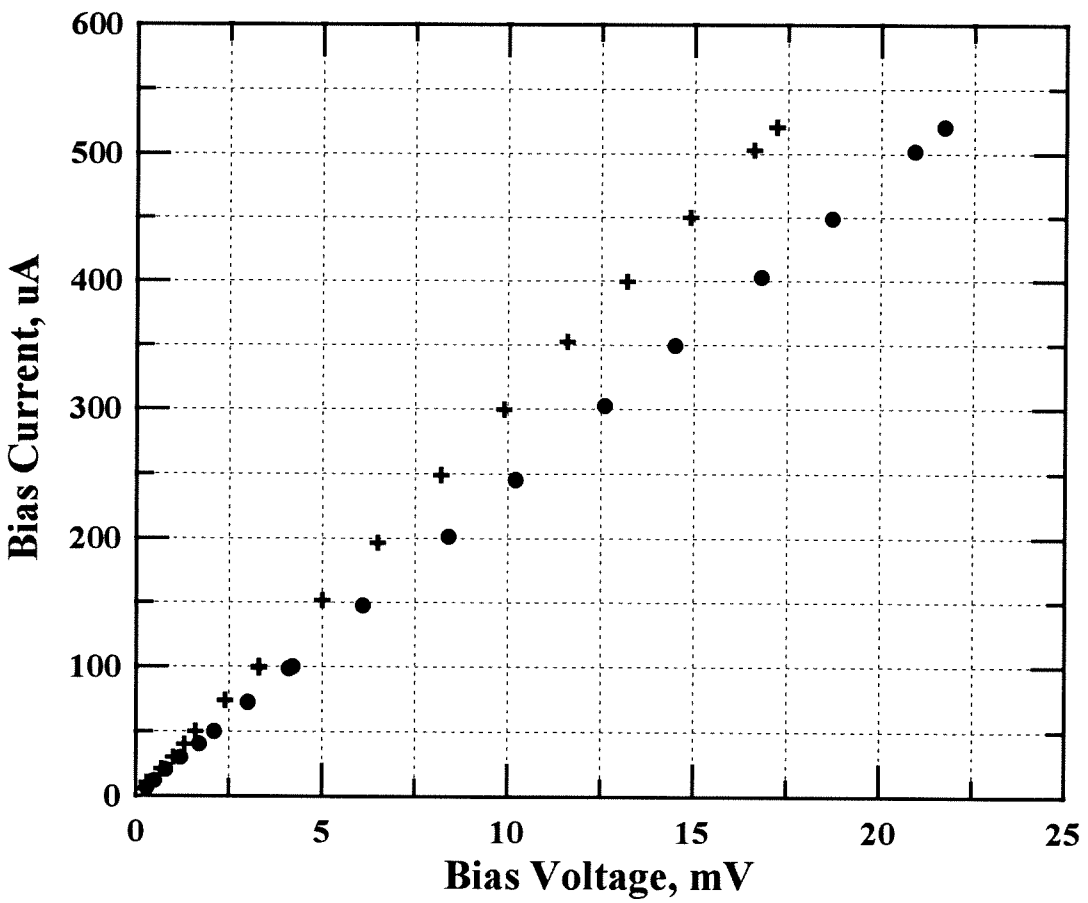

Figure 5.7 DC I-V characteristics for the two thin-film bismuth detectors. The 42 Ω detector (•) and 33 Ω detector (+) appear in parallel as 18.5 Ω for the RF circuit.

is shown in Figure 5.8. Data obtained by sweeping the parallel tuning element, point-by-point over a range of three guide-wavelengths for two different positions of the series tuning element are shown in Figure 5.9. These results were recorded over several experimental runs spaced some hours apart, and different symbols have been plotted to represent groups of data recorded in each run. Data for each sweep were normalized to a reference measurement taken with the SPB which created the parallel susceptance positioned near $\lambda_g/4$, and the SPB which created the series reactance positioned near $\lambda_g/2$. The series tuning element was not swept over the full three guide-wavelengths because of a mechanical flaw in its fabrication. In each measurement sweep, the SPB's functioned to vary the power through multiple peaks and nulls in a repeatable manner.

A theoretical model for the circuit was created and is shown in Figure 5.10. The response for the circuit with respect to SPB positions was calculated as

$$P_n(l_s, l_p) = \frac{\left| \dfrac{\dfrac{R_b Z_{tl}(l_p)}{R_b + Z_{tl}(l_p)}}{Z_a + Z_{tl}(l_s) + \dfrac{R_b Z_{tl}(l_p)}{R_b + Z_{tl}(l_p)}} \right|^2}{\left| \dfrac{\dfrac{R_b Z_{tl}(l_p^r)}{R_b + Z_{tl}(l_p^r)}}{Z_a + Z_{tl}(l_s^r) + \dfrac{R_b Z_{tl}(l_p^r)}{R_b + Z_{tl}(l_p^r)}} \right|^2} \tag{5.1}$$

where P_n is the power delivered to the detector as a function of SPB positions l_s and l_p, normalized to that for reference positions l_p^r and l_s^r. These positions were $l_p^r = 0.321\lambda_g$ for the *parallel* element and $l_s^r = 0.488\lambda_g$ for the *series* element, corresponding to the positions for the measurements used to normalize the data. The calculated antenna impedance is Z_a (24 Ω) [6], and R_b is the measured DC resistance of the two bismuth detectors (33 Ω and 42 Ω), which appear in parallel for this circuit (18.5 Ω). The impedance of each CPW transmission line tuning stub, Z_{tl}, is given by Equation 4.4, using Z_0 for the CPW line (78 Ω) from Equation 2.5 and the equivalent termination impedance for the SPB on CPW ($|s_{11}| = -0.06$ dB).

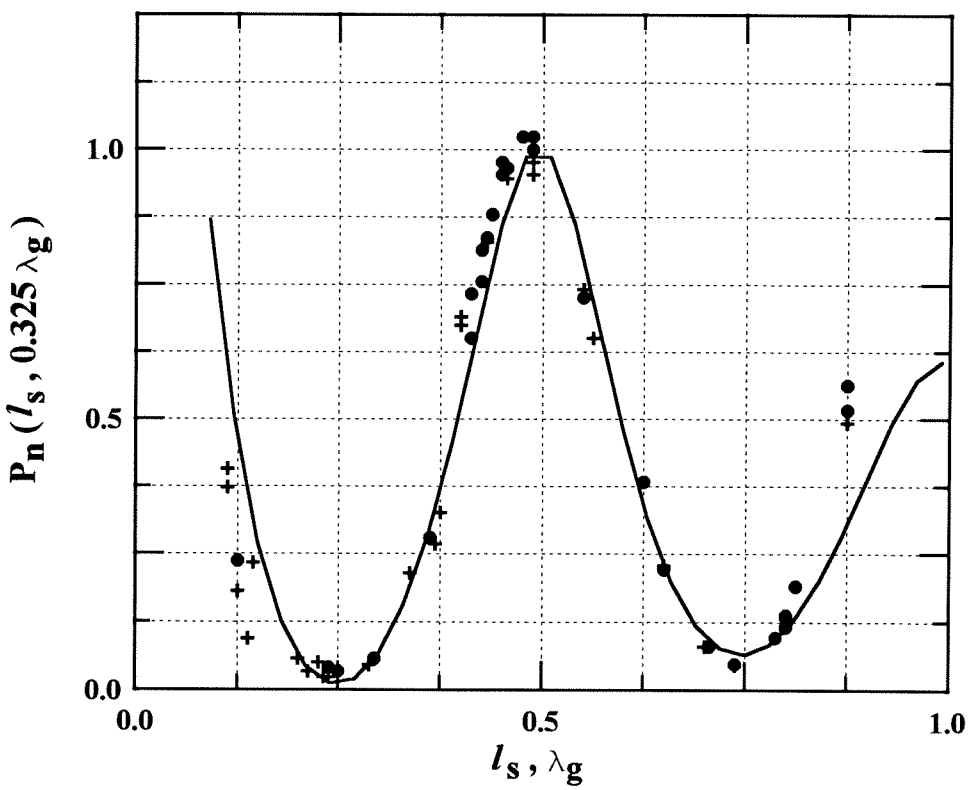

Figure 5.8 Measured (•)(+) and theoretical (—) response for 620 GHz detector circuit. The power absorbed by the detector is shown as a function of the series tuner position, normalized to that for a fixed position ($l_p = 0.321\lambda_g$, $l_s = 0.588\lambda_g$).

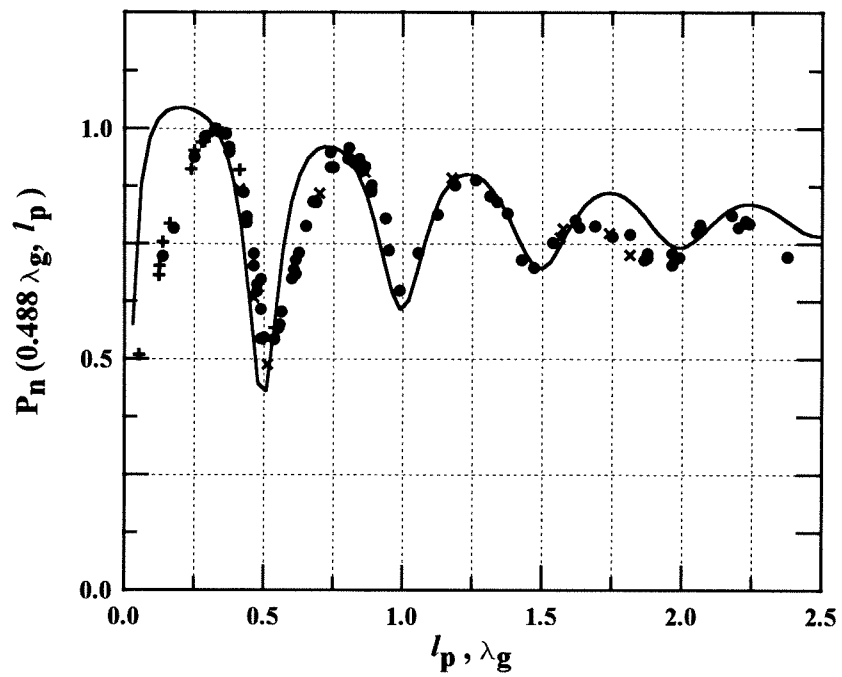

(a)

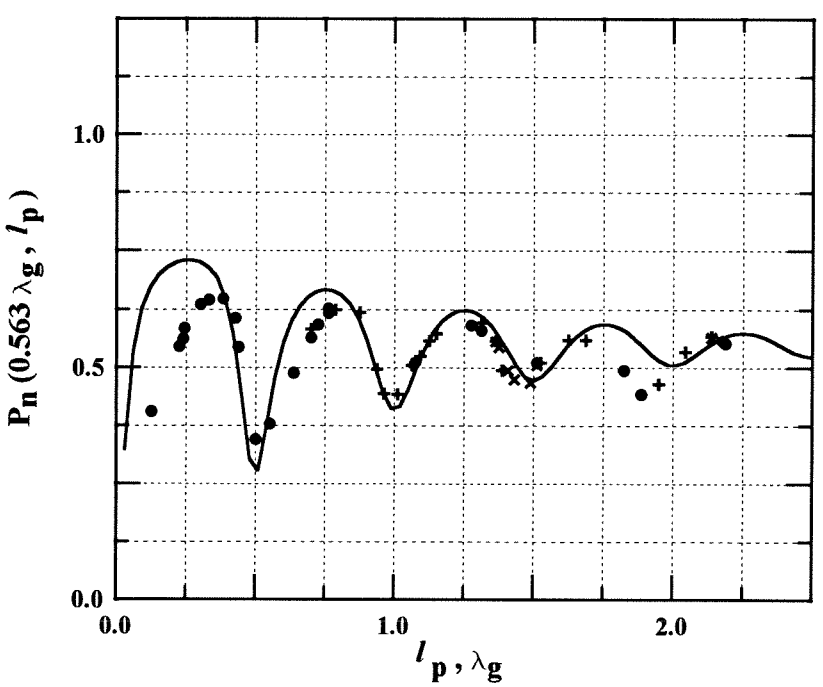

(b)

Figure 5.9 Measured (•)(+)(×) and theoretical (—) response for 620 GHz detector circuit. The detected power, maintaining the reference of Figure 5.8, is shown as a function of the parallel tuner position, for two series tuner positions (a),(b).

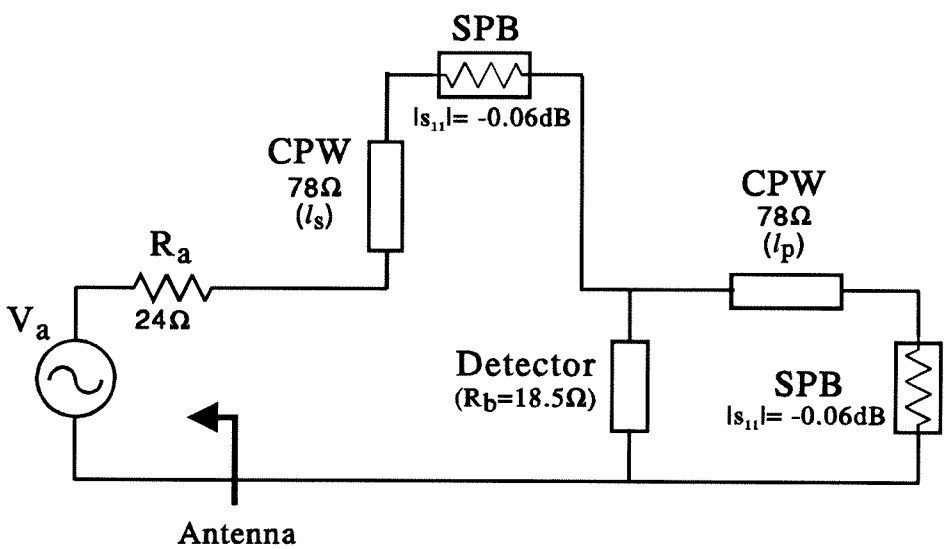

Figure 5.10 Schematic diagram of the equivalent circuit. Two tuning elements vary the impedance match between the antenna and detector.

The attenuation constant, α ($0.6\,\mathrm{dB}/\lambda_g$), and λ_g ($312\,\mu\mathrm{m}$) come from equations 2.13 and 2.6, respectively.

The theoretical response has been included with the measured data in Figures 5.8 and 5.9. While there seems to be some additional coupling-phenomena between the SPB and the antenna, particularly for distances of less than $\lambda_g/2$, the results appear to be consistent with theory. The theoretical range of detector impedances for which this circuit can provide an impedance match to a $24\,\Omega$ antenna is shown in Figure 5.11.

This work demonstrates at 620 GHz, the fabrication and function of a micromechanical tuning element in a monolithic integrated circuit. Two of the micromechanical SPB's were integrated with CPW transmission lines in a quasi-optical detector circuit, and their performance measured. Performance was consistent with a theoretical model, indicating that each SPB showed a return loss of approximately –0.06 dB. The tuning elements were used to vary the power delivered to the detector over a range of almost 15 dB by adding a variable reactance in series with the antenna and a variable susceptance in parallel with the detector. Their fabrication involves processes and materials common to, and compatible with, those typically used in the production of millimeter wave and submillimeter wave integrated circuits.

Such tuning elements can be implemented in a wide variety of monolithic circuit configurations, are easily scaled for use at higher frequencies, and can provide a means for post-fabrication circuit optimization.

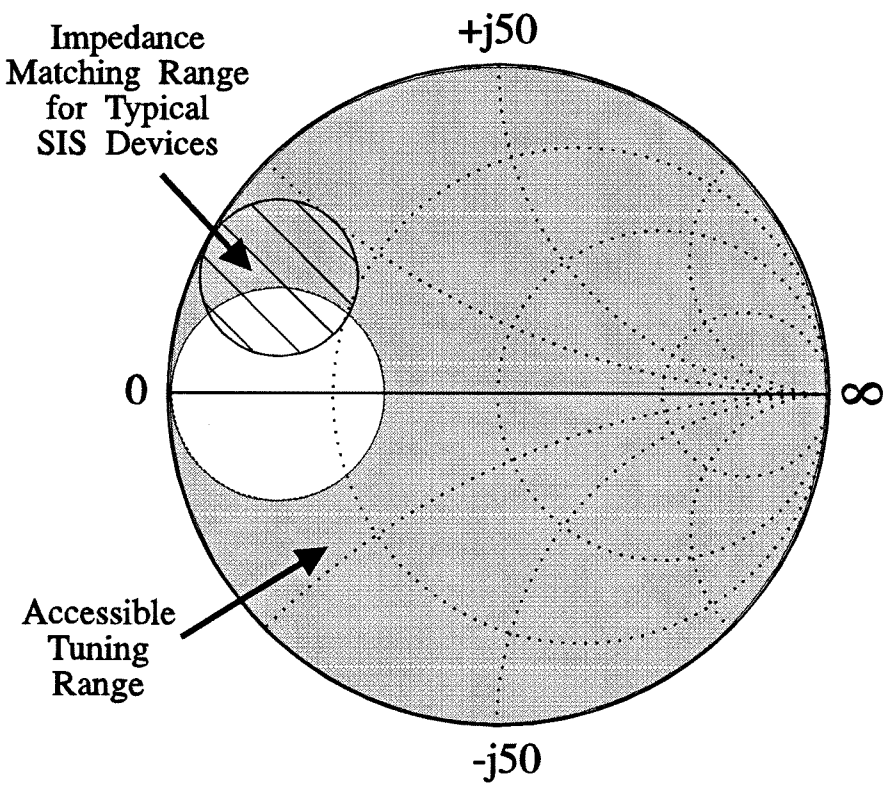

Figure 5.11 Smith chart showing the range of impedances to which the tuning circuit can transform a 24 Ω antenna. The range is based on a lossless system, and includes impedances suitable for matching to SIS devices.

References

[1] V.M. Lubecke, W.R. McGrath, and D.B. Rutledge, "A Micromechanical Tuning Element for a 620 GHz Circuit," *Nineteenth International Conference on Infrared and Millimeter Waves: Conference Digest*, pp. 431–432, October, 1994.

[2]V.M. Lubecke, W.R. McGrath, D.B. Rutledge "Millimeter Wave Performance of a Sliding Planar Backshort," *SPIE International Conference on Millimeter and Submillimeter Waves and Applications-Conference Digest*, pp. 543–544, January, 1994.

[3] J. Zmuidzinas, H.G. Leduc, J.A. Stern, and S.R. Cypher, "Two Junction Tuning Circuits for Submillimeter SIS Mixers," *IEEE Transactions on Microwave Theory and Techniques*, vol. 42, no. 4, pp. 698–706, April 1994.

[4] S.S. Gearhart and G.M. Rebeiz, "A Monolithic 250 GHz Schottky-Diode Receiver," *IEEE Transactions on Microwave Theory and Techniques*, vol. 42, no. 12, pp. 2505–2511, December 1994.

[5] P.A. Stimson, R.J. Dengler, H.G. LeDuc, S.R. Cypher, and P.H. Siegel, "A Planar Quasi-optical SIS Receiver," *IEEE Transactions on Microwave Theory and Techniques*, vol. 41, no. 4, pp. 609–615, April 1993.

[6] G.V. Eleftheriades and G.M. Rebeiz, "Self and Mutual Admittance of Slot Antennas on a Dielectric Half-Space," *International Journal of Infrared and Millimeter Waves*, vol. 14, no. 10, October 1993.

[7] T.-L. Hwang, S.E. Schwartz, and D.B. Rutledge, "Microbolometers for Infrared Detection," *Applied Physics Letters*, vol. 34, no. 11, pp. 773–776, June 1979.

[8] D.P. Neikirk and D.B. Rutledge, "Self-heated Thermocouples for Far-Infrared Detection," *Applied Physics Letters*, vol. 41, no. 5, pp. 400–402, September 1992.

[9] A.B. Frazier and M.G. Allen, "Metallic Microstructures Fabricated Using Photosensitive Polyimide Electroplating Molds," *Journal of Microelectromechanical Systems*, vol. 2, no. 2, pp. 87–94, June 1993.

[10] *Insight Products*, Brighton, MA.

Chapter 6

Discussion and Suggestions for Future Work

In this thesis, the design and fabrication of a new tool for the development and optimization of submillimeter wave monolithic integrated circuits has been described. It is a tuning element called a *sliding planar backshort*, and it can be included as part of a monolithic integrated circuit circuit to allow mechanical adjustment of the electrical length of a planar transmission line.

A semi-empirical approach was employed in its design. Measurements showing an $|s_{11}|$ of better than –0.5 dB over a bandwidth of 50% or more were made for the SPB on both CPS and CPW transmission lines. A frequency scaled version of the SPB was made through photolithographic techniques, and applied in a quasi-optical 100 GHz planar hybrid detector circuit. Its millimeter wave performance was consistent with that of the 2 GHz microwave design model. The SPB was successfully used to vary the response of a Schottky diode in a planar circuit over a range of 14 dB– creating a 3 dB improvement over the untuned response. A technique for fabricating a micromechanical version of the SPB for submillimeter wave circuits was developed, drawing on the advanced MEMS technologies: LIGA and silicon surface-micromachining. Two SPB's were fabricated as part of a fully integrated quasi-optical 620 GHz monolithic detector circuit. Measurements showed that the SPB's were able to successfully vary the power delivered to a thin-film thermoelectric detector over a range of almost 15 dB.

The original motivation for this work was the application of such a device in millimeter and submillimeter wave radiometer circuits. The SPB was demon-

strated to be both realizable and effective in planar circuits operating in the millimeter and submillimeter wave band. While somewhat more complex to fabricate than the fixed tuned structures in existing planar SIS and Schottky heterodyne mixers, the SPB can be employed as a direct replacement for many designs that already utilize CPS and CPW circuitry [1], [2]. This may, however, require that the effect of a cryogenic environment on the materials be addressed.

It has been said that the key word in the future of SIS mixers is *tunerless* [3]. This may be so, in light of the advances being made in planar device technology and fixed broad-band matching circuits used in millimeter wave mixers [4]. Some compromise is made on sensitivity, in return for simplicity of fabrication and operation. At higher frequencies however, limits in device characterization, computer modeling, and fabrication tolerances still lead to circuits which will not function, without some type of post-fabrication tuning. The SPB can play a crucial role in such circuits. It can be used not only as a means for mechanically optimizing performance in a finished mixer design, but also to assist in device characterization and to provide a means for semi-empirical optimization of fixed circuit dimensions in developmental mixers [5].

Applications for this device are not limited to receivers. Recent developments in the fabrication of planar varactor diodes [6], [7], and monolithic transistors [8], have resulted in a strong interest in the development of planar multipliers and oscillators for terahertz frequencies.

One promising new approach for a submillimeter wave frequency tripler circuit employs a novel integrated back-to-back barrier-N-N^+ (bbBNN) varactor diode in a split-waveguide block [9]. This device is a significant advance over whisker-contacted varactors in terms of mechanical robustness. Although novel, the split-waveguide implementation does not take full advantage of the planar bbBNN structure, as evidenced by the complex waveguide tuning circuit shown in Figure 6.1. The device is integrated with microstrip RF and bias filters, and inserted in an

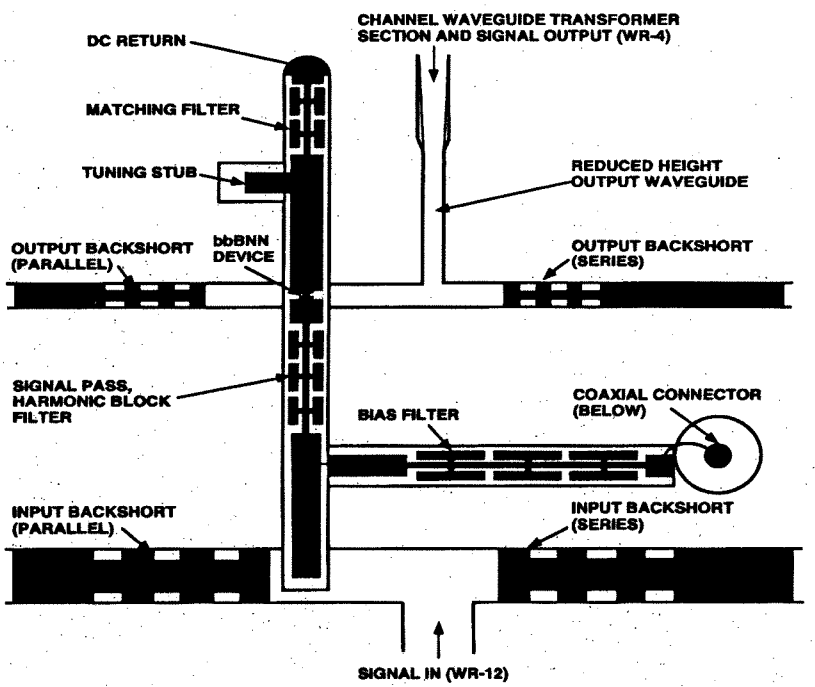

Figure 6.1 Integrated back-to-back barrier-N-N^+ varactor diode tripler using a split-waveguide block [9]. A coplanar version of this circuit with SPB's would better exploit the planar structure of the device.

arrangement of waveguide channels which include two backshort tuners at both the input and output. A fully planar version of this tunable multiplier, on coplanar media, would benefit from simplicity of fabrication, reproducibility, and reliability. As with receivers, several multipliers can be combined in a focal plane array without complicating the fabrication procedure. An SPB could play an essential role in the development of such a circuit.

A quasi-optical planar approach for a frequency doubler is shown in Figure 6.2. It was designed by Kim *et al.* [10] and uses a novel planar quad-bridge diode along with two cross-polarized slot antenna pairs on a dielectric substrate-lens. The unique symmetry of the quad-bridge diode alleviates the need for complex input and output filters. This allows for the design of a circuit whose bandwidth is governed primarily by the antennas. The addition of CPW tuning stubs with integral SPB's (as shown in Figure 6.2) could create a variable reactance in series with each antenna, and allow for adjustment of the frequency of operation. As with receivers, the SPB could play a role in the semi-empirical development of a fixed-tuned circuit, as well as provide post-fabrication tuning for a final product.

The development of submillimeter wave oscillators can also benefit from the use of SPB's. A design for a quasi-optical planar three-terminal transistor oscillator is shown in Figure 6.3. It consists of a slot antenna coupled to a transistor with a CPW transmission line. The antenna impedance is a parameter in the oscillator design, and fixed length CPW tuning stubs at the source and gate are used to maximize the reflection coefficient at the drain of the device [11]. This circuit was used for an oscillator employing an InP-based HFET to achieve oscillations of 155 GHz and 215 GHz. The integrated-quasi-optical approach provided the freedom to fabricate many different designs between 150 GHz and 500 GHz, yet the lack of tuning capabilities prevented initial designs from oscillating, and thus, from providing useful information for the iterative design process [12]. The length of the CPW tuning stubs, as well as the impedance of the antenna, could be made

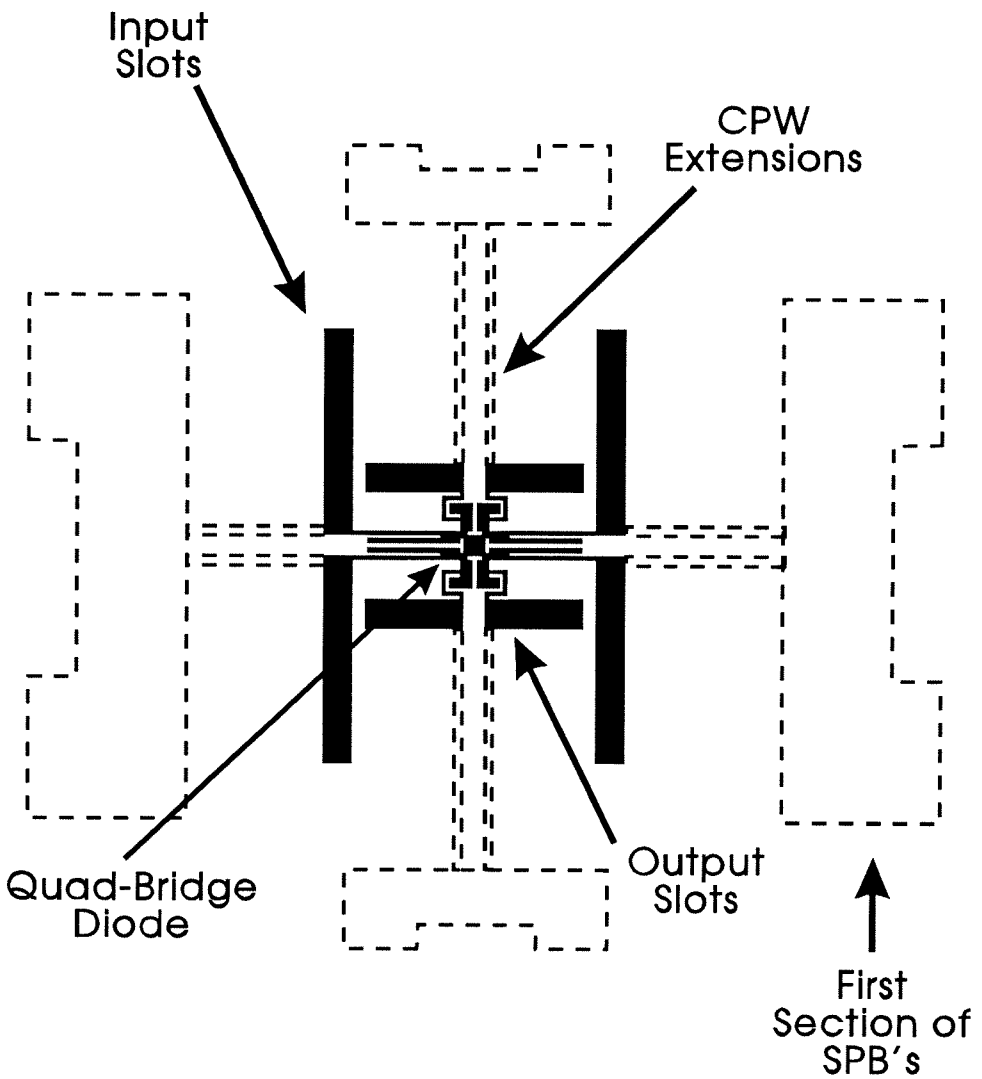

Figure 6.2 Planar quad-bridge diode frequency multiplier [10]. Dashed lines illustrate how SPB's can be added to the circuit to provide post-fabrication tuning.

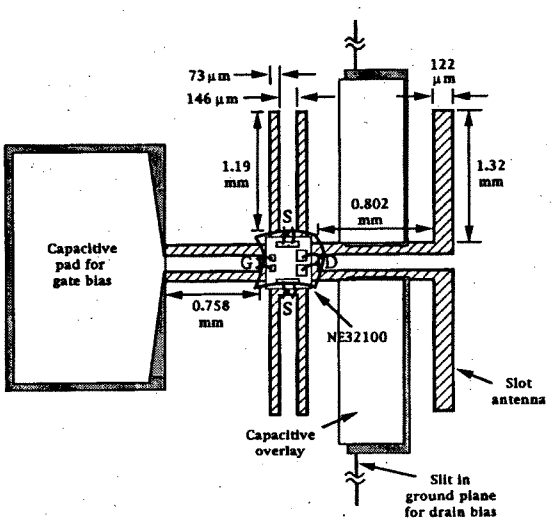

(a)

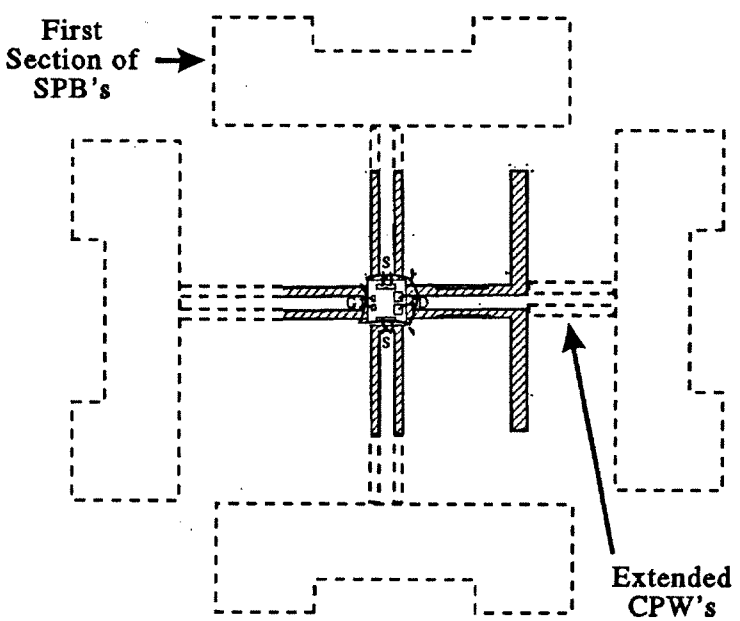

(b)

Figure 6.3 CPW-fed active slot antenna (a). Dashed lines illustrate how SPB's can be added to the circuit to provide post-fabrication tuning (b).

adjustable by direct addition of one or more SPB's, as shown in Figure 6.3.

One remaining issue of note, is the challenge presented in the manipulation of higher frequency SPB's. At 620 GHz the SPB described in Chapter 5 was only 200 μm-wide, and difficult to position manually. As the frequency of operation increases, SPB dimensions become even smaller. One method of addressing this problem appeared in the original design of the 620 GHz quasi-optical detector circuit shown in Figure 6.4, which placed the circuit near the second elliptical focus of an extendable hyperhemispherical lens [13]. This design separated the mechanical side of the circuit from the incoming signal, thus isolating them sufficiently for the use of optical fiber micro-positioners, which held probes in permanent contact with each SPB to facilitate high precision manipulations. The low signal levels available from the BWO source used for the measurements described in Chapter 5 prohibited the detection of any signal in this configuration, thus preventing optical optimization. The approach described in Chapter 5, which placed the circuit much closer to the source in a more robust optical arrangement, was therefore adopted.

Various micron-scale electromechanical stepper-motors and linear translators have been photolithographically fabricated, and could potentially be combined with an SPB [14]. Unfortunately, these motors typically involve fabrication processes and high-voltage driving pulses which are incompatible with the sensitive active devices addressed in this work. Alternatively, electromechanical positioning could be accomplished through the use of thin-film materials which expand and contract with application of DC current or voltage. This concept is illustrated in Figure 6.5, where the deformation of a half-loop of current sensitive material is used to displace an SPB.

Adjustable tuning elements have played an invaluable role in the development of a wide range of microwave circuits. As planar submillimeter wave device technology matures, many new circuits will be developed for this frequency band and beyond, and micromechanical planar tuning elements, like the SPB, can prove

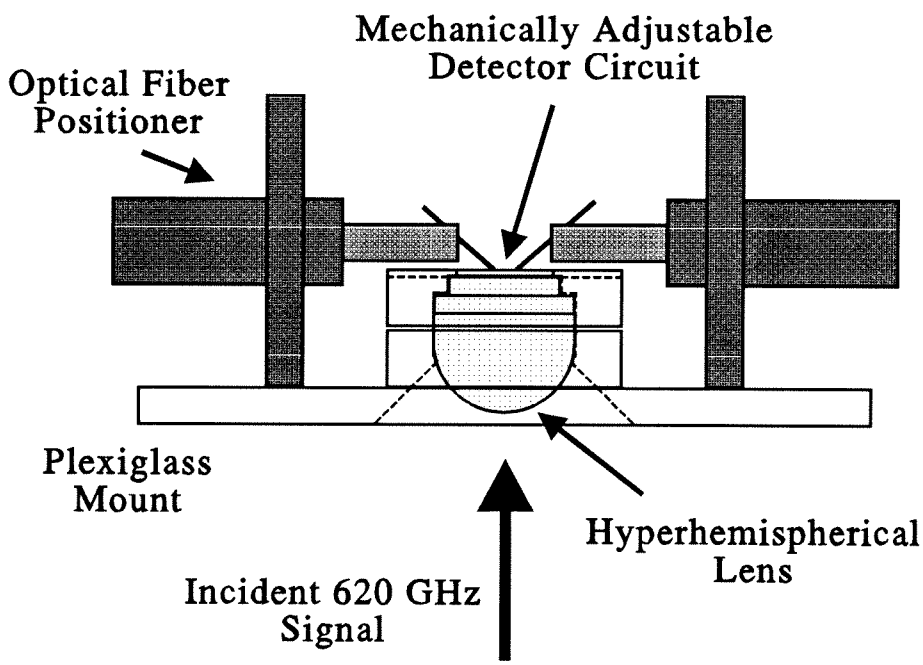

Figure 6.4 Hyperhemispherical mount for planar quasi-optical submillimeter wave circuit with SPB's. Fiber optic micropositioners move the SPB's and are isolated from the incoming signal.

to be useful tools in this process.

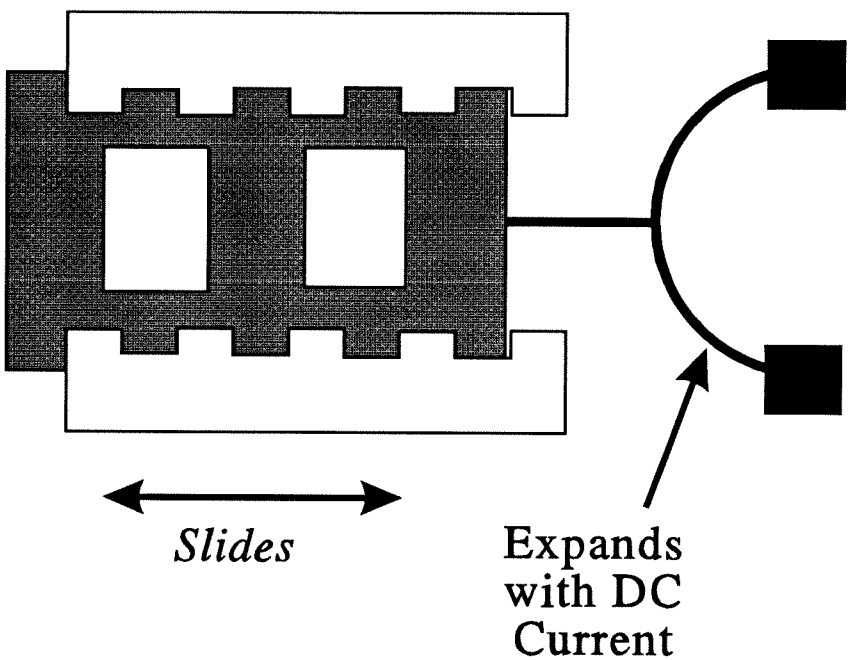

Figure 6.5 An electromechanical SPB. A half-loop of current sensitive material moves the SPB upon application of a DC current.

References

[1] S.S. Gearhart and G.M. Rebeiz, "A Monolithic 250 GHz Schottky-Diode Receiver," *IEEE Transactions on Microwave Theory and Techniques*, vol. 42, no. 12, pp. 2505–2511, December 1994.

[2] P.A. Stimson, R.J. Dengler, H.G. LeDuc, S.R. Cypher, and P.H. Siegel, "A Planar Quasi-optical SIS Receiver," *IEEE Transactions on Microwave Theory and Techniques*, vol. 41, no. 4, pp. 609–615, April 1993.

[3] S. Weinreb, private communication, June 1994.

[4] A.R. Kerr, S.-K. Pan, A.W. Lichtenberger, and D.M. Lea, "Progress on Tunerless SIS Mixers for the 200–300 GHz Band," *IEEE Microwave and Guided Wave Letters*, vol. 2, no. 11, pp. 454–456, November 1992.

[5] C. Mann, private communication, June, 1995.

[6] M.A. Frerking and J.R. East, "Novel Heterojunction varactors," *Proceedings of the IEEE*, vol. 80, pp. 1853–1860, November 1992.

[7] T.W. Crowe, R.J. Mattauch, H.P. Roser, W.L. Bishop, W.C.B. Peatman, and X. Liu, "GaAs Schottky Diodes for THz Mixing Applications," *Proceedings of the IEEE*, vol. 80, no. 11, pp. 1827–1841, November 1992.

[8] L.D. Nguyen *et al.*, "50-nm Self-Aligned Pseudomorphic AlInAs/GaInAs High Electron Mobility transistors," *IEEE Transactions on Electron Devices*, vol. 39, no. 9, pp. 2007–2014, September 1992.

[9] D. Choudhury, P.H. Siegel, R.P. Smith, A.V. Räisänen, S.C. Martin, and M.A. Frerking, "Integrated Back to Back Barrier-N-N^+ Varactor Diode Tripler Using a Split-Waveguide Block," *IEEE Transactions on Microwave Theory and Techniques*, vol. 43, no. 4, pp. 948–954, April 1995.

[10] M. Kim, *et al.*, "Planar Quad-Bridge Diode Frequency Multiplier, to be submitted to *IEEE Transactions on Microwave Theory and Techniques*, 1995.

[11] B.K. Kormanyos, W. Harkopus Jr., L.P. Katehi, and G.M. Rebeiz, "CPW-Fed Active Slot Antennas," *IEEE Transactions on Microwave Theory and Techniques*, vol. 42, no. 4, pp. 541–545, April 1994.

[12] G.M. Rebeiz, "The Highest-Frequency (155 GHz and 215 GHz) Three Terminal Transistor Oscillator in the World Reported," *IEEE Antennas and Propagation Magazine*, vol. 36, no. 2, pp. 36–38, April 1994.

[13] D.F. Fillipovic and G.M. Rebeiz, "Double-Slot Antennas on Extended Hemisphperical and Elliptic Quartz Dielectric Lenses," *International Journal of Infrared and Millimeter Waves*, vol. 14, no. 10, pp. 1905–1924, October 1993.

[14] T. Akiyama and K. Shono, "Controlled Stepwise Motion in Polysilicon Microstructures ," *IEEE Journal of Microelectromechanical Systems*, vol. 2, no. 3, pp. 106–110, September 1993.

Appendix

Fabrication of the Micromechanical Integrated Circuit

The following is a step-by-step description of the fabrication process for the micromechanical 620 GHz integrated circuit used in the experiment described in Chapter 5. Development and optimization of this procedure formed a major part of the thesis. Micromechanical circuits are often more difficult to fabricate than purely electrical ones, as layer mechanical properties are critical, in addition to their electrical properties. They also require the application of many consecutive structural layers and attention must be paid to their vertical characteristics as well has horizontal patterns. Film thickness and uniformity must be tightly controlled to ensure the correct behavior of sacrificial layers, guides, sliders, etc. In many cases, several different layer materials and application techniques were tried before determination of the optimum layer composition.

The circuit was fabricated on a fused-quartz wafer, 18 mm in diameter and 250 μm thick. Three to eight wafers were typically processed, simultaneously. The eight layer fabrication process requires seven masks which consisted of chrome or iron-oxide patterns (completely opaque to 400 nm UV radiation) on white-crown glass laid out by a CAD program and written using electron beam technology.

1. *Wafer Cleaning:* Scrupulous cleanliness is essential for circuits with features on the micron scale, especially if these features span a relatively large area. A single particle of contaminant, such as polishing grit, dust, or lint can ruin the entire circuit by interrupting a narrow track or bridging a narrow gap. The wafer was thoroughly cleaned by first rubbing soapy distilled (DI) water

on the surface with a gloved hand, then soaking the wafer in 40°C DI water within an ultrasonic bath, and then rinsing in DI water, again in an ultrasonic bath.

2. *Antenna and CPW, Layer 1:* This layer forms the antenna and CPW's, and contains a high-resolution pattern which must span a large area on the wafer. It is formed by multiple etchings rather than lift-off, in order to insure a smooth-edged metal interface where the detector is ultimately applied.

   (a) *Wafer Mounting:* Several wafers onto a 3×2 in glass slide by resting each wafer on the slide, over a dab of Apiezon M® [1] vacuum grease, and heating the slide to 55°C on a hot plate. This tightly affixes the wafers to the slide in a simple, quick and removable fashion, and simplifies wafer mounting in the evaporator. Wafers with resist and metal on them can be safely removed after evaporation by again heating the slide and pushing the wafer off the the edge with tweezers. The wafers can then be cleaned by a brief dip in trichloroethylene, with mild agitation.

   (b) *Layer 1 Deposition:* A 60 Å-thick adhesion layer of chrome, followed by a 1000 Å layer of gold, and then another 60 Å layer of chrome was evaporated onto the wafer. The final chrome layer served as an adhesion layer for the following evaporation, and also served as a protective coating over the regions of gold which were ultimately exposed before deposition of the bismuth detector film. An electron-beam evaporator was used for this step, at an initial vacuum level of 1×10^{-7} torr (cryopump) and a 10-30 mA beam current (at 4 kV) which produced deposition rates of 10-30 Å/sec.

   (c) *Layer 1 Pattern:* The first mask was used to create photoresist patterns for the etching of the antenna and CPW's. The wafers were primed by applying AZ Adhesion Promoter-fineline® [2] (hexamethyldisilizane), waiting for 10 sec, and then spinning at 4000 r.p.m. for 60 sec. Al-

though this adhesion promoter was developed for improving adhesion to silicon, the priming step seemed to assist adhesion on most surfaces, possibly acting as a final cleaning-dehydration step. Then AZ 5214E [2] photoresist was applied from a syringe through a 0.2-μm filter and each wafer spun at 5000 r.p.m. for 60 sec to obtain a 1.3 μm-thick coating. The wafers were softbaked on a hotplate at 90°C for 60 sec. Each wafer was aligned under Mask 1, taking care that no flaws in the resist or metallization appeared along the CPW patterns of the mask. The resist was exposed at 180 mJ/cm^2 of 400 nm UV radiation. The patterned resist was then developed by soaking for approximately 60 sec in a 3:1 solution of DI water and AZ 400K® Developer [2], then rinsing for 60 sec in DI water, applying mild agitation throughout the process. The wafers were blown dry and the patterns inspected under a microscope for residual debris. Unwanted particles were removed from along the CPW patterns by sweeping the general area with a small delicate fiber. The resist was then hardbaked by heating the wafer to 115°C on a hot-plate for 5 min. Baking too long or at too high a temperature will make the resist difficult to remove, while too little baking will leave the photoresist pattern susceptible to over etching.

(d) *Layer 1 Etch:* Using tweezers, each wafer was dipped in Transene® [3] chromium mask etchant (a ceric sulfate solution) and gently agitated for 40 sec. This was followed by a brief dip in a solution of 10 parts DI water and 1 part sulfuric acid, before rinsing in DI water. The wafers were then dried and inspected to see that the gold layer was exposed within the pattern, and repairs were made to any problem areas in the patterned resist, as before. The gold layer was etched in Transene type TFA® [3] gold etchant (an iodine-base solution) using mild agitation, and then rinsed in DI water. The wafers were then dried and inspected,

and the chrome etch process repeated.

(e) *Layer 1 Re-Pattern and Etch:* The circuit was patterned with photoresist as before, this time using Mask 2. This step made the circuit highly transparent to 620 GHz radiation by removing most of the ground plane. This can be seen in Figure A.1. This etching step required more time than the first, but could be processed more vigorously since its pattern was far less critical. By etching this pattern separately, better control was allowed when etching the more critical patterns in Step 2(d).

3. *Insulator, Layer 2:* This layer forms the dielectric coating which separates the CPW and the SPB.

(a) *Layer 2 Pattern:* Photoresist was applied to the wafers as before, and exposed at 180 mJ of UV radiation under Mask 3; this step defined windows in the dielectric coating which will allowed for subsequent application of the detector and bonding wires for external electrical connection. The wafers were soaked in chlorobenzene for $3\frac{1}{2}$ min to harden the outer surface of the resist. The wafers were blown dry, then baked on a hotplate at 90°C for 20 sec, and developed as before. The hardened surface of the photoresist develops more slowly, but once penetrated, the inner photoresist develops more rapidly. After 2-3 min, the outer photoresist still holds the pattern, while the inner photoresist had develops beyond the pattern. This resulted in an inverted-slope resist edge profile which prevents the next deposition from coating the sidewalls of the resist, and produces a clean lift-off edge. An alternative, image-reversal process [4] was used in making the circuit actually tested in the experiment described in Chapter 5, however, the process described here was found to be more reliable, and the results were more easily reproduced. Care should be taken not to hard-bake this photoresist, as it must be exposed to high temperatures in the following step which could lead to

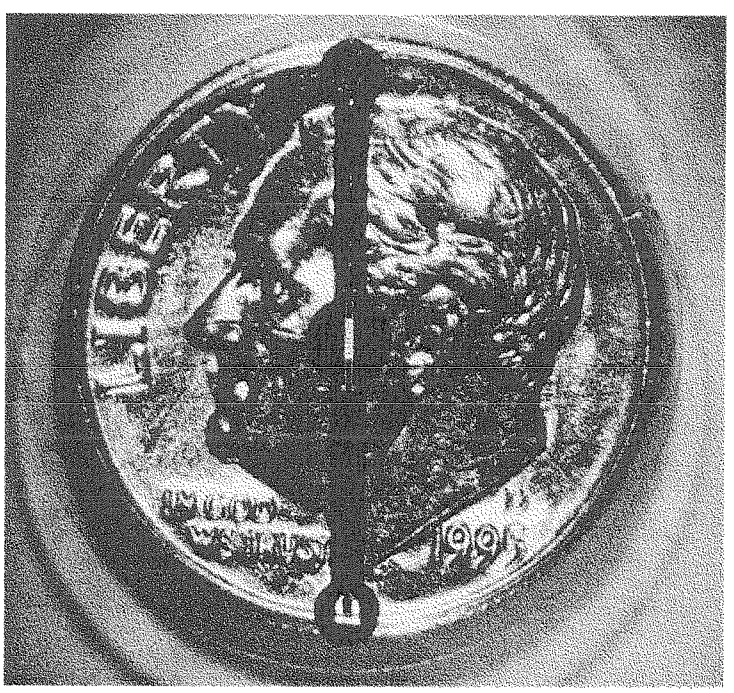

Figure A.1 Micrograph of the submillimeter wave circuit on a fused-quartz wafer. The size of the wafer is comparable to that of a common U.S. coin (dime).

over-baking.

(b) *Layer 2 Deposition:* A 1000 Å layer of silicon-dioxide was sputtered onto the wafer. Reactive RF magnetron sputtering was used for this step to obtain good adhesion and edge coverage without exposing the wafer to excessive temperatures. The process was carried out in a 3×10^{-7} vacuum (cryopump), with a 3 in Si wafer used as a target, and 225 W of power. Total gas pressure was 1×10^{-3} torr with flow rates of 50 cm^3/sec for argon, and 10 cm^3/sec for oxygen.

(c) *Layer 2 Lift-Off:* The photoresist and unwanted portions of silicon-dioxide were then removed (lift-off) by soaking the wafer in acetone for one hour, then in an acetone bath with ultrasonic agitation for 1 min, then placing the wafer in isopropyl alcohol (IPA) and scrubbing the pattern with a cotton swab, and finally placing this solution in an ultrasonic bath for 1 min. The results are shown in Figure A.2(a).

4. *SPB, Layers 3-6:* These layers make up the SPB. A copper sacrificial layer and coating are used to create a sliding gold backshort, captivated by polyimide guides.

(a) *Sacrificial/Seed Film, Layer 3 Pattern, Deposition, and Lift-Off :* A reverse-profile photoresist pattern was formed as in Step 3(a), now using Mask 4. A 60 μm adhesion layer chrome was evaporated, followed by a 1700 Å layer of copper. This was carried out as in Step 2(b), and formed a sacrificial-seed layer for the sliding gold element. The pattern was lifted in acetone, this time using only mild agitation during the soak. Stubborn lift-off's were assisted by placing the problem wafer in a shallow dish of IPA and gently disturbing the lose metal film with a soft, teflon probe. This layer is shown in Figure A.2(b).

(b) *SPB Mold Application:* The wafers were primed and AZ 4620® photoresist was applied as before when using with AZ 5214E®, but this time

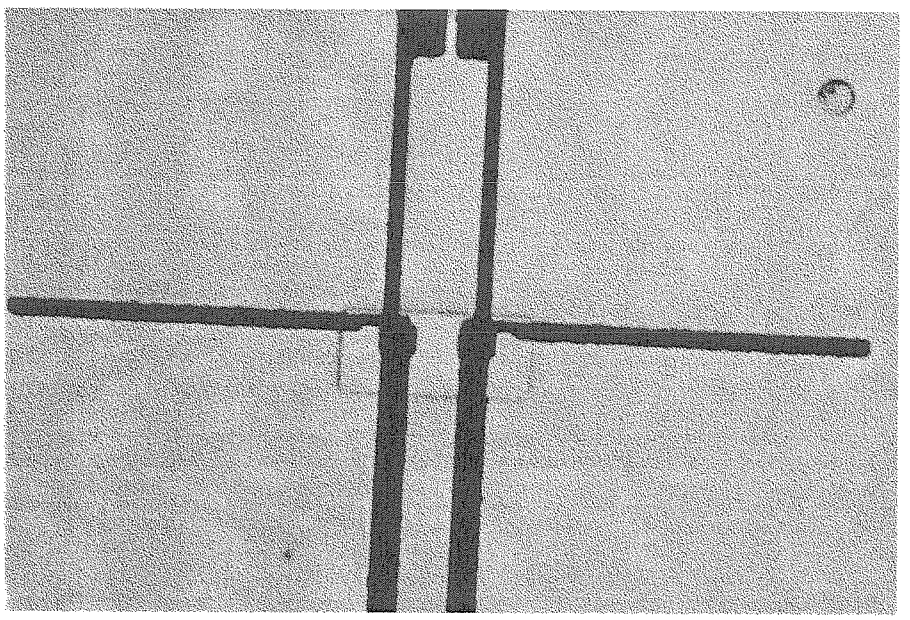

(a)

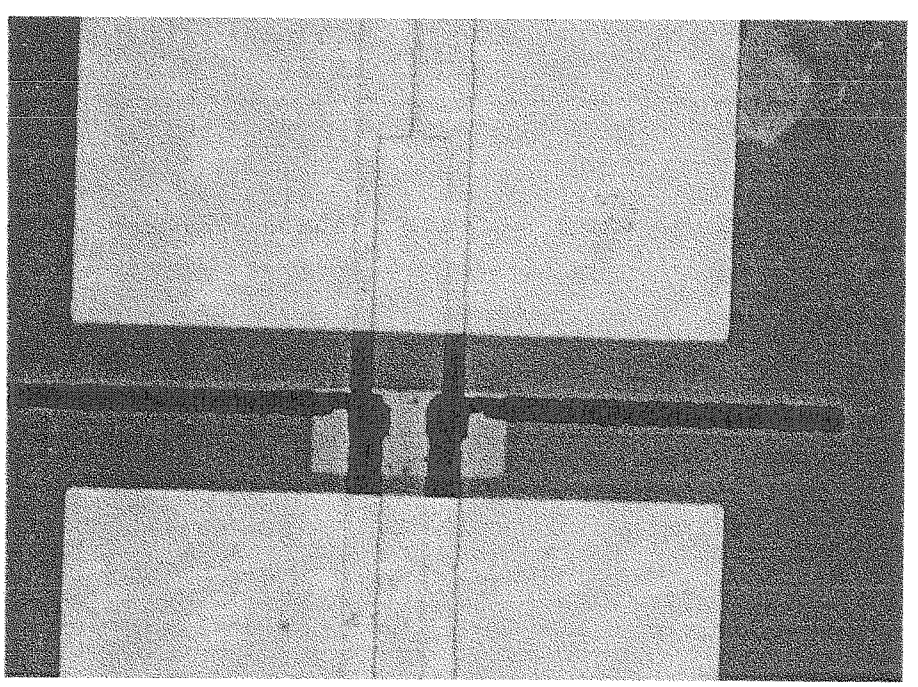

(b)

Figure A.2 Micrographs of the circuit after deposition of Layer 1, the dielectric insulator (a), and Layer 2, the sacrificial/seed metal (b). This circuit included a CPW choke filter which allowed it to operate with only one SPB.

spun at 3000 r.p.m.. This was exposed at 540 mJ of 400 nm UV radiation under Mask 5, developed as in Step 2(c), and hardbaked at 115°C to obtain an 8 μm-thick mold in which gold could be electroplated onto the exposed regions of the copper sacrificial-seed layer. This layer is shown in Figure A.3 along with a plot of the vertical profile.

(c) *SPB, Layer 4 Deposition:* Each wafer was soaked in DI water using a small polyethylene beaker, and placed in an ultrasonic bath for a few seconds. This was done to gently remove any trapped gasses from the mold. An electrode (cathode) was connected to the copper pattern at the edge of each wafer using a small, toothless alligator-clip, and the circuit was submersed in Sel-Rex®Pur-A-Gold® 125 gold electroplating solution [5] (cyanide-based). The solution was kept at 40°C and agitated with a magnetic spinner. Using 70 μA, it took about 25 min to plate 5 μm of gold onto the 2.3 mm^2 of exposed copper, including two 1mm^2 openings which allowed for the use of a higher and more maintainable plating current. The circuit was monitored during electroplating to prevent the formation of bubbles on the pattern, and the final thickness tested with a Sloan Dektak IIA surface profiler. The results of this step are shown in Figure A.4. After rinsing the wafer in DI water, the photoresist mold was removed by soaking in N-methyl pyrrolidone at 60°C for one hour. Residue from this layer can be stubborn, but must be thoroughly removed for the next step to be successful.

(d) *Sacrifical Coating, Layer 5 Deposition:* Again, an electrode (cathode) was connected to the copper pattern at the edge of the wafers, and this time the each circuit was submersed in Sel-Rex®Cubath®acid copper electroplating solution [5] (sulfuric acid solution), deep enough to cover the metal pattern up to a reference mark. The solution was kept at 25°C, agitated with aeration and/or a magnetic spinner, and 570 mA

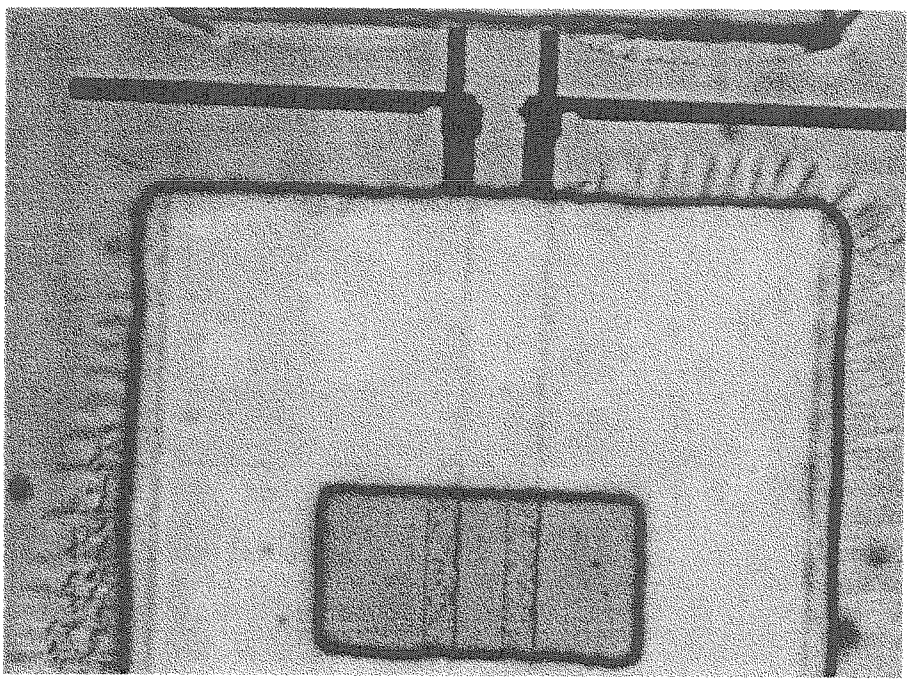

(a)

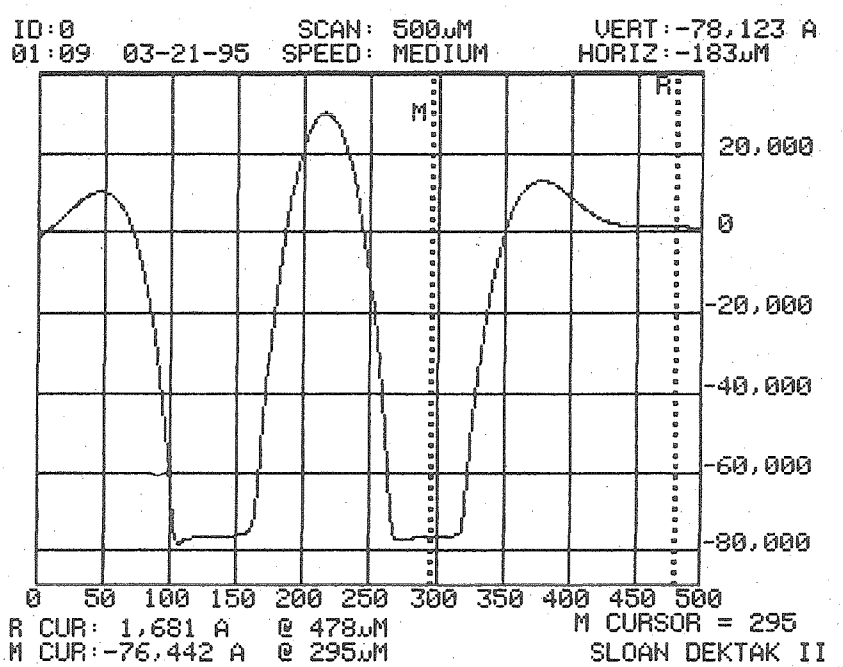

(b)

Figure A.3 Micrograph of the circuit after deposition of the SPB mold (a), and Dektak plot of the vertical profile across the width of the SPB pattern (b).

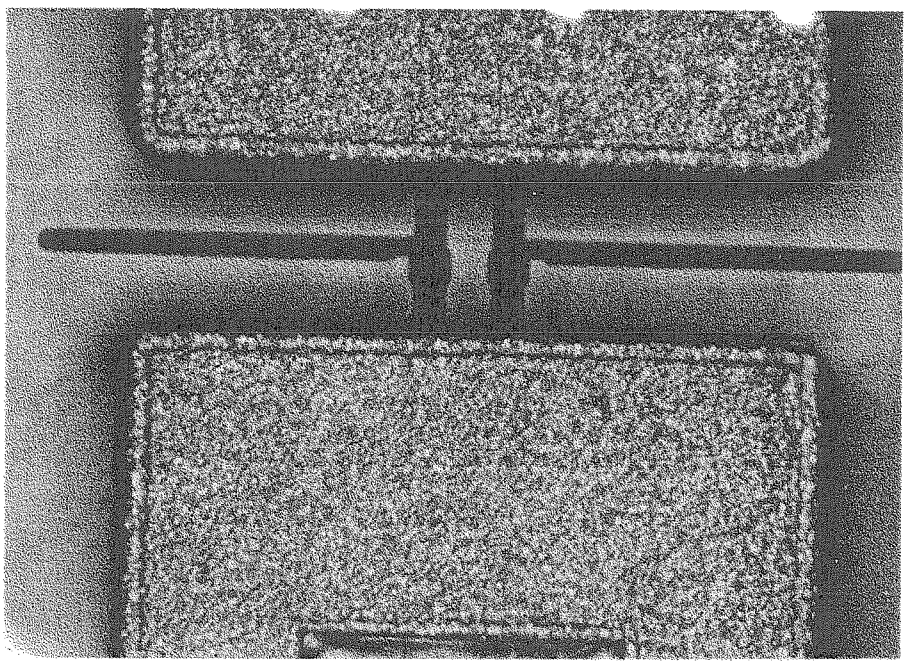

(a)

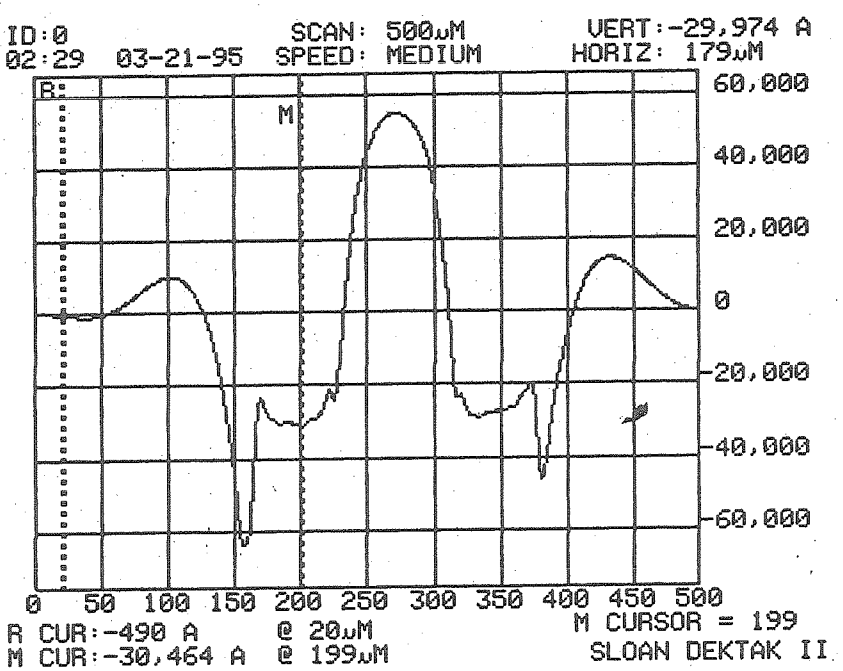

(b)

Figure A.4 Micrograph of the circuit after deposition of the Layer 4, the metal SPB (a), and a plot of the surface profile across the width of the SPB and mold (b).

of current was applied for 3 min 10 sec to plate approximately 1 μm of copper onto the 5.2 mm^2 of submersed metal, forming a sacrificial coating. The results of this step are shown in Figure A.5.

(e) *Guides, Layer 6 Deposition and Pattern:* To promote adhesion for polyimide, each wafer was primed by applying a few drops of fresh 9:1 (QZ 3290® Adhesion Promoter Solvent : QZ 3289® Adhesion Promoter Concentrate® [6]) aminosilane solution, pausing 10 sec, spinning the wafer at 3000 r.p.m. for 60 sec, and then baking the wafer at 110°C for 20 sec. Then HTR 3-200® Photosensitive Polyimide Precursor [6], was spun on at 3000 r.p.m. for 60 sec, and softbaked for 3 min at 100°C. After testing the 13 μm-thick film to insure that it was not still tacky (especially the edge bead), each wafer was exposed at 720 mJ/cm^2 of 400 nm UV radiation under Mask 6, which defined the geometry for the guide structures. The thick film was develop by dipping each wafer first in pure HTR D-2® Selectiplast® Developer [6] for 40 sec (with vigorous agitation), then 1:1 (HTR D-2® : IPA) for 20 sec (again with agitation), and finally in pure IPA for 20 sec (agitated).

(f) *Layer 6 curing:* The patterned film was cured to form a robust polyimide structure. Using a hot-plate, each wafer was heated to 250°C by increasing the temperature at a rate of 150°hr. The wafers were in an inert gas environment while at temperatures exceeding 150°C, in order to prevent oxygen from reacting with the film. This was accomplished by surrounding the wafers with a hollow cylinder (a glass lantern globe or column of aluminum foil can be used), and running a copper pipe down from its top to a point near the surface of the hot-plate, to feed a weak but steady flow of dry nitrogen to the wafers. The curing temperature was maintained for three hours, and then the wafers were returned to room temperature at the same rate used for heating. This produced

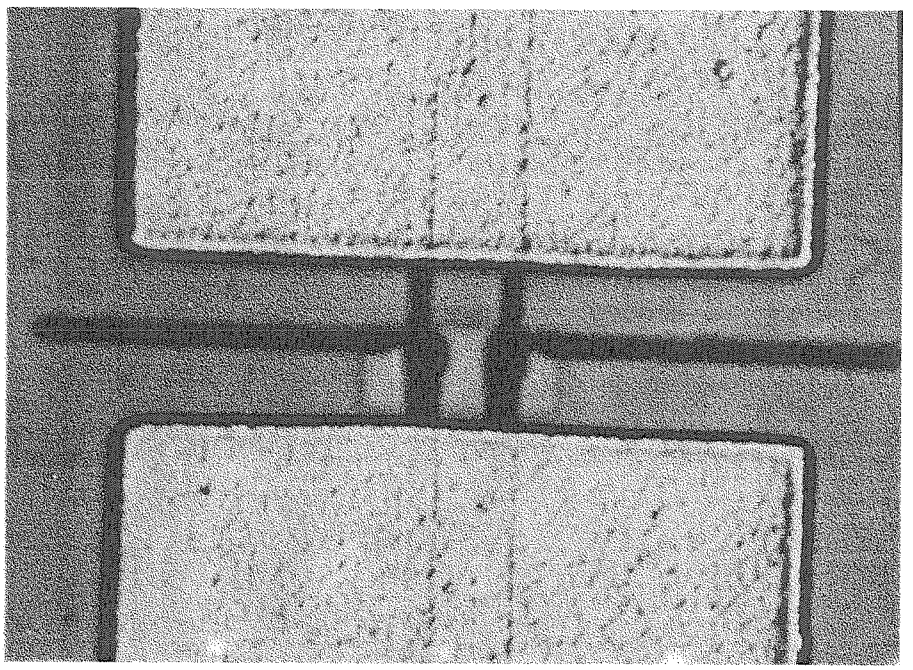

(a)

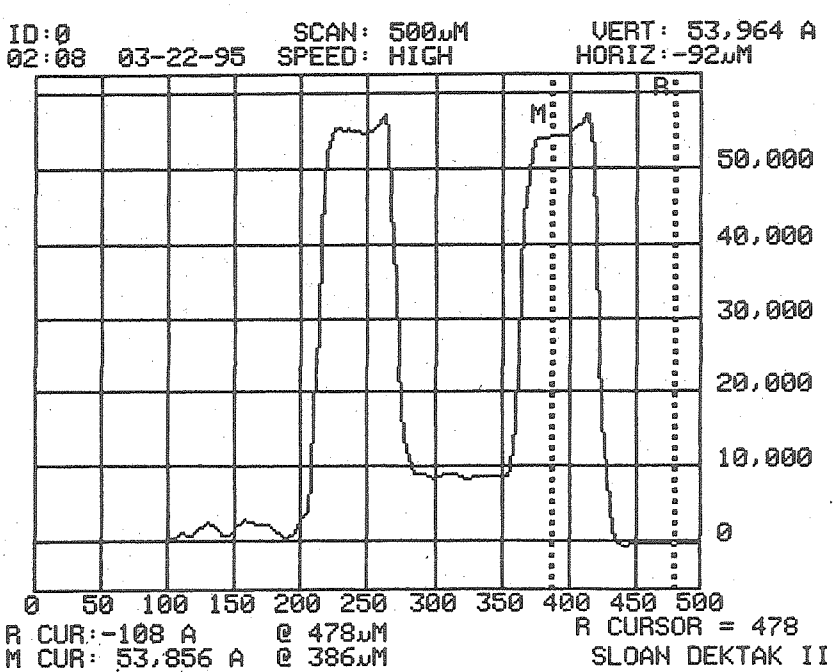

(b)

Figure A.5 Micrograph of the circuit after deposition of the Layer 5, the sacrificial coating (a), and Dektak plot of the vertical profile across the width of the coated SPB (b).

two 9 μm-thick strips of polyimide which anchored to the wafer on one edge, and overlapped the copper-coated gold structures on the other. The results of this step are shown in Figure A.6.

(g) *Release of SPB:* Each wafer was soaked in Transene®Copper Etchant Type CE-100 (a hydrochloric acid mixture) for 1–3 hours to dissolve the sacrificial copper, and thus release the gold SPB structures to slide freely under the polyimide guide structures. The remaining chrome adhesion layer, as well as the chrome within the windows in the dielectric, was then etched away as in Step 2(d). Each wafer was rinsed in DI water and blown dry. It should be noted that this technique sometimes allows the sliding structures to cling to the wafer. An alternative approach is to dry the circuit by rinsing in methanol, and then boiling the methanol away on an 80° hot-plate. Released SPB structures are shown in Figure A.7.

5. *Detector, Layer 7:* This layer forms the thermal detector.

(a) *Layer 7 Pattern and Deposition:* Using AZ 5214E, a photoresist lift-off stencil was patterned as in Step 3(a), this time using Mask 7. The large mechanical structures prevent the mask from making good contact with the resist, and can result in a slightly over-sized pattern. This can be compensated for in the design of the mask, and by varying the final thickness when evaporating the detector film. Attempts were made to use AZ 4620 to get a planarized resist layer, but it was not possible to get a profile that was adequate for lift-off. At this point, bismuth had to be deposited in such a way as to ensure a good-quality film with good edge coverage, which would lift-off cleanly to form a detector with the desired resistance. Bismuth was deposited using a thermal evaporator at a vacuum level of 1×10^{-7} torr, using a current of 45 mA. A total thickness of 6000 Å was quickly deposited (40 Å/sec), through two sequential 45°-angled evaporations, each from opposing sides of the CPW.

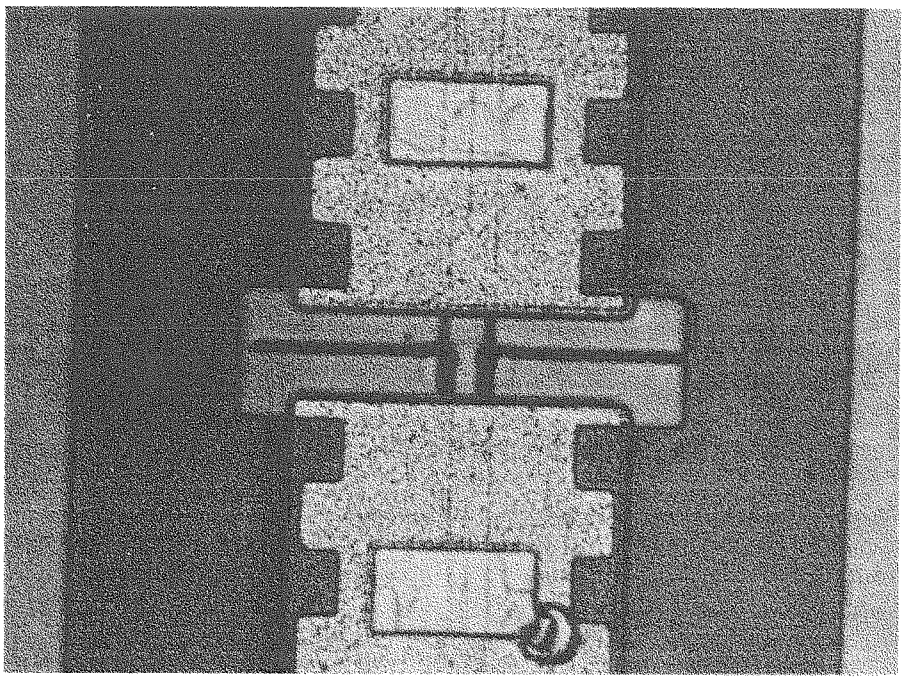

(a)

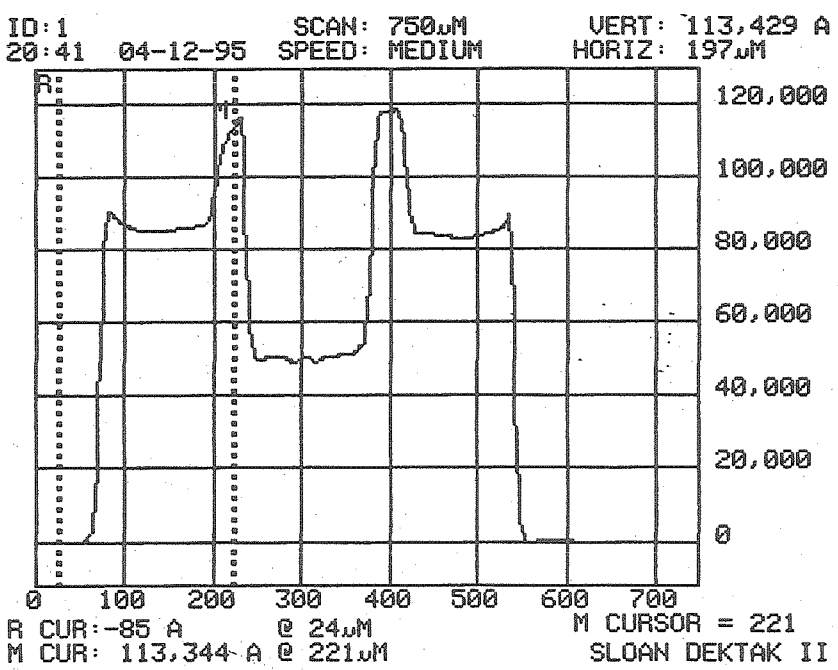

(b)

Figure A.6 Micrograph of the circuit after deposition of the Layer 6, the guide structures (a), and Dektak plot of the vertical profile across the width guides and coated SPB (b).

The wafers were removed from the glass slide mount using temperatures less than 30°C, as heat is detrimental to the bismuth film.

(b) *Layer 7 Lift-Off:* The pattern was lifted in acetone, with some subsequent manual assistance applied while soaking the wafer in a shallow dish of IPA. The finished circuit is shown in Figure A.8.

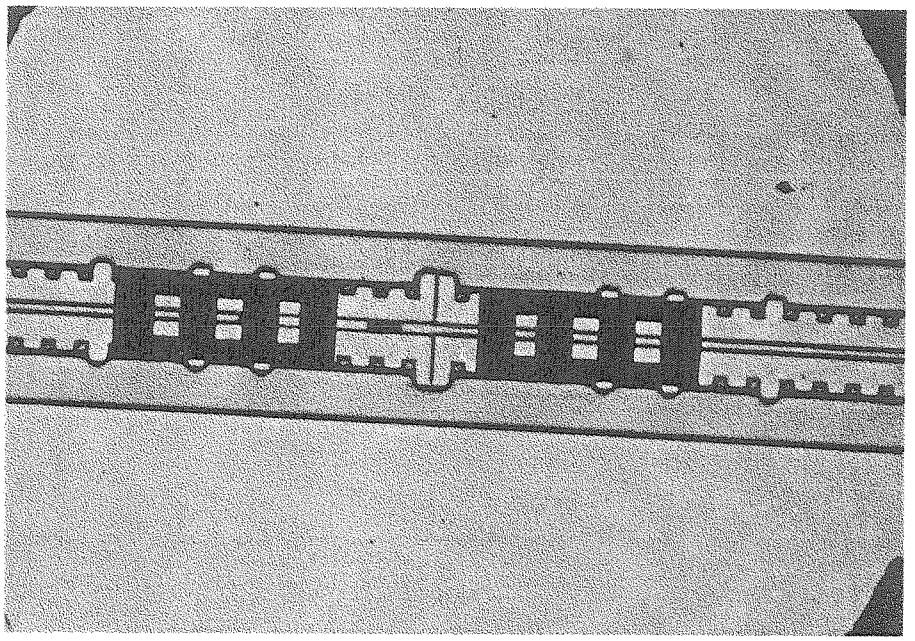

(a)

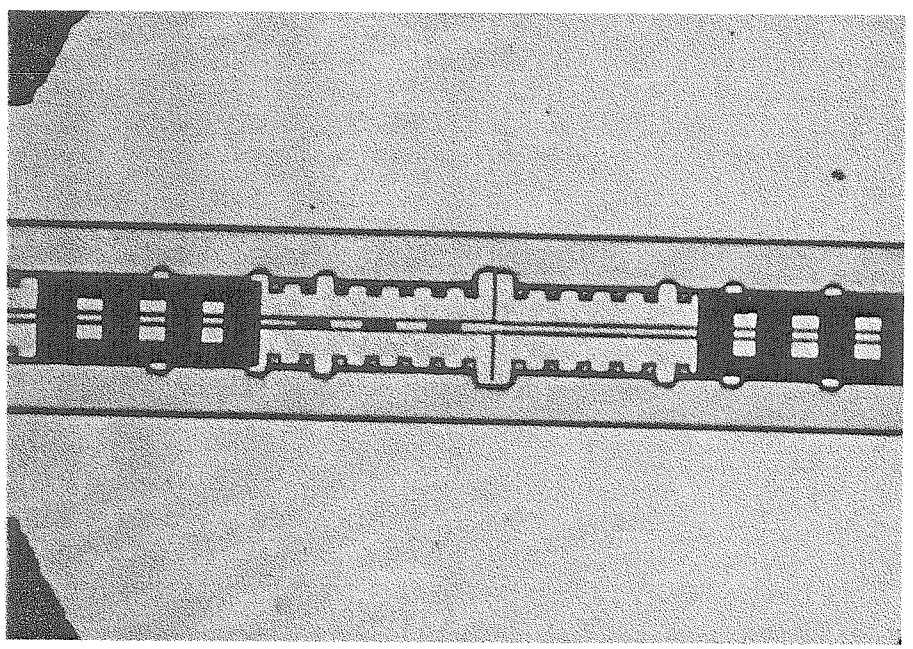

(b)

Figure A.7 Micrographs of a circuit with two released SPB's, in two different sets of positions.

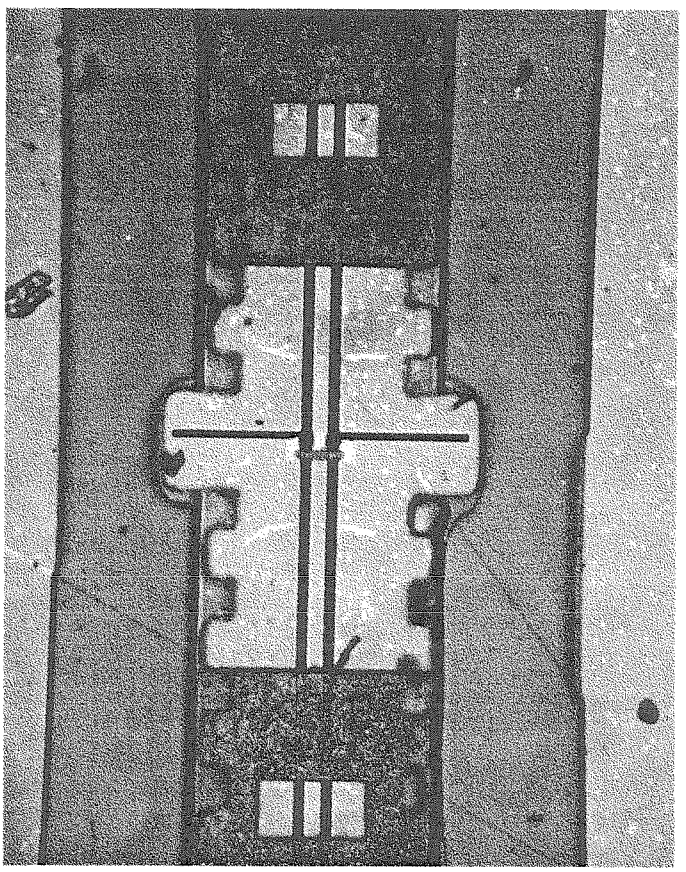

Figure A.8 Micrograph of a micromechanical circuit with a thin-film bismuth detector.

References

[1] Registered trademark of *Apiezon Products Limited*, London, England.

[2] Registered trademark of the *Hoechst Celanese Corporation*, Phoenix, AZ, USA.

[3] Registered trademark of the *Transene Company, Inc*, Rowley, MA, USA.

[4] "Image Reversal with AZ 5200 Series," AZ Product Bulletin.

[5] Registered trademark of the *Oxy Metal Industries Corporation*, Nutley, NJ, USA.

[6] Registered trademark of *OCG Microelectronic Materials, Inc.*, Tempe, AZ, USA